NBS TECHNICAL NOTE 1307

U.S. DEPARTMENT OF COMMERCE / National Bureau of Standards

Limits to the Precision of Electro-Optic and Magneto-Optic Sensors

G. W. Day
P. D. Hale
M. Deeter
T. E. Milner
D. Conrad
S. M. Etzel

The National Bureau of Standards[1] was established by an act of Congress on March 3, 1901. The Bureau's overall goal is to strengthen and advance the nation's science and technology and facilitate their effective application for public benefit. To this end, the Bureau conducts research to assure international competitiveness and leadership of U.S. industry, science and technology. NBS work involves development and transfer of measurements, standards and related science and technology, in support of continually improving U.S. productivity, product quality and reliability, innovation and underlying science and engineering. The Bureau's technical work is performed by the National Measurement Laboratory, the National Engineering Laboratory, the Institute for Computer Sciences and Technology, and the Institute for Materials Science and Engineering.

The National Measurement Laboratory

Provides the national system of physical and chemical measurement; coordinates the system with measurement systems of other nations and furnishes essential services leading to accurate and uniform physical and chemical measurement throughout the Nation's scientific community, industry, and commerce; provides advisory and research services to other Government agencies; conducts physical and chemical research; develops, produces, and distributes Standard Reference Materials; provides calibration services; and manages the National Standard Reference Data System. The Laboratory consists of the following centers:

- Basic Standards[2]
- Radiation Research
- Chemical Physics
- Analytical Chemistry

The National Engineering Laboratory

Provides technology and technical services to the public and private sectors to address national needs and to solve national problems; conducts research in engineering and applied science in support of these efforts; builds and maintains competence in the necessary disciplines required to carry out this research and technical service; develops engineering data and measurement capabilities; provides engineering measurement traceability services; develops test methods and proposes engineering standards and code changes; develops and proposes new engineering practices; and develops and improves mechanisms to transfer results of its research to the ultimate user. The Laboratory consists of the following centers:

- Applied Mathematics
- Electronics and Electrical Engineering[2]
- Manufacturing Engineering
- Building Technology
- Fire Research
- Chemical Engineering[3]

The Institute for Computer Sciences and Technology

Conducts research and provides scientific and technical services to aid Federal agencies in the selection, acquisition, application, and use of computer technology to improve effectiveness and economy in Government operations in accordance with Public Law 89-306 (40 U.S.C. 759), relevant Executive Orders, and other directives; carries out this mission by managing the Federal Information Processing Standards Program, developing Federal ADP standards guidelines, and managing Federal participation in ADP voluntary standardization activities; provides scientific and technological advisory services and assistance to Federal agencies; and provides the technical foundation for computer-related policies of the Federal Government. The Institute consists of the following divisions:

- Information Systems Engineering
- Systems and Software Technology
- Computer Security
- Systems and Network Architecture
- Advanced Computer Systems

The Institute for Materials Science and Engineering

Conducts research and provides measurements, data, standards, reference materials, quantitative understanding and other technical information fundamental to the processing, structure, properties and performance of materials; addresses the scientific basis for new advanced materials technologies; plans research around cross-cutting scientific themes such as nondestructive evaluation and phase diagram development; oversees Bureau-wide technical programs in nuclear reactor radiation research and nondestructive evaluation; and broadly disseminates generic technical information resulting from its programs. The Institute consists of the following Divisions:

- Ceramics
- Fracture and Deformation[3]
- Polymers
- Metallurgy
- Reactor Radiation

[1]Headquarters and Laboratories at Gaithersburg, MD, unless otherwise noted; mailing address Gaithersburg, MD 20899.
[2]Some divisions within the center are located at Boulder, CO 80303.
[3]Located at Boulder, CO, with some elements at Gaithersburg, MD

Limits to the Precision of Electro-Optic and Magneto-Optic Sensors

G. W. Day
P. D. Hale*
M. Deeter**
T. E. Milner**
D. Conrad***
S. M. Etzel

Electromagnetic Technology Division
Center for Electronics and Electrical Engineering
National Engineering Laboratory
National Bureau of Standards
Boulder, Colorado 80303

*Also with the Department of Physics, Colorado School of Mines, Golden, Colorado
**Also with the Optical Sciences Center, University of Arizona, Tucson, Arizona
***Also with the Department of Electrical and Computer Engineering, University of Colorado, Boulder, Colorado

U.S. DEPARTMENT OF COMMERCE, Malcolm Baldrige, Secretary

National Bureau of Standards, Ernest Ambler, Director

Issued March 1987

National Bureau of Standards Technical Note 1307
Natl. Bur. Stand. (U.S.), Tech Note 1307, 128 pages (March 1987)
CODEN:NBTNAE

U.S. GOVERNMENT PRINTING OFFICE
WASHINGTON: 1987

For sale by the Superintendent of Documents, U.S. Government Printing Office, Washington, DC 20402

PREFACE

Research in the Optical Electronic Metrology Group at the NBS Boulder Laboratories aimed at understanding the characteristics and limitations of sensors for electromagnetic quantities began in 1982 and has continued under the auspices of NBS and several other government and private agencies. The work reported in this document was undertaken with the specific support of NBS, the U.S. Department of Energy through Bonneville Power Administration (BPA), and, through BPA, the Electric Power Research Institute (EPRI) and the Empire State Electric Energy Research Corporation (ESEERCO). However, in some respects, it is inseparable from related research conducted presently under the support of the Department of Energy through Los Alamos and Sandia National Laboratories and previously supported by the Department of Defense through the Calibration Coordination Group.

Numerous people have contributed to the authors' understanding of these topics in recent years. Of these, Lynn Veeser, George Chandler, and Franz Jahoda of Los Alamos National Laboratory, Richard Cernosek of Sandia National Laboratory, Dennis Erickson of Bonneville Power Administration, and Gordon Frank of British Columbia Hydro Research Labs deserve special mention. We are also greatly indebted to Edie DeWeese for ably and patiently assembling this manuscript.

Where trade names are mentioned in this manuscript, they should not be considered a recommendation or endorsement by the National Bureau of Standards or an indication that other, similar items may not perform equally well or better. This report will be published subsequently by EPRI as part of an EPRI Report.

CONTENTS

LIST OF FIGURES

LIST OF TABLES

Section 1

INTRODUCTION

The material in this report has been prepared in response to a seemingly simple question, "What precision (that is to say stability, or reproducibility) can be achieved with an electro-optic voltage sensor or a magneto-optic current sensor?"

The basic principles of the linear and quadratic electro-optic effects (sometimes known as the Pockels and Kerr effects, respectively) and the Faraday magneto-optic effect have been known, studied, and occasionally used, for nearly a century. The decade of the 60s, following the discovery of the laser, saw substantial research on these effects, mostly motivated by their potential for optical modulation, and the development of numerous materials with enhanced properties. Beginning in 1970, with the development of cw, room temperature, semiconductor lasers that are easily modulated and nicely compatible with low loss optical fiber developed at about the same time, interest in electro- and magneto-optic materials waned. Now, however, the pendulum seems to be swinging again with interest revived by two applications areas. One is the need for high speed switching, control, etc. in the advanced optical communications systems now being developed. The other is the topic of concern here, namely the potential for nonconducting, noninvasive sensors for electromagnetic quantities.

Throughout their history, very little attention has been paid to the stability of electro- and magneto-optic devices, so that when the question stated above was originally posed, no reliable answers could be provided. This was particularly the case in view of needed precisions of the order of 0.1 percent over very broad temperature ranges (100°C). True, the temperature dependence of the Faraday effect in paramagnetic materials is well known and the temperature dependence of the static birefringence in certain electro-optic materials has been studied, but these cases are not applicable to high precision devices. It seemed clear then, that a critical review of the technology, with a view both to the precision that could be obtained with present technology and to that which might be achieved with further development, was in order. This represents the motivation and background for the present study.

Our intent in this report is to follow the approach that one attempting to design a high precision current or voltage sensor would follow, namely to examine the transfer functions of such devices (i.e., their terminal characteristics), then to relate the properties of those functions to individual components of a sensor, and finally to examine the properties of those components in sufficient detail to project eventual performance.

It became apparent in the early stages of this study that the transfer functions of optical sensors are sufficiently different from those of measurement devices familiar to most power engineers that significant discussion of that topic was needed, hence a fairly lengthy treatment in Section 2. An important example in this regard is that most optical sensors of the sort that may have applications in the power industry provide an instantaneous response over a high bandwidth. They are thus very different from transformer based systems and provide substantially enhanced capability for measuring high frequency or distorted signals. The intent of Section 2 is to be generic, that is, not to relate the transfer functions to any particular sensor or sensor parameter but to examine the implications of the transfer function shape and anticipated changes in shape for the precision of such a sensor.

In Section 3 we begin to relate the transfer functions of Section 2 to specific sensor types and to the components of those sensors. Numerous examples of current or voltage sensor configurations are briefly described as a basis for the more detailed and critical reviews later. It has not been our intent to describe or examine all possible sensor designs, but to cover the basic principles.

Section 4 is a review of the limitations that the properties of various components pose to the precision of electro-optic voltage sensors. The treatment is at a fundamental level, without much attention to the manner in which the sensor would be used. Wherever possible, we have attempted not only to point out problems, but to discuss possible solutions and future developments. The section concludes with a prognosis for the development of high precision voltage sensors. Similarly, Section 5 is a review of the limitations to the precision of magneto-optic current sensors, and also concludes in a prognosis.

In Section 6 we offer our opinions on the steps that should be taken to accelerate the development of high precision current and voltage sensors. These include specific research to be undertaken and other developments that should be pursued.

Finally, Section 7 summarizes the results and recommendations.

Several appendices that should be useful to the designer of electro-optic and magneto-optic sensors are included. The publication of several archival papers on the subject covered here is anticipated.

Section 2

CONCEPTS OF PRECISION AND ACCURACY IN ELECTRO-OPTIC AND MAGNETO-OPTIC SENSORS

In the introduction to this report, we pointed out that the use of optical sensors in the power industry will require entirely different ways of thinking about the relationship between the quantity to be measured (the measurand) and the output of the sensor. In this section we will examine the factors that determine the reproducibility of an optical sensor quantitatively, but in a generic sense, that is without relating the changes in the transfer function to specific material or component properties.

GENERIC TRANSFER FUNCTIONS

In most cases, where a sensor is to be used to determine the instantaneous value of a measurand (i.e., a waveform), the most desirable transfer function is a linear function,

$$R(x) = K\,x, \tag{2-1}$$

where x is the measurand, R(x) is the output of the sensor, and K is a constant. In some cases, specifically the measurement of dual polarity measurands, the anti-symmetric nature of the waveform is important. Unfortunately, in the field of optics, one is rarely able to obtain truly linear functions.

In all of the cases described in this report and in many others, the output of an optical sensor, understood usually to mean either optical power at a detector or the detector output, is related to a measurand (current, voltage, electric or magnetic field) by a function of the form

$$R(x) = A \sin^2(x/x_0 + \Phi), \tag{2-2}$$

where R(x) is the instantaneous output corresponding to a value, x, of the measurand, x_0 is a constant typically depending on the type of sensor, the material used and the wavelength, A is a constant related to the amount of optical power

available from the source and the optical losses in the sensor, and Φ is a constant characteristic of a particular configuration. Note that a single value of R(x) corresponds to multiple values of x, that the function is nonlinear, and that it is always positive--characteristics that are generally undesirable in a sensing device.

The four choices of Φ illustrated in Figure 2-1, (0, $\pi/2$, and $\pm\pi/4$) are the most useful. For greatest sensitivity (i.e., maximum dR/dx) and linearity, $\Phi = \pm\pi/4$ are obviously the best choices. When very large signals are to be measured (those that exceed x_0) or when the rms value of the waveform rather than the waveform itself is to be determined (see below), it may be advantageous to choose Φ to be 0 or $\pi/2$.

A further possibility is to utilize both the + and $-\pi/4$ choices and to take their difference. This yields a transfer function of the form (Figure 2-2)

$$R(x) = A \sin [2x/x_0 + 2(\Phi - \pi/4)] \qquad (2\text{-}3)$$

where the second term in brackets is obviously equal to zero if the value of Φ is chosen accurately. This function now represents a reasonable approximation to the ideal transfer function, at least over a range of positive and negative values of x. It can, however, be improved one step further by noting that the sum of the $\Phi = \pm\pi/4$ choices is identically equal to A. The A dependence, which is a significant factor in determining precision, can thus be removed by division. This additional complexity, which probably requires a computer, may or may not be appropriate in a specific application.

TRANSFER FUNCTION DISTORTIONS

Having identified what is probably the most useful transfer function available from an optical sensor, Eq. 2-3, we are now in a position to examine how that function can be distorted and the impact those distortions will have on the performance of the sensor. Various specifications of sensor precision could be chosen. For present purposes, we choose to compare the rms value of the sensor output waveform to the rms value of the measurand waveform.

We begin by noting that this ratio will be dependent on both the amplitude and shape of the measurand waveform. The dependence on amplitude can be readily computed and is shown in Figure 2-3 for the case of a sinusoidal measurand waveform.

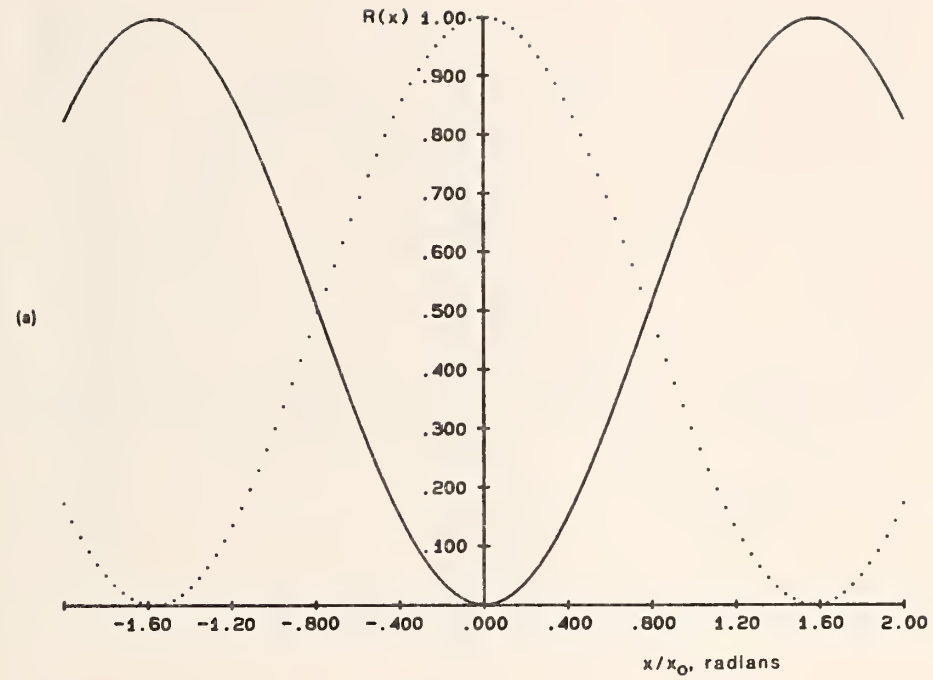

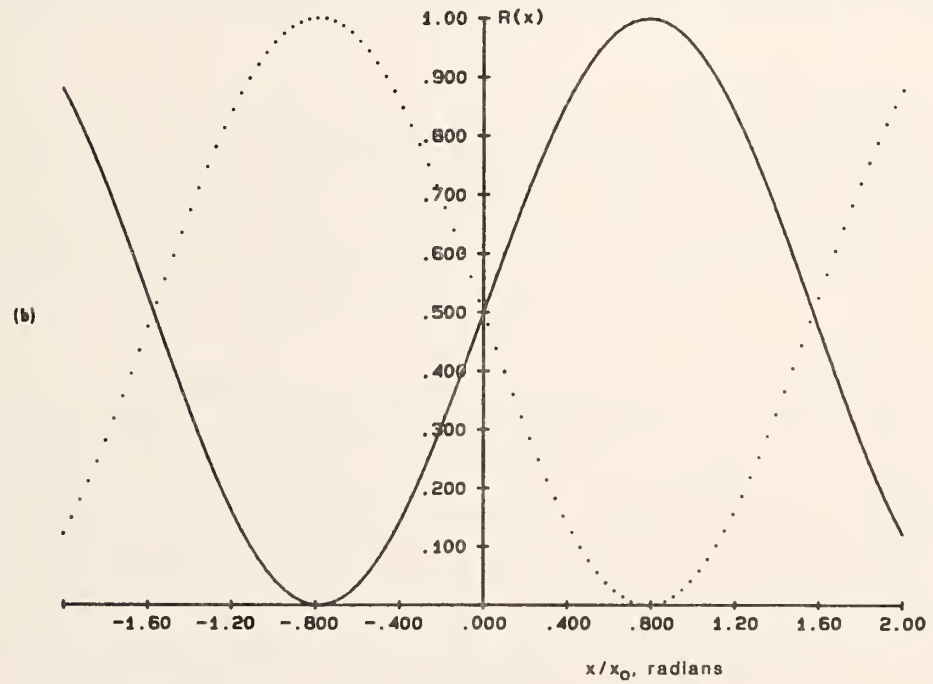

2-1. Transfer functions corresponding to Eq. 2-2 for 4 values of Φ: (a) 0, $\pi/2$; (b) $\pm\pi/4$.

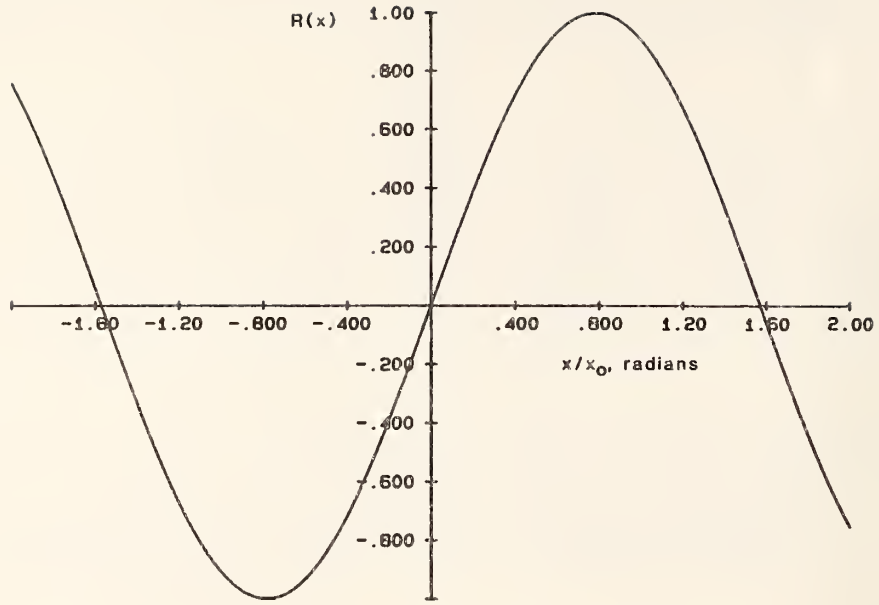

2-2. Transfer function corresponding to Eq. 2-3 for $\Phi = \pi/4$.

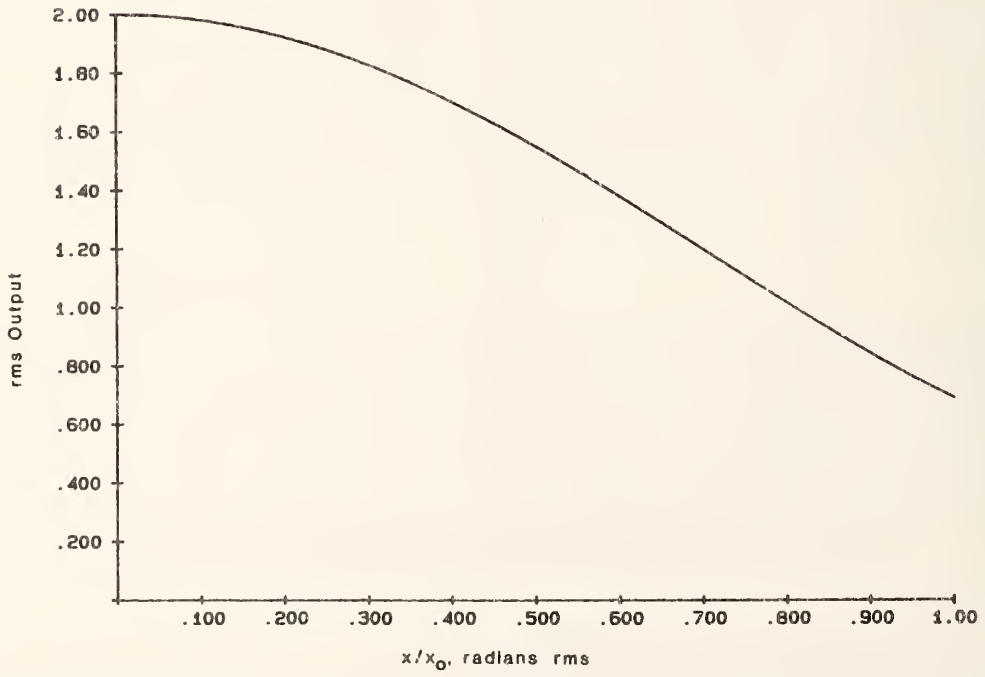

2-3. Generalized calibration curve for a sensor with a transfer function of the form of Eq. 2-3 ($\Phi = \pi/4$) and Figure 2-2.

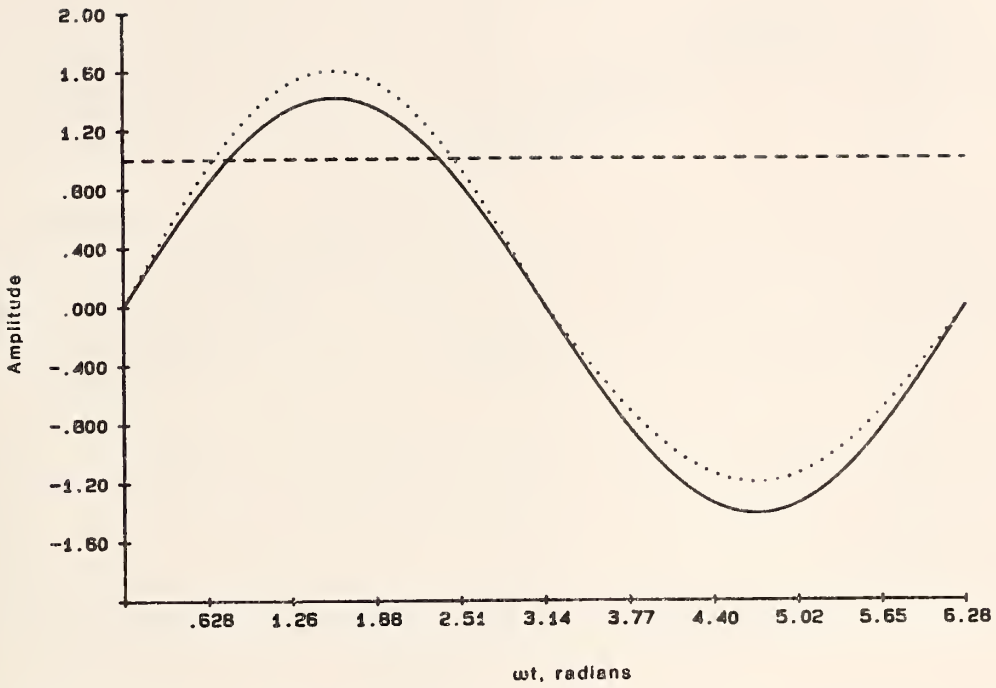

2-4. Three waveforms used for testing the sensitivity of the calibration curve to waveform shape. Solid curve is a true sinusoid, dotted curve is a distorted sinusoid, dashed curve represents a dc measurand. Each is normalized to an rms value of one.

Note that for small values of x/x_0 the ratio is 2 (actually 2A) which is equal to the first derivative of Eq. 2-3 at the origin. Figure 2-3 thus represents a generalized calibration curve for such a sensor. From the point of view of precise measurements the fact that the ratio varies with measurand amplitude is not important; only changes in the curve need to be considered.

In principle, the calibration curve must be determined for every waveform used. It is therefore useful to determine the sensitivity of the calibration curve to waveform shape. Figure 2-4 shows three waveforms used here for illustration. The solid curve is a perfectly sinusoidal waveform. The dotted curve is a distorted sinusoid, with the positive half-cycle being somewhat larger than the negative half-cycle; it therefore has a dc component. The dashed curve indicates a dc measurand. As shown, each has been normalized to have an rms value of one.

Figure 2-5 shows the calibration curves corresponding to these three waveforms. It appears that for nominally sinusoidal waveforms with relatively small values of x/x_0 the calibration curves are relatively insensitive to waveform shape.

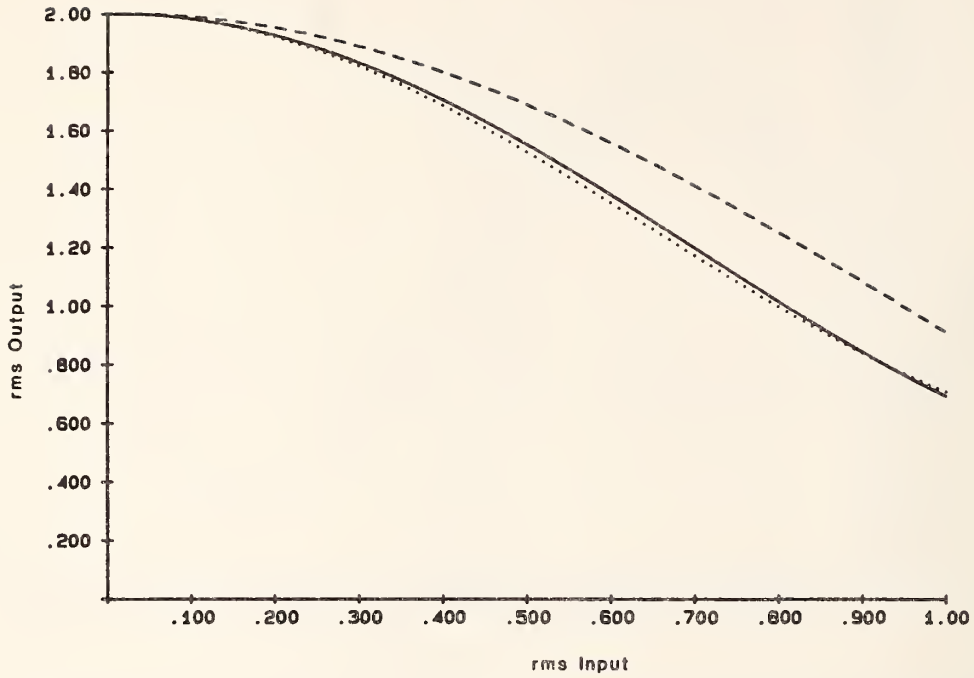

2-5. Computed calibration curves for the three waveforms shown in Figure 2-4. Solid curve is the same as Figure 2-3. Dotted and dashed curves refer to the respective waveforms in Figure 2-4.

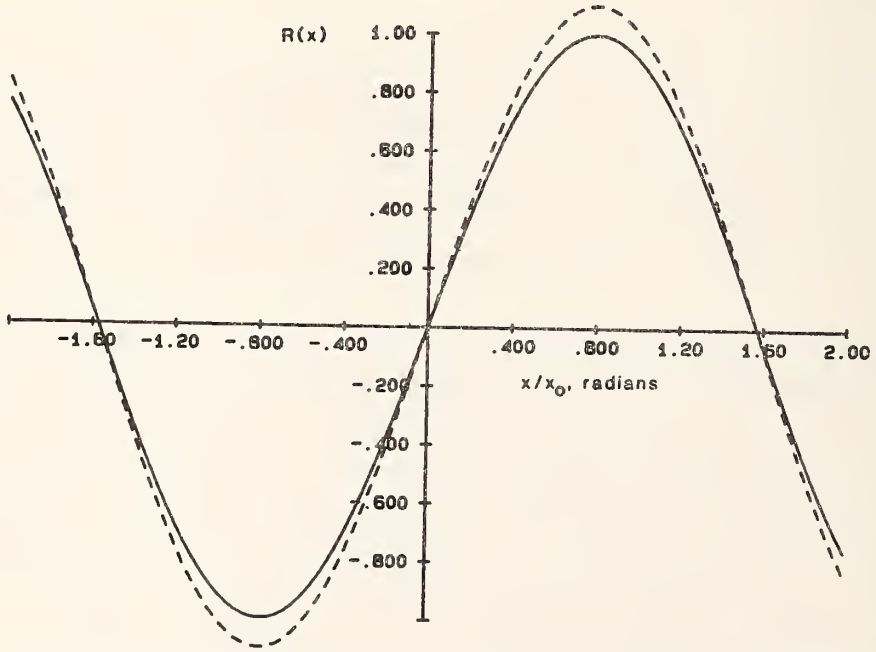

2-6. Illustration of the effect on the transfer function of an increase in the parameter A. Solid curve is the unchanged curve. Change in slope at the origin is directly proportionate to the change in A.

The effect on the transfer function of an increase in the parameter A is shown in Figure 2-6. The result is a proportionate change in the transfer function and therefore in the calibration curve. That is, the parameter A must be maintained constant with exactly the same precision as is required in the overall sensor, or the A dependence must be removed as described above.

The effect of an increase in the parameter x_0 is shown in Figure 2-7. The result is a proportionate change in the periodicity of the transfer function, hence the slope at the origin, and the calibration curve. Therefore, x_0 must also be maintained with the same precision as is required in the overall sensor.

The effect of a change in Φ is different, and is shown in Figure 2-8. The shape of the transfer function is unchanged, but the origin is shifted. This has three significant effects, as follows: (1) The output now has an average value (i.e., a dc level); (2) for sinusoidal signals, there is a phase shift between the input and output of magnitude 2Φ; and (3) if the change in Φ is large enough or the signal is large enough, the calibration curve will change.

If a sensor is to be designed so that it can measure dc components, then the most serious of these three effects is the appearance of an average value which represents an offset in the measurement. Figure 2-9 shows the result of small changes in Φ on the calibration curve. From that analysis, we can determine, for example, that to maintain a precision of 0.1 percent for dc coupled sensors with rms values of x/x_0 no smaller than 0.1, one must maintain Φ to within 0.004 radians. Figure 2-10 shows a plot of the errors in the transfer functions for several values of Φ. Of course, if the sensor designer is willing to forego information about the dc component of a measurand waveform, this requirement can be relaxed.

Sometimes more than one of the three parameters in Eq. 2-3 can change at the same time, yielding a more complex distortion of the transfer function. Figure 2-11 shows an example of such a case, derived for a particular sensor configuration described in more detail in a later section.

The type of analysis described in this section is the first step in determining the sort of precision that can be obtained for a particular sensor. Having determined, quantitatively, what level of distortion in the transfer function can be tolerated, one can then associate the particular defects encountered with the properties of specific components of the sensor, and thus determine the effectiveness of a design. These steps are taken in later sections of this report, but before

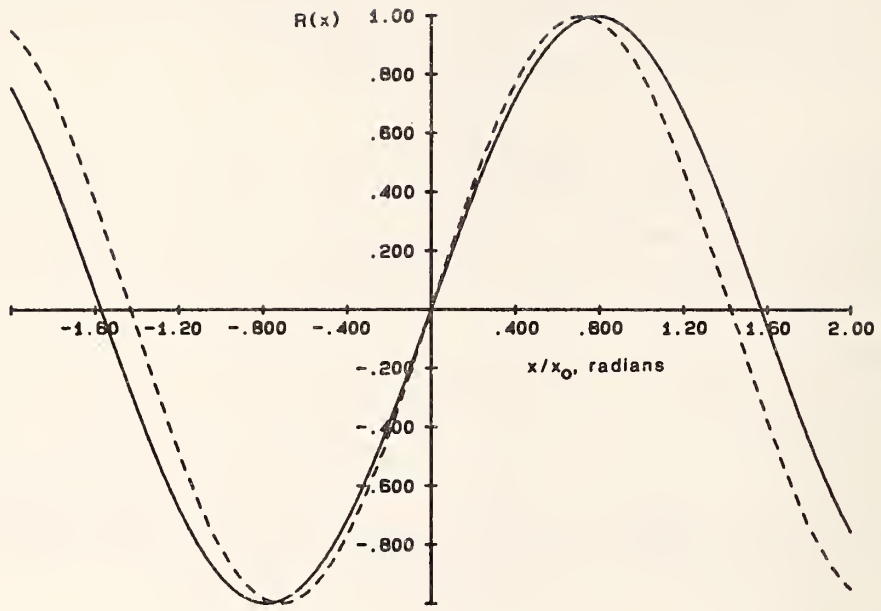

2-7. Illustration of the effect on the transfer function of an increase in the parameter x_0. Solid curve is the unchanged curve. Change in slope at the origin is directly proportionate to the change in x_0.

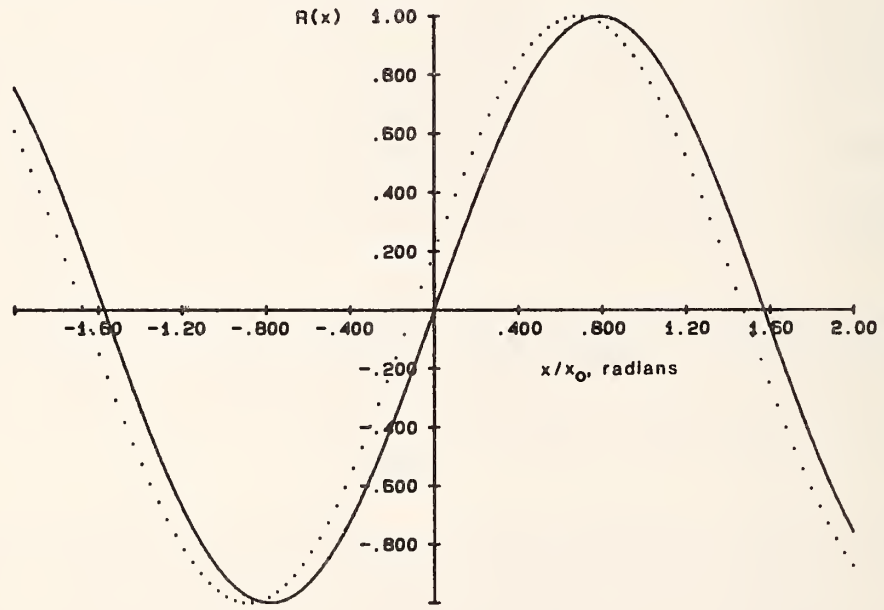

2-8. Illustration of the effect on the transfer function of a change in the parameter Φ. Solid curve is the unchanged curve. The result is the appearance of an average value, a shift in phase, and a change in the calibration curve.

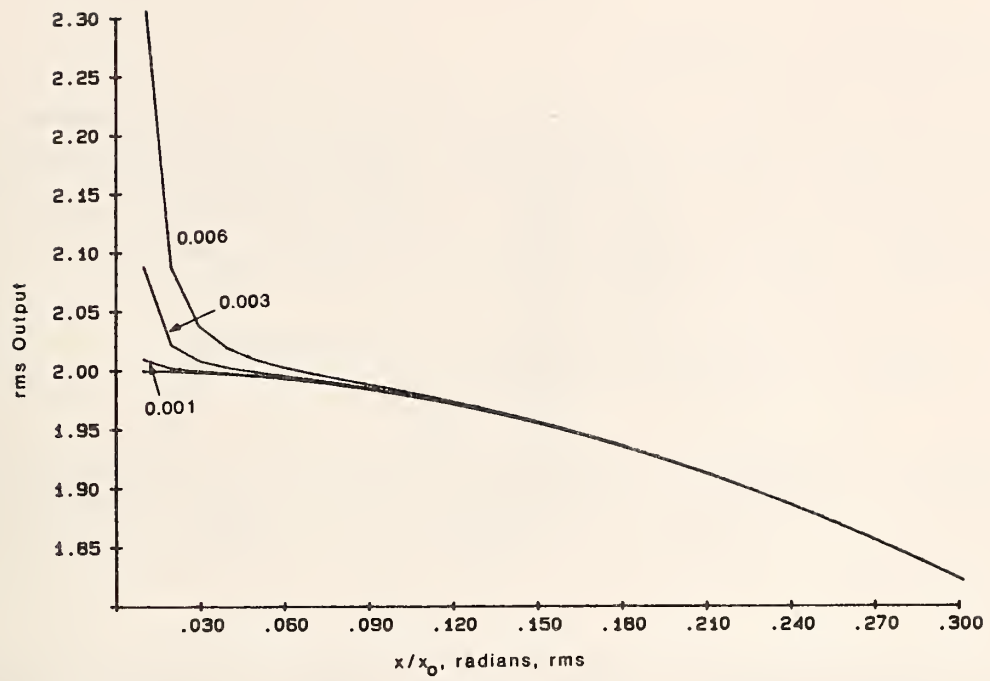

2-9. Result of small changes in Φ on the calibration curve for sinusoidal signals. Labels indicate differences in radians from $\pi/4$.

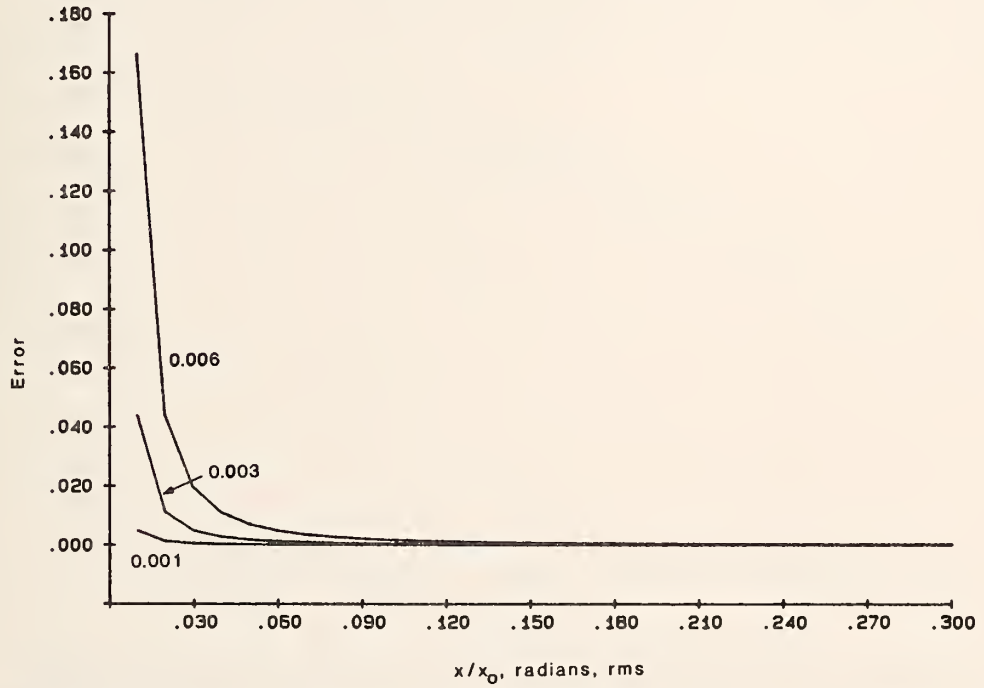

2-10. Fractional errors in the distorted curves of Figure 2-9. Specifically, the differences between each of the distorted calibration curves and the undistorted curve divided by the undistorted curve.

that, it is useful to consider, briefly in the next section, an alternative type of transfer function to that described above.

INSTANTANEOUS VERSUS rms MEASUREMENTS

The assumption that instantaneous measurements of current or voltage waveforms are preferred should not be viewed as a requirement. Another interesting possibility is that of a sensor designed to give directly a response proportional to the true rms of an arbitrary input waveform. Such a device can be produced, based on Eq. 2-2 with $\Phi = 0$ (see Figure 2-1). That is,

$$R(x) = A \sin^2 x/x_0 = A[(x/x_0)^2 - (x/x_0)^4/3 + \ldots], \qquad (2\text{-}4)$$

where the quantity in brackets is a Taylor series expansion. To the extent that the second term in brackets in Eq. 2-4 is negligible, one can obtain the true rms value of the waveform by determining the average output of the sensor over the period of the waveform.

Since this is not a true parabolic function, the ratio of average output to the rms value of the measurand will depend, as with the case described above, on both the amplitude and shape of the measurand. For the three waveforms used for illustration above (Figure 2-4), the computed calibration curves are shown in Figure 2-12.

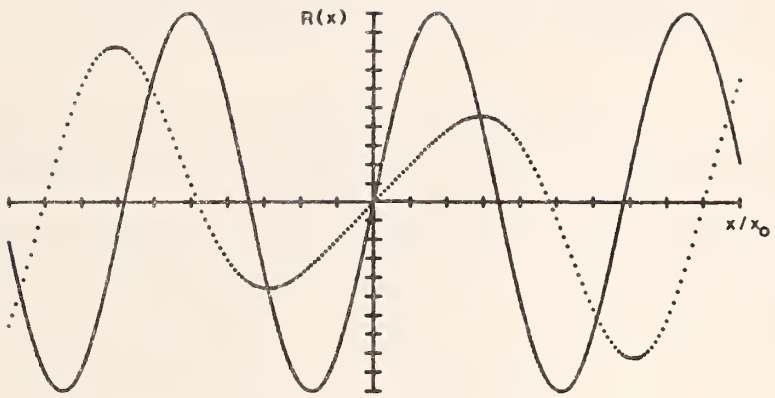

2-11. Illustration of a complex distortion of a transfer function arising from nonideal characteristics of a current sensor described in Section 3.

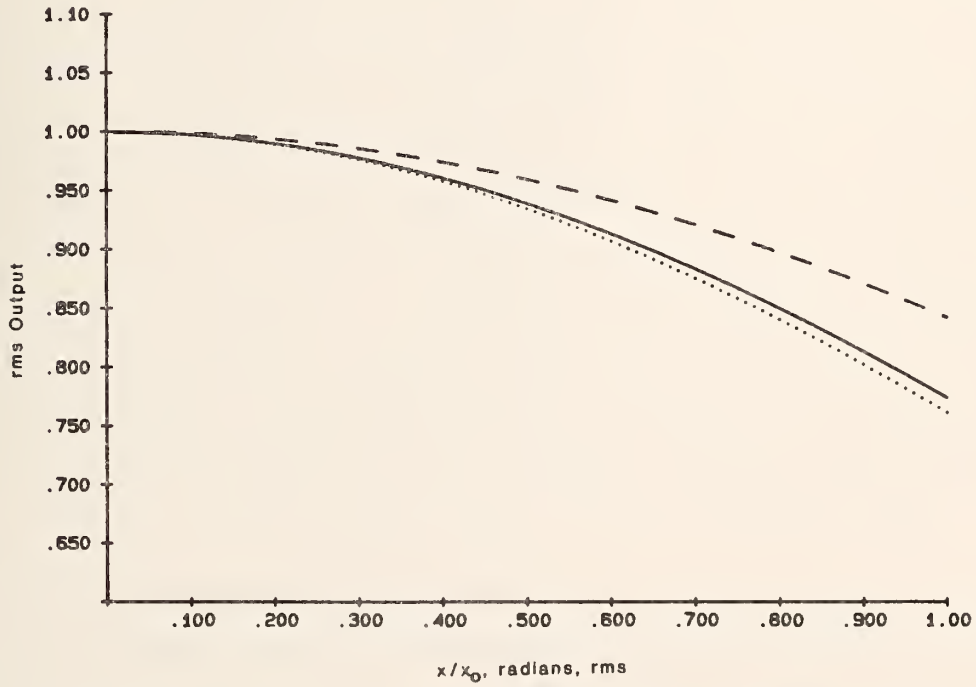

2-12. Calculated calibration curve for a true rms reading sensor for the 3 waveforms of Figure 2-4.

Section 3

ELECTRO-OPTIC AND MAGNETO-OPTIC SENSOR CONFIGURATIONS SUITABLE FOR CURRENT AND VOLTAGE MEASUREMENTS

A very large number of optical approaches to the measurement of current and voltage have been discussed in the literature. Of these, there are a relatively small number that have been examined in sufficient detail that we might expect them to yield at least a first generation of useful devices. In this section we describe some of the more promising approaches, which will allow us, in later sections, to relate specific sensor properties, such as those described in the previous section, to particular component and material properties.

ELECTRO-OPTIC VOLTAGE SENSORS

Numerous effects involving a change in the optical propagation characteristics of a material in the presence of an electric field have been reported in the literature. Of these the two most widely studied and developed are the linear electro-optic effect, sometimes known as the Pockels effect, and the quadratic electro-optic effect, sometimes known as the Kerr effect. Both of these effects may be described as an induced linear birefringence, that is to say an induced anisotropic change in the refractive index of the material. The linear electro-optic effect appears only in crystalline materials and of those, only crystals that do not have a center of symmetry. The quadratic electro-optic effect appears in all materials. Unfortunately, it is very small in glass, though that is the material in which it was discovered, so except perhaps for extremely high fields, it is probably not practical to use fiber itself as the sensing element for a voltage sensor. We therefore concentrate here on sensors based on the linear electro-optic effect though most of the discussion applies also to quadratic devices.

Polarimetric Electro-optic Voltage Sensors

The basic configuration of an electro-optic voltage sensor using polarimetric techniques is shown in Figure 3-1. A suitable crystal is chosen and oriented so that, when an electric field is applied in a certain direction, light passing through the crystal experiences a linear birefringence or change in linear

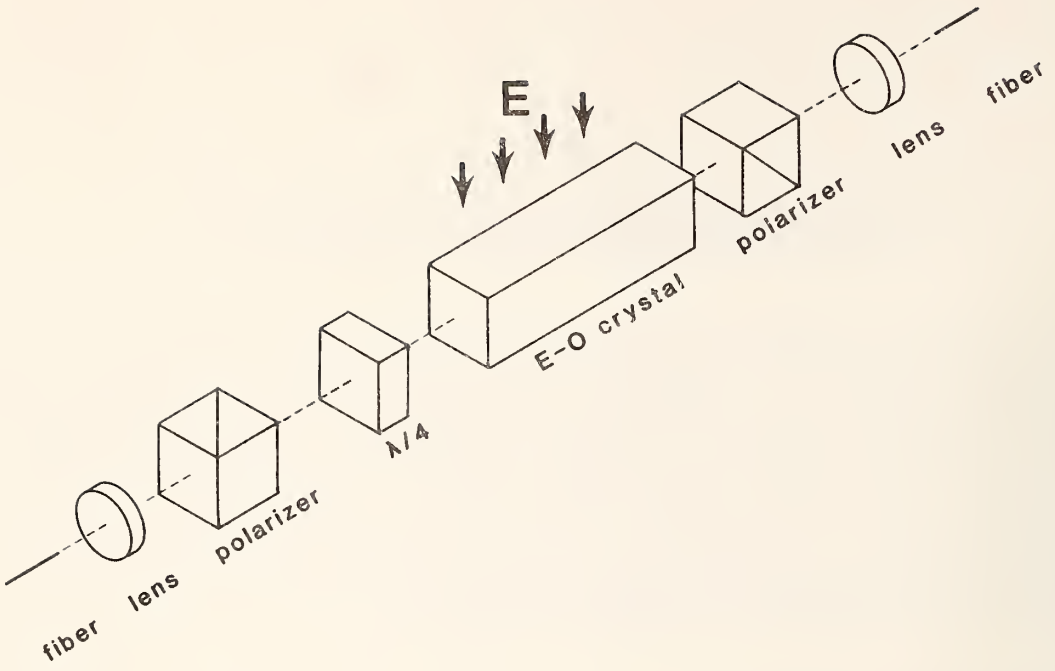

3-1. Basic configuration of an electro-optic voltage sensor. In addition to the electro-optic crystal, normal components include polarizers, a waveplate (retardation plate) shown as a quarter-wave plate, and lenses required to transmit light efficiently from one optical fiber through the bulk components and back into another fiber. Many modifications of this basic geometry can be used, including, particularly a double-pass arrangement in which light is reflected back through the crystal and either into the input fiber or another fiber.

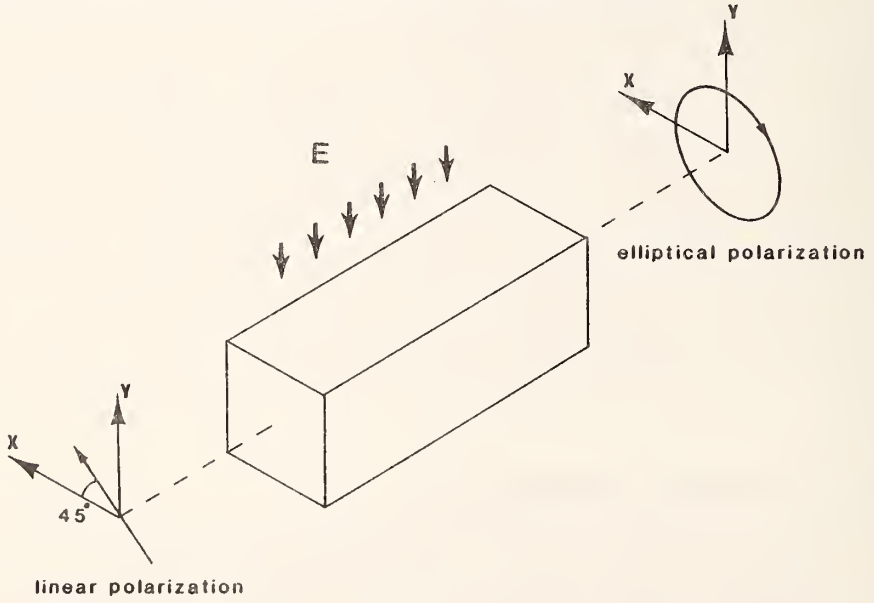

3-2. Linear birefringence induced in the crystal by an electric field causes the polarization state of light to change as it passes through the crystal. The changes in polarization state can be converted to changes in transmittance with polarizers.

birefringence proportional to the field. (Precisely, linear birefringence is the difference between the refractive indices that apply to two specific orthogonal linearly polarized components of the transmitted light.) When the transmitted light contains components parallel to both the axes of birefringence, the polarization state at the output is dependent on the magnitude of the birefringence incurred. Changes in polarization state can be converted to changes in transmittance using a polarizer.

More specifically, consider the case illustrated in Figure 3-2. The axes of linear birefringence are taken to be the x and y axes. Light incident on the material at 45° to these axes gives equal components parallel to the x and y axes. If the refractive index for these components is taken to be n_x and n_y respectively, the two components will differ in phase at the output by an amount given by

$$\Gamma = 2\pi(n_x - n_y)h/\lambda, \tag{3-1}$$

where h is the crystal length and λ is the wavelength. The polarization state at the output as a function of Γ is depicted in Figure 3-3. The quantity Γ may be expressed as a function of the electric field as follows,

$$\Gamma = \frac{2\pi Bh}{\lambda} + C_{eo}E, \tag{3-2}$$

3-3. Illustration of the change in polarization with Γ for the case of light that is initially linearly polarized at 45 deg to the axes of linear birefringence.

where Bh is the value of $n_x - n_y$ at zero field and C_{eo} may be called the effective electro-optic coefficient. C_{eo} depends on the specific material, its crystalline (point group) symmetry, and both the orientation of the electric field and the direction of propagation relative to the crystalline axes.

When the device is placed between crossed polarizers, the transmittance is given by

$$R(E) = \sin^2(\Gamma/2). \tag{3-3}$$

If Bh = 0, we obtain

$$R(E) = \sin^2(C_{eo}E/2) \tag{3-4}$$

which, when $C_{eo}/2$ is identified as $1/x_0$ and E as x, is the function shown as the solid curve in Figure 2-1a. When the polarizers are aligned, the function shown as the dotted curve in Figure 2-1a is obtained.

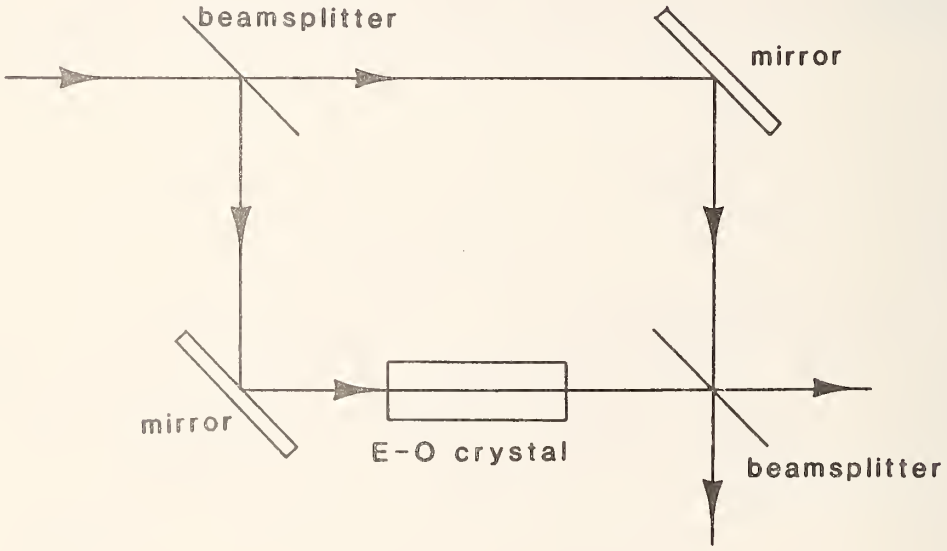

3-4. Illustration of a Mach-Zehnder interferometer used as an electric field or voltage sensor. An electro-optic crystal is placed in one arm of the interferometer. A change in refractive index of the crystal causes a fringe shift in the interferometer. The transfer function can span the full range of functions shown in Figure 2-2 depending on how closely matched the arms of the interferometer are in zero field.

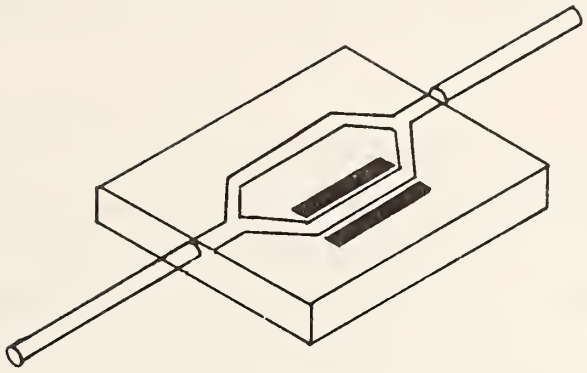

3-5. A planar waveguide (integrated optic) version of the Mach-Zehnder interferometer. The substrate would be of an electro-optic material in which a permanent waveguide structure could be created by locally changing the refractive index. By applying a voltage to electrodes (black areas) near the guide the optical path length of one path can be changed relative to the other in the same manner as in Figure 3-5.

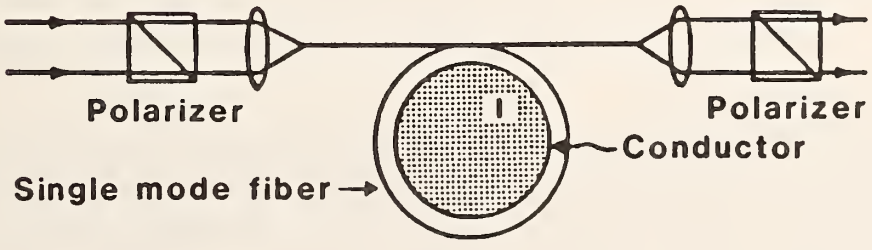

3-6. Basic configuration of an optical fiber current sensor.

Functions in between these two cases may be obtained when Bh is not zero. Specifically, the functions shown in Figure 2-1b are observed when $2\pi Bh/\lambda$ is equal to ±90 deg. These can also be obtained when Bh = 0 by placing a quarter-wave plate (a device that introduces a 90 deg phase shift) in series with the electro-optic crystal.

Interferometric Electro-optic Voltage Sensors

An alternative to the use of polarimetric techniques with an electro-optic sensor is to place the active material in one arm of an interferometer, for example the Mach-Zehnder interferometer shown in Figure 3-4. In this case the polarization of the light is oriented along one of the axes of induced birefringence in the crystal. The effect of the electric field then is to change the optical path length of the interferometer arm containing the crystal relative to the other. The change in output power is then again given by a function in the form of Eq. 2-1. The value of A is determined by the total power transmitted by the interferometer. The value of Φ is the difference in phase between light transmitted through the two arms of the interferometer with no applied field, and the value of x_0 is related to the material, symmetry, and orientation of the crystal.

Interferometric devices constructed of bulk components are not particularly attractive for measurement purposes because a high degree of mechanical and thermal stability is required for a stable output. However, such devices have been constructed using planar waveguide technology (integrated optics) and these show more promise of yielding useful devices (Figure 3-5). A particular advantage of this approach is that much more sensitive devices can be constructed and also that the number of components is minimized. The causes of instability in planar devices are similar to those in polarimetric devices, and therefore the discussion of stability in electro-optic devices presented in a later section will largely apply.

MAGNETO-OPTICAL CURRENT SENSORS

Magneto-optic current sensors are based on the Faraday magneto-optic effect, a rotation of the plane of polarization of linearly polarized light propagating through a material in the presence of a magnetic field. The Faraday effect is present to some degree in all materials, but is most often exploited in glass, either bulk glass or single mode optical fiber. Utilization of the effect in fiber allows great freedom in configuration and requires a minimum number of components and fabrication steps. On the other hand, a greater choice of materials

is available in bulk, bulk materials are more stable, physically, and it is easier to design for certain configurations using bulk materials. Both choices have been examined in detail in this study; their basic design and performance is described here.

Optical Fiber Current Sensors

The basic configuration of an optical fiber current sensor is shown in Figure 3-6. One or more turns of single mode fiber is looped around the conductor. The principles of the Faraday effect predict that the plane of polarization of linearly polarized light propagating through the fiber will be rotated by an angle θ given by

$$\theta = V \int \vec{B} \cdot \vec{d\ell}, \tag{3-5}$$

where V is a constant characteristic of the material in the fiber, called the Verdet constant, $B = \mu H$ is the magnetic flux density, and $d\ell$ is a differential vector in the direction of propagation. From Ampere's law the integral of the magnetic field (H) along any closed path around a conductor is equal to the current (I) passing through the path, i.e.,

$$\int \vec{H} \cdot \vec{d\ell} = I. \tag{3-6}$$

Thus we obtain a linear relationship between the rotation and the current,

$$\theta = \mu VNI, \tag{3-7}$$

where N is the number of turns of fiber around the conductor. In typical fiber, the ratio of rotation to current is small; for a single turn sensor and an operating wavelength of 633 nm it is approximately 265 deg/MA. It is shown in an appendix, however, that it is possible to detect very small rotations.

The most common method of measuring the rotation induced by the current is to place polarizers at the input and output, as shown in Figure 3-6. The rotation then results in a change in transmittance which is detected as a change in power at an optical detector. Depending on the relative orientation of the polarizers, any of the transfer functions shown in Figure 2-1 can be obtained. The case where the polarizers are aligned for maximum transmittance at zero current corresponds

to $\Phi = \pi/2$; alignment for zero transmittance at zero current to $\Phi = 0$; the two orientations giving 50 percent transmittance correspond to $\Phi = \pm\pi/4$.

The transfer function shown in Figure 2-2 is obtained with a polarizing beam splitter, such as a Wollaston prism, oriented so that both the + and $-\pi/4$ components are detected and their difference taken. It is often convenient to incorporate a half-wave plate (a polarization rotator) into the system in order to simplify the orientation of the polarizer (Figure 3-7).

To obtain, simultaneously, transfer functions with $\Phi = 0$ and $\pm\pi/4$ or $\pi/2$ and $\pm\pi/4$, to count fringes requires a beam splitter and two separate polarizers, as shown in Figure 3-8. The beam splitter must be designed and used in such a way that the polarization states of the transmitted and reflected beams are not altered.

Other configurations for determining the rotation can be considered. One is shown in Figure 3-9. If the plane of polarization of the linearly polarized light injected into the fiber is caused to rotate rapidly with time, the plane of polarization of the light at the output rotates at the same frequency, but with a phase shift that is proportional to the induced rotation in the fiber. Standard phase measurement instrumentation can thus be used to determine the current, as shown. Any method of creating a rotating linear polarization state, such as a rotating mechanical polarizer, can be used, but it is best if a very high rotation rate can be used. A convenient method depicted in Figure 3-9 is to start with two orthogonally polarized beams at slightly different wavelengths (i.e., slightly different optical frequencies). When these beams are passed through a quarter-wave plate oriented with its axes at 45 deg to the directions of polarization, the resulting beams is linearly polarized with its orientation rotating at the optical difference frequency. The two beams can be obtained from a Zeeman-split gas laser, where the difference frequencies are of the order of 0.1 MHz or using acousto-optic modulators, where the difference frequencies are of the order of tens of megahertz.

Another possibility is to incorporate the fiber coil into a Sagnac interferometer, as shown in Figure 3-10. The Sagnac interferometer is the same device used in a fiber optic gyroscope, and many of its properties are well known. Light entering the input fiber is divided with a 3 dB fiber coupler, the fiber equivalent of a 50/50 beamsplitter. Equal components thus propagate in opposite directions through the sensing coil, and are recombined at the coupler. It is a property of

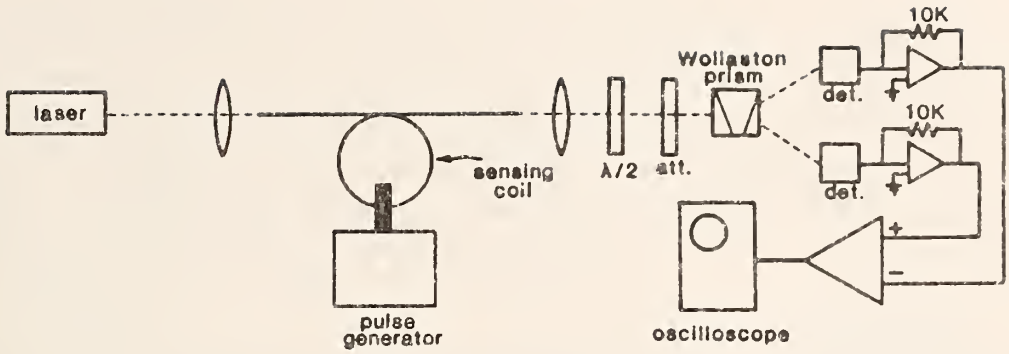

3-7. An optical fiber current sensor in which two orthogonal output polarizations are detected using a Wollaston prism polarizer.

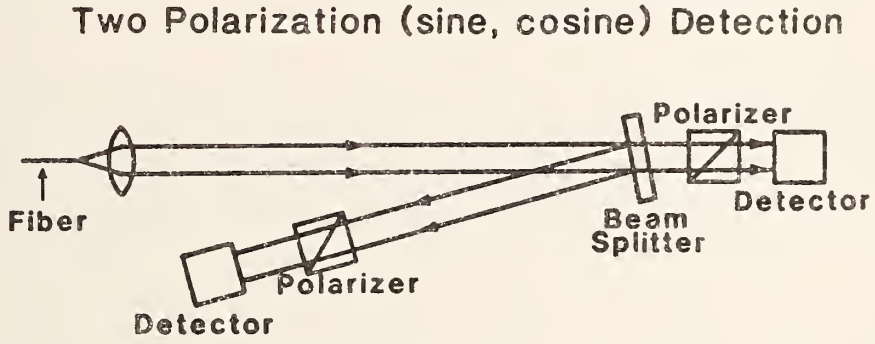

3-8. Polarizer arrangement for detecting two output polarizations oriented at 45 deg to each other.

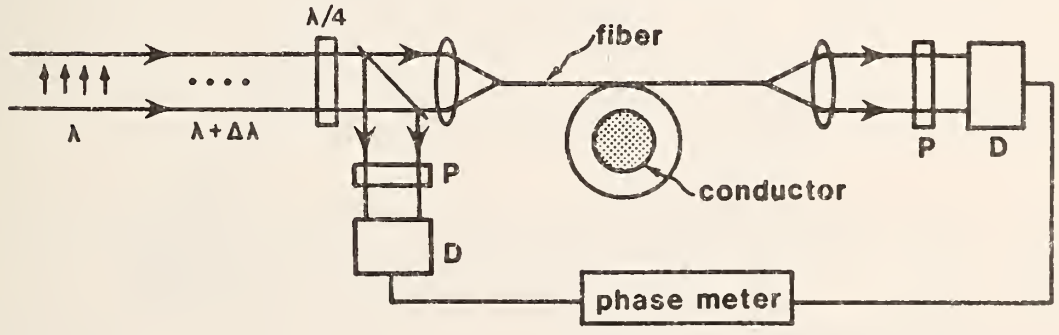

3-9. Rotating polarization technique for observing Faraday rotation in an optical fiber coil. The rotating input polarization is created by passing two orthogonally polarized optical beams at slightly different optical frequencies through a quarter-wave plate. The phase of the rotation is shifted in proportion to the current.

such couplers, as with beam splitters, that the two output components differ in phase by $\pi/2$ radians. One can then quickly show that, if the coil is reciprocal, the two components arriving at the output port differ in phase by π radians and interfere distructively, while the components arriving at the input port are in phase. Because the Faraday effect is nonreciprocal (i.e., it depends on the sign of the magnetic field) light is shifted from one port to the other by the presence of a current though the coil. The actual transfer function is given by Eq. 2-1 with $\Phi = 0$.

Because there is no easy method of choosing another value of Φ, the Sagnac device is not well suited to the measurement of small signals. It is extremely attractive for other reasons. It is a particularly simple device, involving no polarizers, and in fact works well with any input polarization state, including unpolarized light.

Bulk Glass Current Sensors

While the fiber current sensors described above have many advantages, there are times when it is preferable to construct a device in which the sensing occurs in a bulk material, with light transmitted to and from the material using fiber. The basic principles of such devices otherwise are identical to the all-fiber sensor. Advantages of this approach include the opportunity to use materials that are not available in fiber form, the possibility of using certain geometries that are not possible with fiber, and, for the present time, greater stability.

For high sensitivity current sensors, fused silica is not particularly attractive because the Verdet constant is low. Other commercial glasses offer a Verdet constant that is as much as twenty times larger and some experimental glasses offer the possibility of still higher values. Some crystalline materials have Verdet constants about three orders of magnitude greater than fused silica.

Figure 3-11 shows the design of a bulk glass sensor that has been reported in the literature. Light is transmitted to and from the sensor using multimode fiber. Polarizers and lenses are placed between the fiber and the sensor. The sensor is constructed of a single piece of glass faceted to reflect light around the conductor by complex path. The reason for the complex path is that when light is reflected from a dielectric interface (in this case total internal reflection is used) a phase shift between light polarized in the plane of the reflection and that polarized perpendicular to the plane of polarization is encountered. This

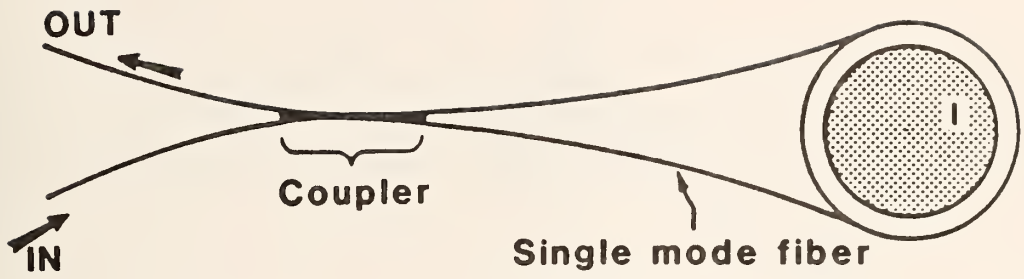

3-10. The Sagnac interferometer. Light entering the input port is split by the fiber coupler, half propagating through the coil in the clockwise direction and half in the counter-clockwise direction. In the absence of current through the conductor all light exits by the input port, but if current flows, the magnetic field causes the fiber coil to become nonreciprocal and light is shifted to the output port. The transfer function is that of Figure 2-1 with $\Phi = 0$.

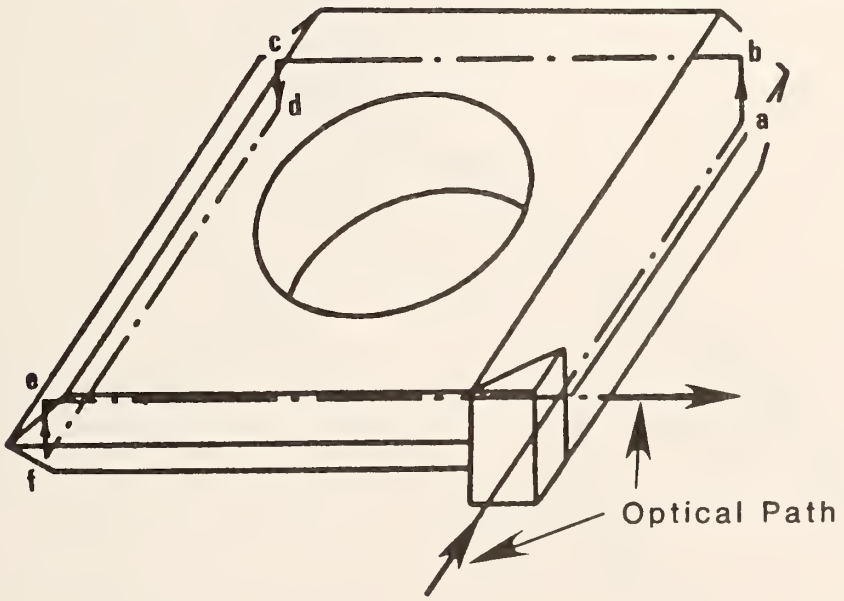

3-11. A Faraday rotation current sensor based on a design by Kanoi, et al. IEEE Trans. Power Delivery, 1986, vol. PWRD-1, p. 91-97. Two complementary reflections are used at each corner to cancel phase shifts that occur in reflection.

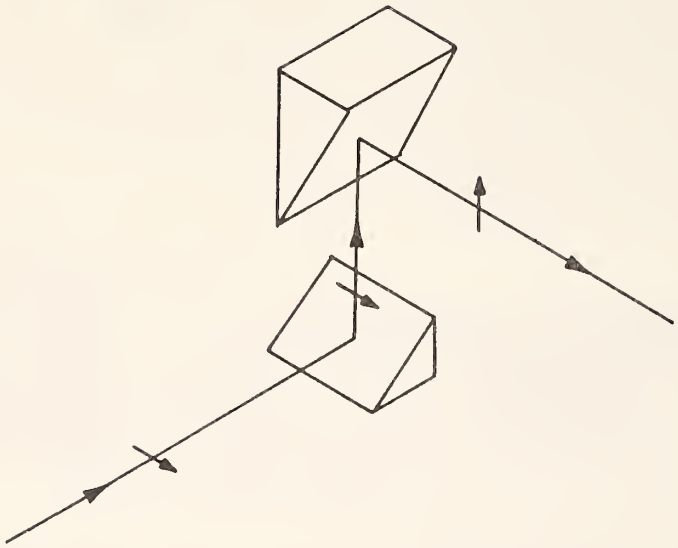

3-12. Illustration of the principle of polarization-independent beam steering using complementary reflections. The component of the optical field that is perpendicular to the plane of incidence in the first reflection is parallel to the plane of incidence in the second and vice versa.

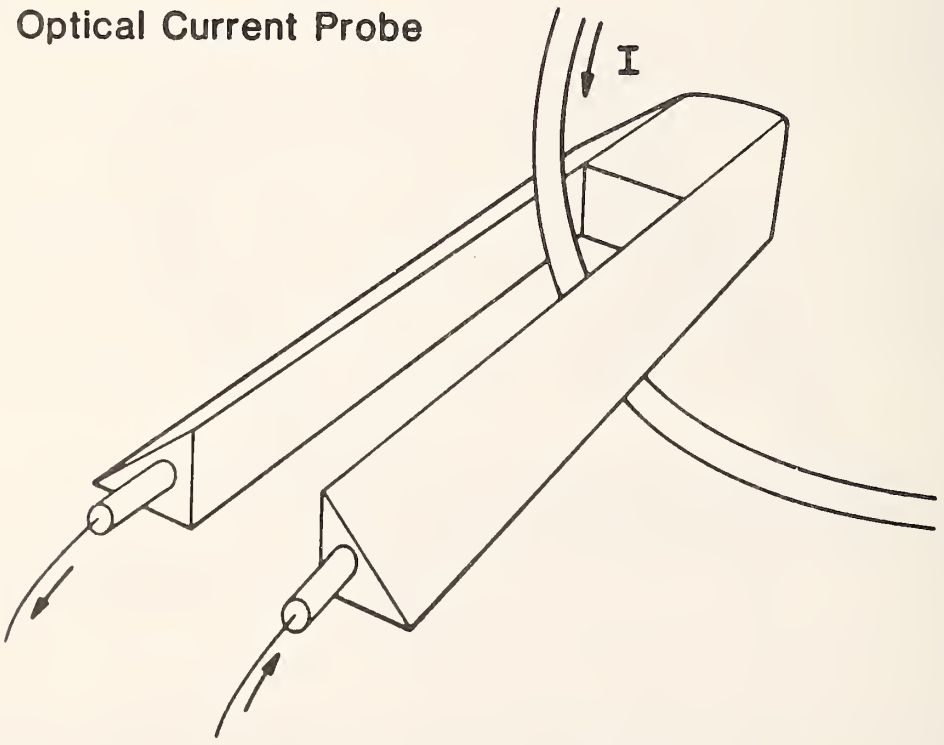

3-13. A bulk-glass current sensor that can be placed around a conductor without breaking either the conductor or the optical path.

results in a change of polarization state at each reflection and a distortion of the transfer function. The solution is to use two reflections wherever one is needed, the two being designed so that the parallel component in the first reflection is the perpendicular component in the second and vice versa, so that the phase shifts cancel. This use of complementary reflections for polarization-independent beam steering is widely used in optics. It is illustrated schematically in Figure 3-12.

Figure 3-13 shows how a bulk current sensor can be designed to slide onto a conductor. In such a device the optical path does not completely surround the conductor, but when carefully designed only a small percentage of the total signal is lost.

Section 4

CRITICAL EVALUATION OF ELECTRO-OPTIC SENSOR TECHNOLOGY

FACTORS LIMITING THE PRECISION OF BULK MAGNETO-OPTIC SENSORS

Properties of Electro-optic Materials

The effective electro-optic coefficient, C_{eo} defined in Eq. 3-2, depends on the specific material, its crystallographic symmetry, its orientation with respect to the directions of propagation and electric field, and its dimensions. A complete description of the electro-optic effect is beyond the scope of this document; the interested reader is referred to two books (4-1,4-2) that provide broad treatments of the subject. Here, we focus on material properties and material selection.

Many of the best known electro-optic materials--$LiTaO_3$, $LiNbO_3$, and KDP and its isomorphs, for example--are naturally birefringent; that is, even in the absence of an applied electric field, different polarizations experience different refractive indices (4-1,4-2,4-3). As a result, in many configurations, the parameter B in Eq. 3-2 is non-zero and is often very temperature dependent. This is particularly true in $LiTaO_3$ when used in its optimum orientation. It is possible in some of these materials to choose an orientation in which this natural birefringence is not, in principle, a problem. In these cases, however, alignment and collimation of the beam become critical and, furthermore, those orientations usually result in a significantly lower electro-optic coefficient.

Our first suggestion in selecting materials for high precision voltage measurements therefore is to restrict the selection to crystals with cubic symmetry; these are not naturally birefringent.

There is a second reason for choosing cubic crystals and that is related to the pyroelectric effect. Certain classes of crystals, specifically 10 of the 32 point symmetry classes, known as polar classes, have the property of developing an electric polarization when their temperature is changed. This represents an internal

electric field that can, by itself, cause changes in the birefringence of the crystal. None of the 10 polar classes is cubic (4-3).

Among the five cubic crystal classes--23, m3, 432, $\bar{4}3m$, m3m--two have a center of symmetry (m3m and m3) and therefore do not exhibit a linear electro-optic effect. One other (432) also does not have a linear electro-optic effect, leaving only classes 23 and $\bar{4}3m$ to be considered.

There is one further effect to be considered, namely optical activity. Optical activity is a rotation of the plane of polarization of plane polarized light of the same sort produced by the Faraday effect, except that both the sign and magnitude of the rotation are fixed by the material rather than a magnetic field. In the same way that linear birefringence tends to quench Faraday rotation, optical activity tends to quench the electro-optic effect. Crystal class 23 exhibits optical activity suggesting that crystals of class $\bar{4}3m$ are perhaps the best choice for voltage sensors. (There is one possible exception to this, discussed under temperature compensation techniques, below.)

Fortunately, a number of common crystals are included in class $\bar{4}3m$. These include GaAs, CdTe, ZnS, ZnSe, GaP, and $Bi_4Ge_3O_{12}$. For the rest of this section we concentrate on the properties of these materials.

For crystals of class $\bar{4}3m$, optimally oriented, the expression for induced birefringence is given by

$$\Gamma = C_{eo}E = \frac{2\pi}{\lambda} n^3 r_{41} h E, \qquad (4\text{-}1)$$

where Γ is the induced phase shift between orthogonal linearly polarized components, λ is the wavelength, h is the length of the crystal, n is its refractive index in zero field, r_{41} is an element of the electro-optic tensor applicable to the specific material, and E is the electric field in the crystal.

With regard to material properties and their effect on precision, we see from Eq. 4-1 that we must focus on the quantity $n^3 r_{41} h$. The fractional change in this quantity with temperature is

$$\xi = \frac{1}{n^3 r_{41} h} \frac{d(n^3 r_{41} h)}{dT} = \frac{3}{n}\frac{dn}{dT} + \frac{1}{r_{41}}\frac{dr_{41}}{dT} + \frac{1}{h}\frac{dh}{dT}. \qquad (4\text{-}2)$$

Because it appears as the third power, the variation of refractive index with temperature is the first consideration. In most semiconductor materials the temperature derivative of the refractive index is of the order of 10^{-5}/°C. Accurate data are available for only a few of the cases of interest here. What data can be obtained are summarized in Table 4-1.

For the materials shown in Table 4-1 the quantity $3(dn/dT)/n$ is between 10^{-4}/°C and 10^{-5}/°C in each case.

The next parameter of concern is dh/dT. For cubic crystals, thermal expansion is isotropic. Representative values of $\alpha = (dh/dT)/h$ are given in Table 4-2.

The final parameter of concern in Eq. 4-2 is r_{41}. The temperature dependences of the electro-optic tensor elements of a few crystals have been measured but no data appear to be available on any of the 43m crystals listed above. (See reference (4-4) for one of the most extensive compilations of data on the electro-optic properties of materials.) We suspect that r_{41} will not be the major contributor to the temperature dependence of the electro-optic effect, but cannot at this point be sure.

While it does not appear explicitly in Eq. 4-1 or 4-2, another property of materials that can effect their thermal stability is the stress-optic effect. Stress applied to any material causes an anisotropic change in its refractive index which may yield a non-zero value of Δn in Eq. 3-2. In a sensor, stress could occur because of differential thermal expansion in a mounting structure. Materials with small stress-optic coefficients are therefore desirable. For those class 43m crystals in which the stress-optic effect has been studied, the coeffecients are similar (4-1).

During this study we have begun to focus on bismuth germanate, $Bi_4Ge_3O_{12}$, as perhaps one of the most attractive of the materials listed in Tables 4-1 and 4-2. It is widely used in nuclear scintillation and therefore readily available. And it has been suggested (4-5) that the temperature dependence of its electro-optic coefficient is smaller than that for other crystals. We have obtained samples of bismuth germanate for complete testing of its properties. These studies have thus far yielded the preliminary data presented in Tables 4-1 and 4-2; work on the complete electro-optic coefficient continues along with work on the stress-optic coefficients. Gallium phosphide is another attractive choice but high resistivity crystals are difficult to obtain.

Table 4-1

TEMPERATURE DERIVATIVE OF THE REFRACTIVE INDEX FOR SEVERAL CRYSTALS

Crystal	n	λ(nm)	(dn/dT)/n 10^{-5}/°C	Ref.
GaAs	3.3	5000	1.7	b
ZnSe	2.5	850	3.1	a
ZnS	2.3	850	2.1	a
GaP	3.2	850	1.3	b
$Bi_4Ge_3O_{12}$	2.1	633	2.	c

[a]A. Feldman, D. Horowitz, R. M. Waxler, M. J. Dodge, Optical Materials Characterization, Nat. Bur. Stand. (U.S.) Tech. Note 993 (1979).

[b]Y. Tsay, B. Bendow, S. S. Mitra, Theory of the temperature dependence of the refractive index in transparent crystals. Phys. Rev. B. 8, 2688-2696 (1973).

[c]G. W. Day, D. Conrad, K. S. Lee, P. D. Hale. "Optical electro-optical and stress-optical properties of bismuth germanate, $Bi_4Ge_3O_{12}$," unpublished.

Table 4-2

THERMAL EXPANSION COEFFICIENTS OF SEVERAL CRYSTALS OF CLASS 43m

Crystal	$\alpha(10^{-6}K^{-1})$	Ref.
GaAs	5.7	c
ZnSe	7.3	a
ZnS	6.8	a
GaP	5.3	c
$Bi_4Ge_3O_{12}$	10.	b

[a]A. Feldman, D. Horowitz, R. M. Waxler, M. J. Dodge, Optical Materials Characterization, Nat. Bur. Stand. (U.S.) Tech. Note 993 (1979).

[b]G. W. Day, D. Conrad, K. S. Lee, P. D. Hale. "Optical electro-optical and stress-optical properties of bismuth germanate, $Bi_4Ge_3O_{12}$," unpublished.

[c]William L. Wolfe. "Properties of optical materials," in Handbook of Optics. Optical Society of America/McGraw Hill, 1978.

Summaries of the properties of several of the more promising electro-optic materials for use in electro-optic voltage sensors can be found in an appendix.

There is one further concern with electro-optic materials. It is that all materials that possess a linear electro-optic effect are also piezoelectric (4-3). Direct piezoelectricity is the property that when stress is applied to a crystal, an electric polarization is developed. Converse piezoelectricity is the property that when an electric field is applied to a crystal, its dimensions change. The consequence, for the study of the electro-optic effect is that the electro-optic coefficients are dependent on the modulation frequency of the applied field and on the manner in which the crystal is mounted.

If a crystal is not physically constrained and if the applied field is electrostatic or varying slowly, the piezoelectric effect causes a small dimensional change that through the stress-optic effect causes a refractive index change in addition to that produced directly by the electric field. The symmetry characteristics of the two processes are identical so that the effects add algebraically. The resulting effective electro-optic tensor elements are often identified with the superscript T.

If the crystal is constrained so that its dimensions cannot change with the electric field, or if the electric field is changing fast enough so that the crystal cannot change dimensions fast enough to follow the field, the piezeoelectric contribution vanishes and the resulting electro-optic tensor elements are often identified with the superscript S. It should be noted clearly that while the symmetry of the piezoelectric and electro-optic contributions is the same, the magnitudes of the effects can be opposite so that S values may be smaller than T values or vice versa.

At certain frequencies, depending on the properties of a crystal and its dimensions, a crystal will exhibit piezoelectric resonances, that is frequencies at which the dimensional changes are enhanced. At these same frequencies, the electro-optic effect is also typically enhanced.

There is little that can be done about piezoelectric effects in electro-optic sensors other than to ensure that the signals to be measured are at frequencies significantly below any resonances. Generally, for most applications in the power industry, this can be achieved.

Further concern relates to the establishment of the electric field in the crystal. In all of the foregoing discussion it has been assumed that the electric field in the crystal is uniform in magnitude and direction. This is a good approximation if electrodes are applied to the crystal and the field established by applying a voltage to the crystal. It may not be a good approximation if a crystal without electrodes is simply placed in a field.

In the latter case the field in the crystal will depend on the dielectric constant of the crystal, the shape of the crystal, and the field distribution outside the crystal. Exact field distributions inside a dielectric material are very difficult to calculate except where simplifying geometries are chosen (4-6). This makes calibration of such a device difficult. Furthermore, the dielectric constant of a material is known to be a function of temperature, thereby introducing an additional source of imprecision.

Generally, therefore, it seems advisable to consider sensor geometries that involve electrodes on the crystal. In a power system application this may require the use of voltage dividers to reduce the voltage at the electro-optic crystal to an acceptable value.

One final concern related to materials is that all materials exhibit a Faraday effect, and if a magnetic field component in the direction of propagation exists, noise, or distortion in the transfer function could result. The problem is somewhat less severe when, as would typically be the case, light propagating through the crystal is circularly polarized, on which the magnetic field has no effect. Design of the sensor so that anticipated magnetic field components are perpendicular to the direction of propagation is also desirable and magnetic shielding could be used if necessary.

Properties of Waveplates

The second most important component in a voltage sensor is the waveplate. The function of the waveplate is to establish the desired value of Φ, as for example, $\Phi = \pi/2$ to achieve the transfer function described in Eq. 2-3, when $\Delta n = 0$ in Eq. 3-2. Three types of waveplates may be considered--birefringent waveplates, reflection waveplates (rhombs), and polymer waveplates. Reference (4-7) provides an extensive review of waveplate designs and properties. Recent work in our laboratory on the characterization of waveplates, in particular

the issue of their stability, is presented in an appendix to this document and in a forthcoming paper by the authors (4-8).

Birefringent Waveplates. Birefringent waveplates are perhaps the best known type of waveplates. They are usually made from uniaxial crystals, such as quartz or magnesium fluoride, cut so that the direction of propagation is normal to the optic axis. In this case, light polarized parallel to the optic axis experiences one refractive index, called n_e, and light polarized perpendicular to the optic axis experiences a different refractive index, called n_o. Either n_e or n_o may be larger. A phase shift between these two polarizations of magnitude

$$\delta = \frac{2\pi}{\lambda} (n_e - n_o)h \equiv \frac{2\pi}{\lambda} Bh \qquad (4\text{-}3)$$

occurs as light propagates through the crystal.

Generally one is interested in a waveplate for which $\delta = \pi/2$ (i.e., a quarter-wave plate), though in double pass sensor configurations, a value of $\pi/4$ (i.e., an eighth-wave plate) may be desired. With $n_e - n_o$ determined by the material, one may construct a waveplate with the desired retardance at a given wavelength by choosing the thickness correctly.

A waveplate with a retardance of δ is, in some respects, indistinguishable from a waveplate that differs in retardance by $2n\pi$. Waveplates with $\delta < 2\pi$ are called zero order waveplates; those with $n > 0$ are called multiple order waveplates of order n. If n is large, a multiple order plate is much less stable than a zero order plate.

For many materials, a true zero order plate would be very thin and thus difficult to fabricate. As a result, the components usually sold as "zero order waveplates" are actually compound waveplates, composed of two multiple order waveplates differing in retardance by the desired value. In most respects such a plate behaves almost exactly the same as a true zero order plate.

The fractional stability of a birefringent waveplate is seen from Eq. 4-3 to be given by

$$\gamma = \frac{1}{\delta}\frac{d\delta}{dT} = \frac{1}{B}\frac{dB}{dT} + \frac{1}{h}\frac{dh}{dT}. \qquad (4\text{-}4)$$

Table 4-3

PROPERTIES OF MATERIALS COMMONLY USED IN BIREFRINGENT WAVEPLATES

Material	γ	Ref.
Quartz	-1.4×10^{-4}	a
MgF	-3.9×10^{-5}	b
Mica	-2.3×10^{-4}	c

[a]T. Toyoda and M. Yabe. "The temperature dependence of the refractive indices of fused silica and crystal quartz." J. Phys. D., 1983, vol. 16, p. 97-100.

[b]A. Feldman, D. Horowitz, R. M. Waxler, M. J. Dodge. "Optical Materials Characterization." Nat. Bur. Stand. (U.S.) Tech. Note 993, 1979.

[c]P. D. Hale and G. W. Day. "The selection of linear retarders (waveplates) for use in high precision electro-optic sensors and other polarimetric appliations," to be published.

The quantity γ is tabulated in Table 4-3 for quartz and magnesium fluoride.

It was suggested in Section 2 that the quantity Φ should be maintained stable to about 1 mrad, at least for a sensor designed to measure dc quantities. From Eq. 4-4 and the data in Table 4-3 we discover that, given a perfectly stable source wavelength, a zero order quarter wave plate made from quartz will change over 100°C by approximately 22 mrad, one made from magnesium fluoride by approximately 6 mrad, and one made from mica by 36 mrad. The temperature stability of a multiple order plate will be worse than that of a zero order plate, in proportion to ratio of retardances. The temperature dependence of a compound plate will be the same as that of an equivalent zero order plate.

Orientation is another problem with birefringent waveplates. If a waveplate is rotated away from normal incidence, the optical path length increases, but in uniaxial crystals n_e also changes with angle. The net result for a zero order plate is that when the rotation occurs about the optic axis the retardance increases by the factor $1/\cos\theta$ where θ is the angle of incidence with respect to

the normal, but rotation about an axis normal to the optic axis causes a decrease in retardance by the factor cos θ (4-9). The change of retardance of a multiple order plate with angle is larger than that of a zero order plate in proportion to the ratio of the total retardances. The change in retardance of a compound waveplate with angle is more complex to describe but is also large compared to a true zero-order plate (4-8). Careful alignment procedures and mechanical design are thus essential parts of sensor design.

The apparent retardance of a waveplate is also dependent on the coherence of the source with which it is used. If the coherence length of the source is long with respect to the thickness of the wave plate, multiple reflections within the wave plate can cause a significant change in its effective retardance (4-10). Furthermore this effective retardance has a strong temperature dependence as shown in Figure 4-1. One obvious solution is to coat the waveplate with an antireflection coating. This substantially reduces the sensitivity to changes in temperature but an extremely low reflection coating is required to completely eliminate the problem. A better solution is to use a low coherence source.

Reflection Waveplates. Reflection waveplates rely on the fact that in reflection from a dielectric surface, the components of the incident light parallel to and perpendicular to the plane of incidence undergo different phase shifts. The best known reflection waveplate is the Fresnel rhomb quarter wave plate, shown schematically in Figure 4-2. It is designed so that incident light is totally internally reflected, twice, yielding a total retardance of $\pi/2$.

From the expression for the retardance, Δ, that occurs in total internal reflection,

$$\tan\left[\frac{\Delta}{2}\right] = \frac{\cos\theta\,(n^2 \sin\theta - 1)^{1/2}}{n \sin^2\theta} \qquad (4\text{-}5)$$

where n is the refractive index of the material and θ is the angle of incidence relative to the normal (4-11) and using data for the temperature coefficient of the refractive index, it is possible to determine the change in retardance with temperature. For a Fresnel rhomb made of BK-7 glass the normalized temperature coefficient is found to be 3×10^{-6}.

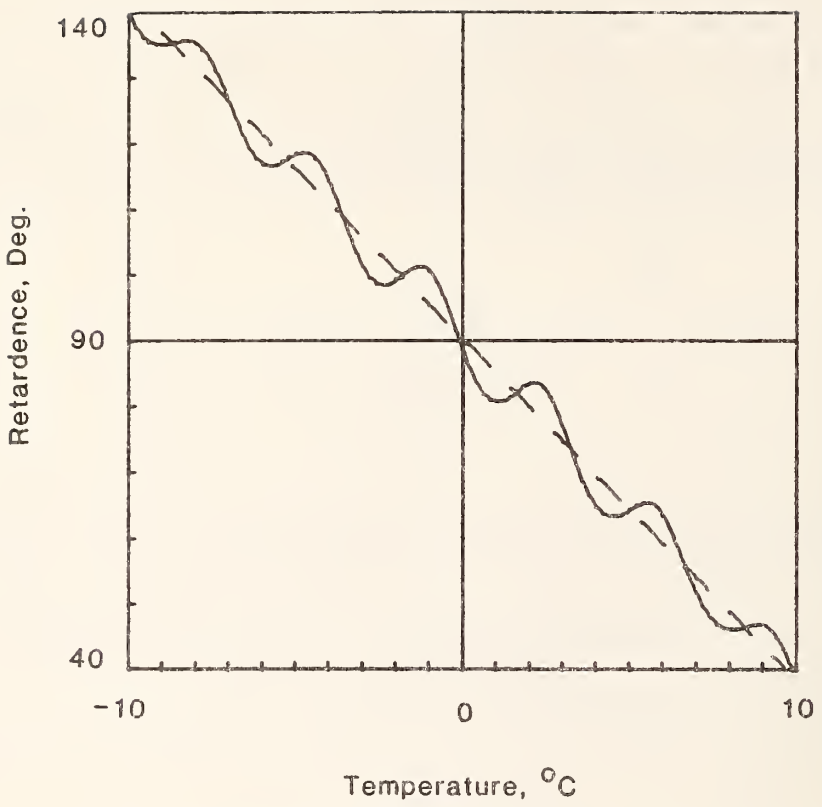

4-1. Retardance of a 100-order quartz quarterwave plate (approximately 1 mm thick) versus temperature for a coherent source (solid) and an incoherent source (dashed).

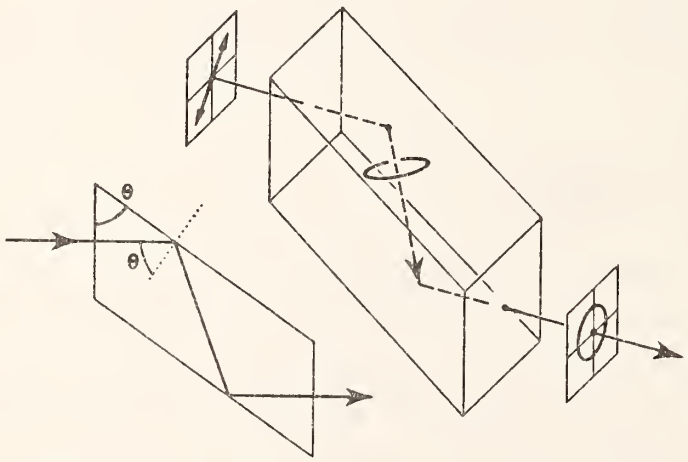

4-2. Representation of a Fresnel romb quarter-wave plate(after (4-11)). Light undergoes two total internal reflections, each time incurring a 45 deg phase shift between components parallel and perpendicular to the plane of incidence. For commonly used BK-7 glass the angle θ is 54.6 deg.

Also using Eq. 4-5, it is possible to determine the sensitivity of the Fresnel rhomb to misalignment. The result is $d\delta/d\theta = 0.01$ rad/deg.

From these results we see that the stability characteristics of a Fresnel rhomb are significantly better than those of a birefringent wave plate. The obvious disadvantages of the rhomb are that it is comparatively large and the input and output beams are not collinear. These are significant considerations, particularly in the design of small sensors.

Polymer Waveplates. The retardance of polymer waveplates derives from the fact that thin polymer films are significantly anisotropic. They have long been known to provide a retardance that is insensitive to wavelength (4-12), and are also attractive because they can be made very thin, even with necessary supporting substrates. Recent commercial literature suggests that they may be relatively insensitive to temperature. Testing in our laboratory confirms these characteristics to some degree, but also indicates that the maximum operating temperature of a polymer waveplate must be kept below about 40°C. They are therefore probably unsuitable for use in power systems applications. Some data on polymer waveplates are presented in an appendix.

Summary of Waveplate Properties. Table 4-4 presents a summary of waveplate properties useful in the design of voltage sensors. From this compilation, it appears that the best choice for high precision sensors may be the Fresnel romb, at least for those cases where its size and configuration can be tolerated. Another possibility is discussed below in the section on temperature compensation techniques.

Properties of Polarizers

A linear polarizer is a device that, when placed in a beam of light, produces a beam in which the electric vector is vibrating almost entirely in one direction. If such a device is placed in a perfectly plane polarized light and rotated about an axis parallel to the direction of propagation the transmittance is given by

$$T = (T_1 - T_2) \cos^2 \theta + T_2 \qquad (4\text{-}6)$$

Table 4-4

TEMPERATURE AND ANGULAR DEPENDENCE OF VARIOUS RETARDERS AT THREE WAVELENGTHS

Device, material, wavelength, nm	$d\delta/dT$, $°C^{-1}$	γ, $°C^{-1}$	$d\delta/d\theta$, rad/deg
Fresnel rhomb BK-7			
1300	4.1×10^{-6}	2.6×10^{-6}	9.3×10^{-3}
850	4.6×10^{-6}	2.9×10^{-6}	1.2×10^{-2}
633	4.7×10^{-6}	3.0×10^{-6}	1.4×10^{-2}
Birefringent retarder MgF_2†			
1300	-6.2×10^{-5}	-3.9×10^{-5}	$\sim 0.09\theta$*
850	-6.2×10^{-5}	-3.9×10^{-5}	$\sim 0.13\theta$*
633	-6.2×10^{-5}	-3.9×10^{-5}	$\sim 0.18\theta$*
Birefringent retarder quartz†			
1300	-2.7×10^{-4}	-1.7×10^{-4}	$\sim 0.08\theta$*
850	-2.3×10^{-4}	-1.4×10^{-4}	$\sim 0.12\theta$*
633	-2.1×10^{-4}	-1.3×10^{-4}	$\sim 0.16\theta$*

†Uncertainty in γ and $d\delta/dT$ for MgF_2 is 5×10^{-6} and 8×10^{-6}, and for quartz 3×10^{-5} and 4×10^{-5}, respectively.[2]

*In a Taylor series expansion the first angle dependent term is quadratic in θ. These values assume a total thickness of 6 mm. θ is measured in degrees.

where T_1 and T_2 are called the principal transmittances (usually $T_1 >> T_2$) and Φ is the angle between the principal transmittance T_1 and the plane of polarization of the incident beam.

A few examples explain the performance and specification further. When a polarizer is placed in an unpolarized beam, the transmittance is

$$T = 0.5\ (T_1 + T_2). \qquad (4\text{-}7)$$

When two identical polarizers with their directions of transmittance oriented at the angle θ to each other are placed in an unpolarized beam the resulting transmittance is given by

$$T(\theta) = 0.5(T_1^2 + T_2^2)\cos^2\theta + T_1T_2\sin^2\theta \qquad (4\text{-}8)$$

from which one obtains

$$T(0) = 0.5(T_1^2 + T_2^2) \qquad (4\text{-}9)$$

when the polarizers are aligned and

$$T(90) = T_1T_2 \qquad (4\text{-}10)$$

when the polarizers are crossed. The ratio T_2/T_1 is usually called the extinction ratio E_x and can be obtained by taking the ratio of T(90) to T(0),

$$T(90)/T(0) \approx 2T_2/T_1 = 2E_x. \qquad (4\text{-}11)$$

Prism Polarizers. Most prism polarizers are made from the crystal calcite, a uniaxial crystal with an extremely large birefringence. Innumerable prism configurations have been used (4-4), to separate orthogonally polarized components of the beam.

The most popular designs, known as Glan-type prisms (also, Glan-Thompson, Glan-Taylor, Glan-Foucault), function through the fact that when light is propagating normal to the optic axis in a uniaxial crystal, the difference in refractive index experienced by components parallel and perpendicular to the optic axis makes it possible for one but not the other to undergo total internal reflection (Figure 4-3).

Except when intended for high power laser applications, the reflected beam is generally absorbed in the prism mounting. In those cases where the reflected beam is available, one may find a significant component of the transmitted polarization in the reflected beam, depending on how close the angle of incidence is to the Brewster's angle. Glan-type prisms are generally superior to an older type known as the Nicol prism, which also relied on total internal reflection but in which

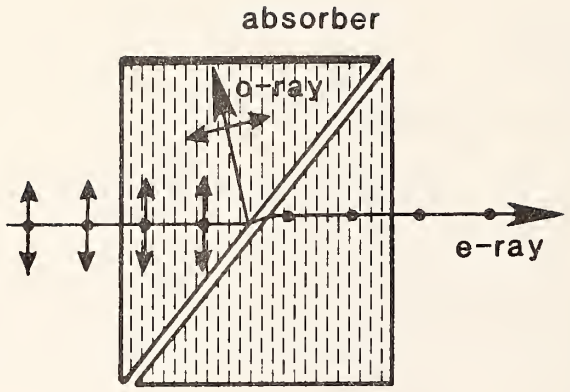

4-3. Representation of a Glan prism polarizer. For the component parallel to the plane of incidence, total internal reflection occurs at the internal surface. The optic axes of the two pieces are parallel to each other and to the entrance and exit surfaces.

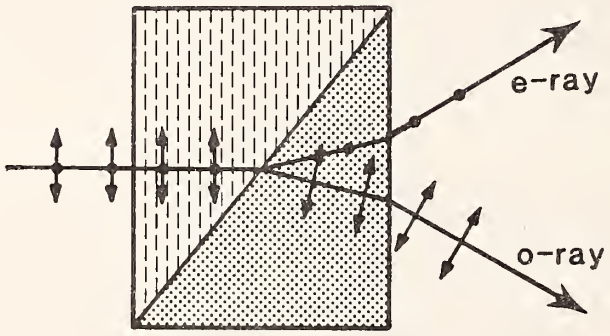

4-4. Representation of a Wollaston prism polarizer. The optic axes of the two pieces are orthogonal. Orthogonal components are refracted by different amounts when passing from the first segment to the second. Output beams are nearly symmetric but the angle of deviation is wavelength dependent.

the entrance and exit faces were not perpendicular to the direction of propagation. Properly used, Glan prisms offer the best extinction ratios available in polarizers--values of 10^5 to 10^6 are generally expected for well collimated light and a well aligned prism.

Common imperfections in Glan prisms include a deviation of the output beam with respect to the input beam and ellipticity of the output beam. Beam deviation can be a very significant when the prisms are used with optical fibers, particularly when the prism is rotated in a beam before the beam is focused into a single mode fiber. Angular deviation of the output beam is translated into a transverse offset at the focal point of the launch lens. The launch efficiency thus depends on the orientation of the polarizer. For such applications it is useful to use polarizers with the smallest beam deviation available, about one arc minute. Ellipticity of the output beam generally occurs because of strain in the output half of the prism and is dependent on mounting. Ellipticity may not normally be specified but should not be a problem with most high quality prisms.

Other specified parameters include the field angle and the length to aperture ratio. The field angle in a Glan prism is determined by the minimum angle at which the unwanted polarization undergoes total internal reflection and the maximum angle at which the wanted polarization is transmitted. It is strongly wavelength dependent, being larger at shorter wavelengths and having typical values of a few degrees. This small angular aperture is in almost all cases smaller than the exit radiation angle of a fiber making it essential to insert a lens between the fiber and polarizer as shown in Figure 3-1. In some cases, the length to aperture ratio can similarly limit the location of a prism polarizer in a sensor configuration.

A second class of prism polarizers relies on a difference in refraction of two orthogonal components to separate them spatially. These include the Rochon, Senarmont, and Wollaston types. Of these, the Wollaston, is the best known and most popular because the two beams emerge at symmetric angles, typically about 1 deg, to the axis of the input beam (Figure 4-4). Because of this geometrical characteristic, it is often useful in sensor designs. There is, however, a potential problem with the Wollaston prism in that the deviation angles are wavelength dependent making it important to insure, for example, that unexpected aperturing does not occur. In principle, we should expect the deviation angle to also be temperature dependent, though we have been unable to observe any significant effect.

A potential problem with all prism polarizers is that the cements used to hold the prisms together and which significantly affect their performance may not withstand the full range of operating temperatures necessary in power system applications. In some cases cements can be avoided. In others it may be necessary to choose nonstandard cements.

Dichroic Polarizers. Dichroic polarizers are those that rely on a difference in attenuation of orthogonally polarized components. Among the best known and widely used types are the H and K sheet polarizers which consist of polyvinyl alcohol, stretched and stained with iodine (4-4,4-13). Sheet polarizers are thin and can be readily incorporated into sensor configurations without deviating the beam and in the visible portion of the spectrum can have extinction ratios of 10^4 or greater, more than sufficient for most sensing application.

There are three problems with the use of sheet polarizers in sensors. One is that they are inherently lossy, with T_1 often being only about 0.6 to 0.7, thus limiting the transmitted power and often ultimately the signal to noise ratio. Second, most types do not perform well in the near infrared, where most sensors are likely to operate. Some sheet polarizer types are designed to function in the 800 to 900 nm region, but their extinction ratios and transmittances do not approach that which can be achieved with prisms at that wavelength. Third, there is concern about the performance of polymer films over the full temperature range required for sensors in the power industry, particularly when the exposure to high temperatures is prolonged.

Dielectric Film Polarizers. Another technique for constructing a polarizer is to take advantage of the difference in reflectivity of a dielectric surface for polarization components parallel and perpendicular to the plane of incidence. Near the Brewster's angle, this effect is strong and is enhanced by using a multilayer coating. However, polarizing beam splitters that use this technique generally have a specified extinction ratio of only about 100; they are therefore probably not the best choice for high precision sensors.

Source Properties

In designing a high precision voltage sensor there are basically three considerations related to the source--amplitude stability, wavelength, and coherence (spectral width).

Various sources may be used for the development and testing of electro-optic sensors, but it is assumed here that practical devices that can be used in the field will utilize semiconductor sources, either lasers, light emitting diodes (LEDs), or perhaps superluminescent LEDs. The latter are devices, intermediate between lasers and LEDs, in which stimulated emission and some line narrowing occur, but in which the optical feedback is weak, so that oscillation does not build up to the same degree as in lasers and modes do not appear. They are therefore relatively efficient, low coherence devices.

As pointed out in Section 2, amplitude stability is related directly to sensor precision, so that, for example, to achieve a sensor that is stable to 0.1 percent, one must stabilize the output power to 0.1 percent. This generally requires temperature control and feedback control, but is well within present capability.

One is likely to choose a wavelength of operation in the range from 0.8 to 0.9 μm where GaAlAs lasers are readily available and where high quality silicon detectors are also available. There is little reason for choosing a specific wavelength within this range, though it might be pointed out that the electro-optic coefficient is inversely proportional to wavelength and the sensor will be more sensitive at shorter wavelengths. That functional dependence leads to greater concern about source stability. A change in wavelength results in an inversely proportionate change in the parameter x_0 in Eq. 2-3, so it seems necessary to achieve a source wavelength stability of the order of 0.1 percent. This is achievable with the same level of temperature control necessary for amplitude stability.

In addition to concerns with amplitude and spectral stability, there is, assuming that the fiber used to convey light to and from the sensing element is multimode fiber, additional concern with the coherence properties of the source. This is related to a phenomenon known in the field of optical communications as "modal noise."

A multimode fiber of the sort commonly used in communications supports 10 or 20 mode groups each comprising many discrete modes having, in principle, the same phase velocity. If the coherence length of the source is long compared to the product of the differences in phase velocity and the propagation time through the fiber, the modes can interfere at the output of the fiber yielding a complex intensity pattern. The details of that pattern are highly dependent on the details of the differences in phase velocity. Because these differences change

with temperature and mechanical disturbances to the fiber, the details of the output near- and far-field patterns generally vary continuously.

If any mode-dependent loss mechanisms are present (coupling from a fiber through various bulk components and back into another fiber is a prime example) the variations in the output patterns will yield noise in the output signals, i.e., modal noise. Modal noise is avoided by using a source with a broad spectral characteristic (a low coherence source) and minimizing mode dependent losses. As a practical matter for high precision sensors it is likely that such systems must be limited to the use of light emitting diodes.

Detector Characteristics

Properly used silicon PIN photodiode detectors are among the easiest and most stable optical detectors available. Prime consideration in their use is with the electronics used to control the operating point and load line on their current-voltage characteristic. For measurement devices, where stability and linearity are principal considerations, the proper operating point is the origin, with a vertical load line (zero resistance load). Under these circumstances the detector can be considered to be a current source, directly proportional to the incident optical power.

The desired conditions are most easily met using an operational amplifier in transimpedance mode (Figure 4-5). The output voltage of this amplifier is related to the input current by the expression

$$V_{out} = I_{in} R_f \qquad (4\text{-}12)$$

where R_f is the feedback resistor. In this case there are three factors related to stability--the responsivity of the detector, the feedback resistor, and the input offset characteristics of the amplifier. All three of these can be adequately addressed by temperature control, and in the case of the last two, suitable choice of components.

Fiber Characteristics

One aspect of fiber selection has already been addressed above in the discussion of modal noise. Others include design for efficient transmission of light through the bulk components and the polarization properties of fiber.

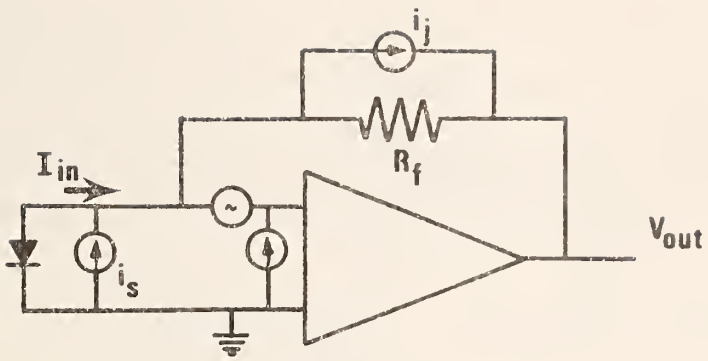

4-5. Current mode (or transimpedance) operational amplifier following a photodiode detector. Principal noise sources, shot noise associated with the average detector current, Johnson noise associated with the feedback resistor, and amplifier input voltage and current noise, are shown. Signal input and output are related by Eq. 4-12.

Coupling of light from a fiber, through bulk components that are long compared to their aperture, and into another fiber is the subject of an appendix. Basically, the design is easier if the input fiber has as small a core as possible and the output fiber as large a core as possible. Purely from the standpoint of transmitted light, using a single mode fiber for the input and a relatively large multimode fiber for the output would thus be appropriate. Depending on the source, however, other considerations, for example, the efficiency with which light can be coupled into a single mode fiber from an LED may dominate.

Polarization properties of the fiber generally become important only when a polarized source is used, but this includes many laser diodes. Multimode fiber largely depolarizes light, but not completely, so that when polarized light is passed through a multimode fiber and then through a polarizer, significant amplitude noise occurs. If a polarized source must be used, another choice is to use polarization maintaining single mode fiber between the source and the sensor and avoid an input polarizer at the electro-optic crystal.

FACTORS LIMITING THE PRECISION OF PLANAR WAVEGUIDE SENSORS

In the long term, planar waveguide sensors, such as those described in Section 3, are likely to provide very attractive sensor characteristics. At the present time, however, almost all devices of the sort shown in Figure 3-5 are being produced in $LiNbO_3$. As pointed out above, $LiNbO_3$ is a very unattractive material for stable devices, because of its high birefringence, and strong temperature dependence, and because it is pyroelectric.

High precision planar interferometric sensors will require the exploitation of other materials, the most likely being the same group suggested here for bulk sensors. Of these, GaAs and related compounds are already the subject of substantial research. If and when devices in these materials are developed, the fundamental limits to performance should be the same as those described for bulk sensors of the same materials. The advantage in the avoidance of bulk components is significant; sensitivity and speed should be enhanced.

TEMPERATURE COMPENSATION TECHNIQUES

Waveplates

A 1970 patent (4-14) suggested that it should be possible to produce a temperature compensated waveplate by using two different birefringent materials having different temperature coefficients of their retardance. If the two materials have temperature dependences of the opposite sign they may oriented with their respective fast and slow axes aligned. However, since waveplates made from most common materials exhibit a decreasing retardance with increasing temperature, it is necessary to align the fast axis of one with the slow axis of the other.

The proposal of reference (4-14) was incomplete in that it did not take into account the thermal expansion of the material, a significant contribution to the change in retardance with temperature, and apparently never resulted in an actual device. We have recently revised the analysis and produced a specific design using two readily available materials, quartz and magnesium fluoride.

The design is achieved by setting the difference in retardance of the two plates equal to the desired value and the temperature dependence of the composite plate to zero. Thus for a quarter-wave plate

$$\delta_1 - \delta_2 = \pi/2 \tag{4-13}$$

and

$$\gamma_1\delta_1 - \gamma_1\delta_2 = 0 \tag{4-14}$$

where δ_1 and δ_2 are the retardances of the two elements and

$$\gamma_1 = \frac{1}{\delta_1}\frac{d\delta_1}{dT} = \frac{1}{B_1}\frac{dB_1}{dT} + \frac{1}{h_1}\frac{dh_1}{dT} \tag{4-15}$$

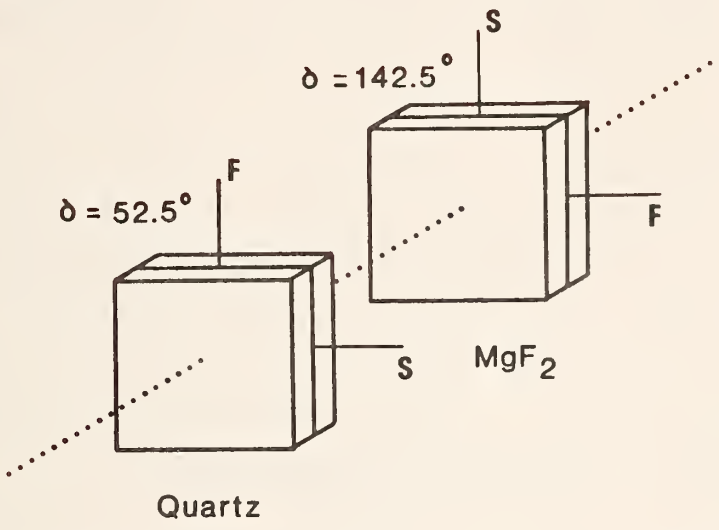

4-6. Design for a temperature-compensated quarterwave plate using quartz and magnesium fluoride. Each segment is assumed to be a compound zero-order waveplate.

$$\gamma_2 = \frac{1}{\delta_2}\frac{d\delta_2}{dT} = \frac{1}{\Delta n_2}\frac{d\Delta n_2}{dT} + \frac{1}{h_2}\frac{dh_2}{dT}. \qquad (4\text{-}16)$$

The desired results are

$$\delta_1 = \frac{\pi}{2}\frac{\gamma_2}{\gamma_2 - \gamma_1} \qquad (4\text{-}17)$$

and

$$\delta_2 = \frac{\pi}{2}\frac{\gamma_1}{\gamma_2 - \gamma_1}. \qquad (4\text{-}18)$$

For the two materials quartz and MgF the results are shown in Figure 4-6.

The production of such a device is made more difficult than might be expected by a greater than desired uncertainty in the numerical value of γ for quartz and because the retardance of a compound plate is significantly dependent on the angle of incidence.

Electro-optic Crystals

A temperature compensation scheme for electro-optic crystals that is similar to that used for waveplates can also be contemplated. Recall from above that the induced retardance of an electro-optic of class $\bar{4}3m$ is given by

$$\Gamma = \frac{2\pi}{\lambda} n^3 r_{41} h E = C_{eo} E. \tag{4-19}$$

If we consider two different crystals in series but rotated about the direction of propagation by 90 deg to each other, the net induced retardance is

$$\Gamma_n = \Gamma_1 - \Gamma_2 \tag{4-20}$$

which must be non-zero. At the same time we would like

$$\frac{d\Gamma_1}{dT} - \frac{d\Gamma_2}{dT} = 0 \tag{4-21}$$

where for each component

$$\frac{1}{\Gamma}\frac{d\Gamma}{dT} = \frac{3}{n}\frac{dn}{dT} + \frac{1}{r_{41}}\frac{dr_{41}}{dT} + \frac{1}{h}\frac{dh}{dT} \equiv \xi. \tag{4-22}$$

This leads to the requirement that

$$\frac{h_1^2}{h_2^2} = \frac{\xi_2}{\xi_1}\frac{C_{eo^2}}{C_{eo^1}} \tag{4-23}$$

and the result that

$$\Gamma_n = C_{eo^2}\left[\frac{\xi_2}{\xi_1} - 1\right] \tag{4-24}$$

which is the effective electro-optic coefficient of the combined crystals.

This technique has not been attempted experimentally, yet, because more data are needed on possible crystals, but the concept seems promising.

PROGNOSIS FOR HIGH PRECISION VOLTAGE SENSORS

The two most critical elements in determining the precision of an electro-optic sensor are the electro-optic crystal, itself, and the waveplate.

We have been able to show that for most purposes, the stability of a Fresnel-romb quarterwave plate will be adequate and that when the use of that device is not possible or adequate, temperature compensated birefringent waveplates should, in principle, be still better.

Obtaining data on the properties of electro-optic materials has proven more difficult than expected at the beginning of this study. Nonetheless, we have been able to show that, because of the temperature dependence of the refractive index and of the dimensions of various promising crystals, the precision of a sensor of the sort shown in Figure 3-1 can not be appreciably better that 1 percent over a 100°C temperature range. On the other hand, informal reports of experimental work elsewhere suggest that a precision not much worse than that may be achieved.

To reach a precision of 0.1 percent over 100°C will clearly require some sort of temperature compensation. The principles of a temperature compensated device have been described above. The practicality of such a device will depend on further understanding of the properties of promising materials.

Some work in this area has already occured [4-15]. In the crystal $Bi_{12}GeO_{20}$ it has been shown that an internal temperature compensation can occur by balancing the temperature dependence of the electro-optic effect with the temperature dependence of the optical activity present in this class 23 crystal.

REFERENCES

4-1. Amnon Yariv and Pochi Yeh. Optical waves in crystals. John Wiley, 1984.

4-2. Ivan P. Kaminow. An introduction to electrooptic devices. Academic Press, 1974.

4-3. J. F. Nye. Physical properties of crystals. Oxford, 1960.

4-4. "Landolt-Bornstein, Aahlenwerte und Funktionen aus Naturwissenschaften und Technik." Neue Serie, K.-H. Hellwege, Ed., Gruppe III:Band11, Elastische, piezoelektrische, pyroelektrische, piezooptische, elektrooptische Konstanten un nichtlineare dielektrische Suszeptibilitaten von Kristallen. Springer Verlag, 1979.

4-5. M. Kanoi, et al. "Optical voltage and current measuring system for electric power systems." IEEE Power Engineering Society Summer Meeting, Vancouver, BC Canada, 1985.

4-6. G. A. Massey, D. C. Erickson, and R. A. Kadlec. "Electromagnetic field components: Their measurement using linear electrooptic and magnetooptic effects." Appl. Opt., 1975, vol. 14, p. 2712.

4-7. Handbook of optics, Optical Society of America/McGraw Hill, 1978.

4-8. P. D. Hale and G. W. Day. "The selection of linear retarders (waveplates) for use in high precision electro-optic sensors and other polarimetric systems," to be published.

4-9. M. Born and E. Wolf. Principles of optics. Pergamon Press.

4-10. D. A. Holmes. "Exact theory of retardation plates." J. Opt. Soc. Amer., 1964, vol. 5, p. 1115-1120.

4-11. See for example, E. Hecht and A. Zajac. Optics. Addison Wesley, 1980.

4-12. Product literature. Meadowlark Optics, 7460 East County Road, Longmont, Colorado 80501.

4-13. The Polaroid Corp. Polarizing filters. Spectral photometric data.

4-14. U.S Patent No. 3529885.

4-15. T. Mitsui, K. Hosoe, H. Usami, and S. Miyamoto. "Development of fiber-optic voltage sensors and magnetic-field sensors." IEEE Power Engineering Society Summer Meeting, Mexico City, Mexico, 1986.

Section 5

CRITICAL EVALUATION OF MAGNETO-OPTIC SENSOR TECHNOLOGY

FACTORS LIMITING THE PRECISION OF BULK MAGNETO-OPTIC SENSORS

The Verdet Constant of Bulk Materials and its Temperature Dependence

The magneto-optic properties of materials have not been studied or tabulated to the same degree as have the electro-optic properties. One of the best compilations is in an unpublished report prepared by M. J. Weber of Lawrence Livermore Laboratory and issued in 1981 (5-1). In it, data on 34 glass and crystalline materials are reviewed. Of particular interest is rarely available data on the spectral dependence of the Verdet constants of these materials. Other useful compilations can be obtained from the Schott Glass Company (5-2,5-3).

Of primary interest in this study is the variation of Verdet constant with temperature. Temperature coefficients in paramagnetic materials have been widely studied and it is generally accepted (5-1) that the Verdet constant of these materials can be expressed as a function of temperature (for temperatures well above absolute zero) as follows:

$$V(T) = V_{dia}(T) + V_{par}/T, \tag{5-1}$$

where V_{dia} is attributable to diamagnetic effects present in all materials, V_{par} is attributable to the presence of a paramagnetic ion, and T is absolute temperature. By convention in the definition of the Faraday effect V_{dia} is positive and V_{par} is normally negative. When fairly large densities of paramagnetic ions are present V_{par} becomes the dominate parameter yielding a negative Verdet constant that varies inversely with absolute temperature, i.e., of the order of 0.3 percent/°C near room temperature. This large coefficient is unacceptable for high precision sensors and leads generally to the use of materials that show only a diamagnetic effect. Unfortunately, the temperature dependence of V_{dia} for most materials is unknown, beyond the fact that it is small compared to that of paramagnetic processes and can often be ignored (5-4).

Very recently, some reports of the variation with temperature of the Verdet constant of a few diamagnetic materials have appeared in the literature. These are listed in Table 5-1.

Table 5-1

TEMPERATURE DEPENDENCE OF THE VERDET CONSTANT FOR SEVERAL MATERIALS

Material	$\left\lvert\frac{1}{V}\frac{dV}{dT}\right\rvert$	$\lambda(\mu m)$	Ref.
ZnSe	2.5×10^{-4}	0.87	a
ZnSe	$<1.4 \times 10^{-4}$	0.82	b
$Bi_{12}SiO_{20}$	1.5×10^{-4}	0.87	a
$Bi_{12}GeO_{20}$	$<2.8 \times 10^{-4}$	0.85	b
SF6 glass	$<0.9 \times 10^{-4}$	0.87	b

[a]T. Mitsui, K. Hosoe, H. Usami, S. Miyamoto. Development of Fiber-optic Voltage Sensors and Magnetic Field Sensors. IEEE Power Engineering Society Summer Meeting, Mexico City, Mexico (1986).

[b]O. Kamada, et al. Matsushita Electric, Moriguchi, Osaka 570, Japan, private communication.

To supplement these data, we have, during this study, constructed a measurement system to measure the Verdet constant of various bulk materials versus temperature. A diagram of that system is shown in Figure 5-1. The system is based on a large electro-magnet with a field region of about 15 cm long by 10 cm diameter, capable of producing a magnetic flux density of about 0.5 T. A small nonmagnetic oven, capable of heating a sample as long as 10 cm is located in the field region. Light from a laser makes two passes through holes in the pole pieces of the magnet. Its rotation as a function of magnetic field is determined for about 10 field values and 5 to 10 temperatures between room temperature and 120°C. Figure 5-2 shows an example of rotation versus field data for a particular material and temperature. Figure 5-3 shows an example of Verdet constant versus temperature data for a particular glass.

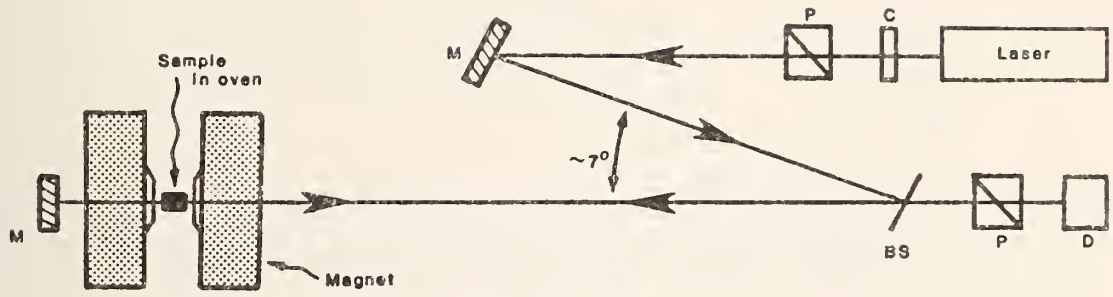

5-1 Measurement system for determining dV/dT. C--Chopper, P--Polarizer, M--Mirror, BS--Beam Splitter, D--Detector. Light makes two passes through the sample, doubling the rotation.

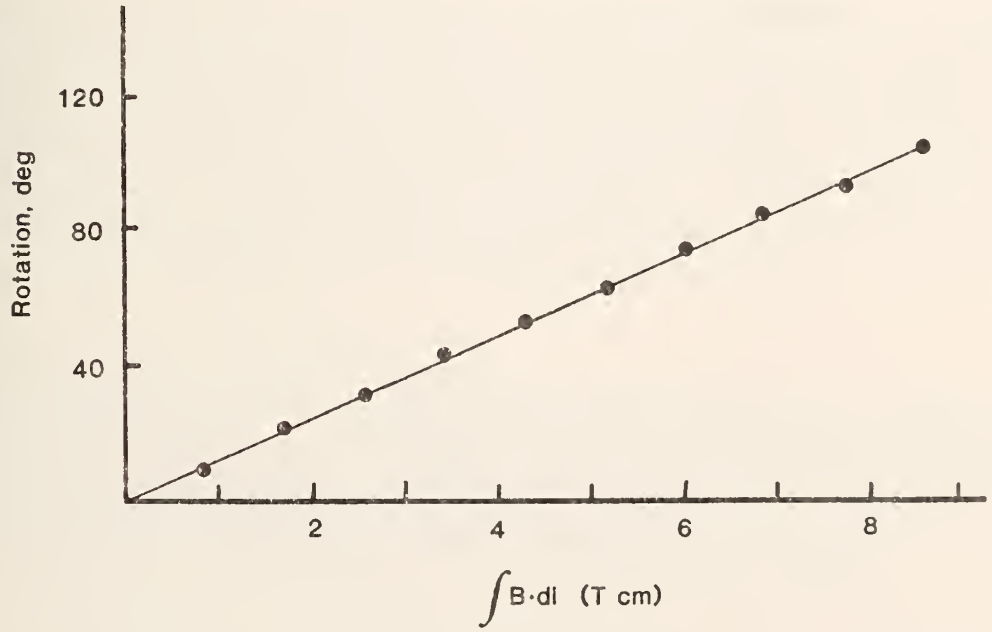

5-2 Rotation versus magnetic field for a sample of SF-57 glass at 25°C. Sample was approximately 10 cm long.

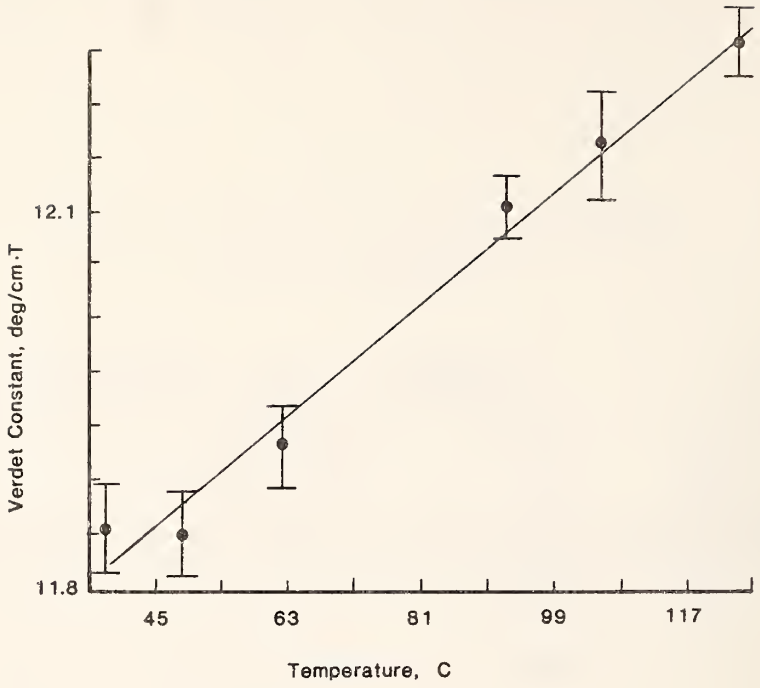

5-3 Verdet constant versus temperature for a sample of SF-57 glass. Error bars represent a one standard deviation uncertainty in the slope of curves of the form shown in Figure 5-2.

To date, we have focused on two glasses, a lead silicate (flint) glass known commercially as SF-57 and fused silica in a grade known commercially as Suprasil. Our best evaluation of the temperature coefficients of these materials to date are given in Table 5-2. These data suggest that, all other problems being solved, a precision no better than ±1 to 2 percent over a 100°C temperature range should be possible with a sensor design similar to those shown in Figures 3-11 and 3-13. Other materials are being studied to determine if smaller values of dV/dT can be found.

One may consider ways to predict the value of dV/dT for various diamagnetic materials from other, more readily available information. The Becquerel equation, derived in the early part of this century using classical physics (i.e., without quantum theory) is useful in predicting the Verdet constant of various materials (5-1,5-5). It is given in SI units by

$$V = \frac{e\lambda\mu}{2mc}\frac{dn}{d\lambda} \qquad (5\text{-}2)$$

Table 5-2

TEMPERATURE DEPENDENCE OF THE VERDET CONSTANT FOR TWO GLASSES

Material	$\left\lvert\frac{1}{V}\frac{dV}{dT}\right\rvert$ (10^{-4})	λ (μm)
SF57	2.8	0.633
SiO_2	2.2	0.633

where e is the electronic charge, λ is the wavelength, m the effective electron mass, c the speed of light, and $dn/d\lambda$ is the dispersion of the refractive index. Predictions based on the Becquerel equation are usually somewhat too large, but can be made to agree if the predicted value is multiplied by a factor, sometimes known as the magneto-optic anomaly, and which is nearly constant for a given class of materials. The magneto-optic anomaly typically takes values between 0.6 and 0.9 for glasses.

One might expect, from Eq. 5-1, that the temperature dependence of the dispersion of the refractive index would be a good predictor of the temperature dependence of the Verdet constant. The dispersion at different wavelengths and temperatures is often available in glass catalogs. We have used these to compute dV/dT for several materials. The predictions are found to be of the same order of magnitude as our measurements, but further work is required before final conclusions can be drawn.

Stress-Optic Effects in Bulk Materials

Because the presence of linear birefringence adversely affects the Faraday effect and because stress in a material, either residual stress arising during fabrication or externally applied, can cause linear birefringence, it is desirable to choose materials for sensors that have a small stress-optic effect.

In isotropic materials such as glass, the stress-optic effect is much more easily described than in crystals. The birefringence induced by applying a uniform pressure P transverse to the direction of propagation (Figure 5-4) is given by

$$\Delta n = CP \tag{5-3}$$

where Δn is the difference in refractive index between the components of transmitted light parallel to and perpendicular to the applied stress, C is the stress-optic coefficient, normally in units of TPa^{-1} (1 terapascal is equal to 10^{12} N/m^2 and is the same as the historical unit called a Brewster), and P is the applied pressure in Pa.

Table 5-3 gives representative values of the stress-optic coefficient for several common glasses. The values range over approximately two orders of magnitude with fused silica having one of the largest values and SF-57 one of the lowest. SF-57 is in fact a good approximation of the so-called Pockels glass (5-6) which resulted from the observation that within the lead silicate glass family it was possible to prepare glasses with either positive or negative stress-optic coefficients and that therefore it might be possible to prepare a glass with zero stress-optic coefficient. Because it also has a relatively high Verdet constant, it therefore becomes one of the leading candidates for bulk Faraday current sensors.

Source Properties: Spectral Stability

With regard to source requirements, magneto-optic devices differ from electro-optic devices only in the spectral dependence of the Verdet constant. The Verdet constant is dispersive, as suggested by the above stated Becquerel equation, and may be modeled with varying degrees of accuracy by any of the traditional material dispersion formulas. A relatively simple and often used formula is (5-1)

$$V(\lambda) = \frac{K}{\lambda_t^2 - \lambda^2} \tag{5-4}$$

where K is a constant and λ_t is a wavelength, typically in the ultra-violet portion of the spectrum. Experimental data fitted to this equation yield values for the two parameters. One may differentiate Eq. 5-1 with respect to wavelength, yielding

$$\frac{dV}{V} = \frac{2\lambda}{(\lambda_t^2 - \lambda^2)}\, d\lambda. \tag{5-5}$$

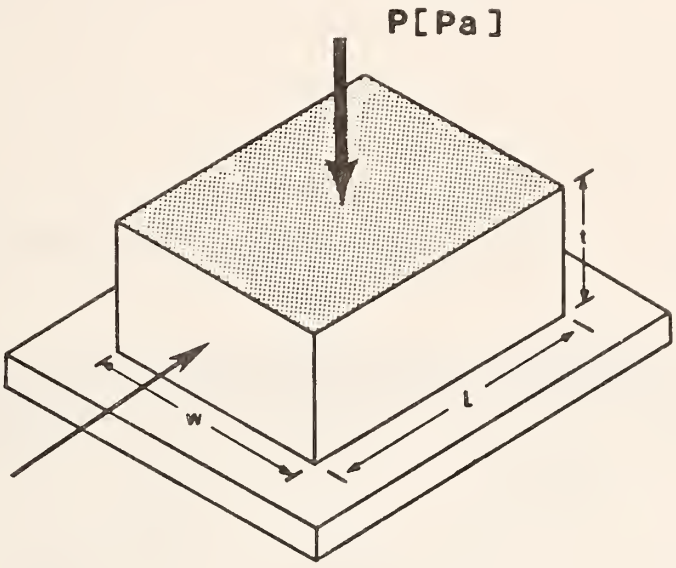

5-4 Configuration for studying the stress-optic effect in isotropic materials, such as glass. A uniform pressure is applied normal to the direction of propagation resulting in a change of refractive index both for light polarized parallel to the direction of the pressure and perpendicular to it. The difference in these refractive indices under applied stress is the induced birefringence.

Table 5-3

VALUES OF THE STRESS-OPTIC COEFFICIENT FOR SEVERAL COMMON GLASSES

Glass	$C(TPa^{-1})$	Ref.
BK-7	2.74	a
SF-6	0.63	a
SF-57	0.03	a
SF-59	-1.46	a
SiO_2	-3.36	b
7070	-4.6	b
8363	1.1	b

[a]Optical Glass, Schott Optical Glass, Inc., York Ave., Duryea, PA 18642.

[b]American Institute of Physics Handbook, McGraw Hill, 1972.

A reasonable first approximation for wavelengths substantially greater than λ_t is

$$V(\lambda) = \frac{K}{\lambda^2} \tag{5-6}$$

or

$$\frac{dV}{V} = \frac{-2d\lambda}{\lambda}. \tag{5-7}$$

The bandgap of a semiconductor material shifts with temperature by an amount that depends on the specific material but which is of the order of 10^{-4}/°C. This suggests that sources for high precision MO sensors must be temperature stabilized to about 0.1°C to achieve a precision of 10^{-3}, a not particularly difficult requirement. It has not been possible during this study to evaluate the possibility of long term shifts in the operating wavelength of semiconductor devices. To our knowledge no such effects have been reported.

Other Components

The other components found in magneto-optic sensors--polarizers, lenses, detectors, etc.--have basically the same performance requirements in a magneto-optic sensor as in an electro-optic sensor. The reader is therefore referred to Section 4 for information on those parameters.

FACTORS LIMITING THE PRECISION OF OPTICAL FIBER MAGNETO-OPTIC DEVICES

Relevant Properties of Optical Fiber

Essentially all efforts to produce a magneto-optic sensor in which the Faraday effect in an optical fiber is utilized have involved single mode fibers of the same basic type as those used for communications. These consist primarily of fused silica, with various dopants incorporated to achieve the required guidance and propagation characteristics. The only attempt that we are aware of to measure carefully the Verdet constant of various fibers were undertaken in our laboratory prior to the beginning of this study. A measurement system, shown schematically in Figure 5-5, was constructed and several different types of fiber were measured. Differences between the Verdet constants of the fibers and pure fused silica of several percent were found but as yet no correlation between the known compositions and guidance characrteristics of the fibers and the variations in Verdet constants have been found. Because silica and the other dopants commonly used in fiber are all diamagnetic we expect the temperature dependence of the Verdet

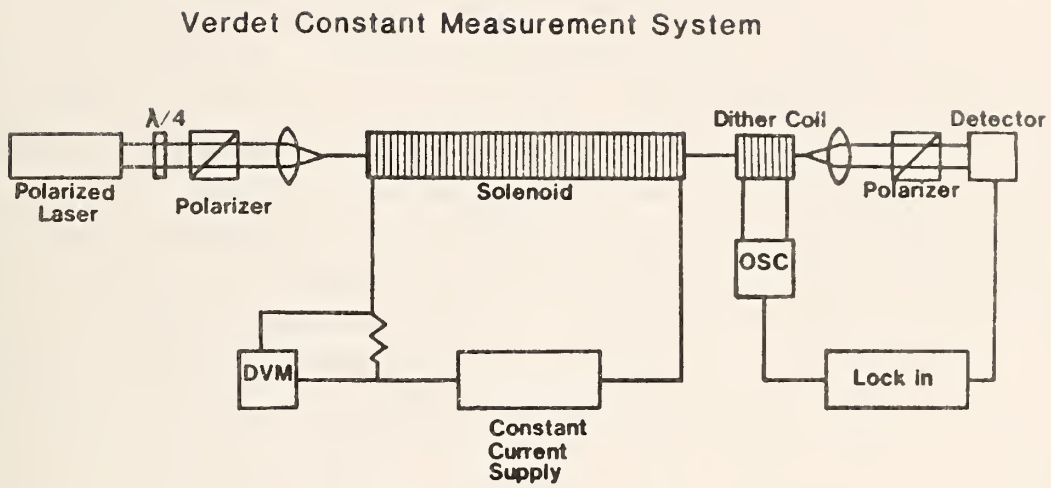

5-5 Measurement system for determining the Verdet constant of optical fiber. It is based on a 1-m long solenoid having approximately 3000 turns and operated at 30 A. Polarizers are oriented manually to determine rotation, the identification of a null being facilitated by the use of a dither coil and a lock-in amplifier.

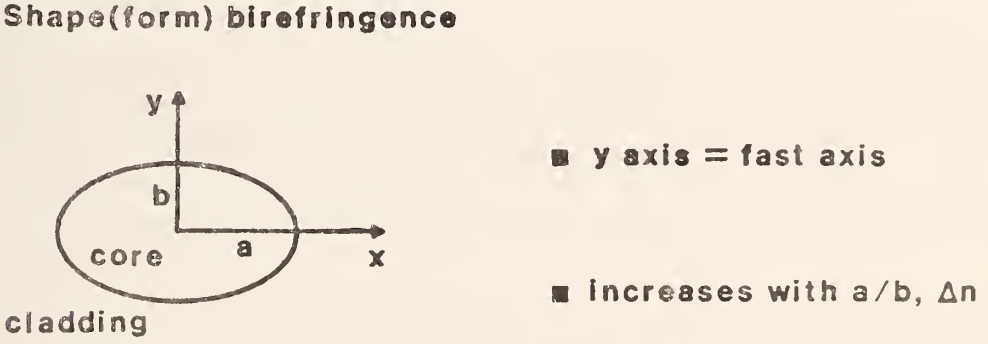

5-6 Geometry of form birefringence in an optical fiber. The fast axis is the minor axis of the ellipse. The magnitude of the birefringence increases with the ellipticity and with the difference in refractive index between the core and cladding.

constant to be similar to that of bulk diamagnetic materials. We also expect, and have observed with the apparatus in Figure 5-5, variations of the Verdet constant with wavelength that are consistent with the properties of the bulk materials. The major fundamental difference in using fiber rather than bulk materials is that the waveguiding propagation characteristics of the fiber can have a very significant effect on the polarization state of light propagating through it. This, in turn, complicates the simple picture of the Faraday effect presented previously, and in severe cases effectively quenches the Faraday entirely. A complete picture of the polarization properties of optical fiber would be too extensive to present here (5-7). However, because of the importance of these considerations in sensor design, the basic considerations are discussed below. The basic concept is that a so-called single mode fiber, that is one that supports only a single spatial mode, in fact supports a pair of orthogonal polarization states, which in general have slightly different phase velocities. It is therefore, more precisely, a two mode fiber. The reason is a lack of perfect circular symmetry, geometric or otherwise, in the fiber either as it was manufactured or because of externally applied perturbations. If the core of a fiber is slightly elliptical (Figure 5-6) it will exhibit what is known as "form birefringence." Form birefringence is a difference between the phase velocities of light polarized parallel to the minor axis of the ellipse and that polarized parallel to the major axis. The minor axis is the "fast axis." The degree of ellipticity and the difference in refractive index between the core and cladding determine the amount of birefringence present. Fibers in which the circular geometric symmetry is imperfect also exhibit "stress birefringence." This is a result of the fact that the various layers of the fiber structure have different thermal expansion characteristics and thereby cause an inherent radial stress. Through the stress-optic effect, additional birefringence appears, having the same axes as the form birefringence, and the two add algebraically. It is possible, through careful design and manufacturing techniques, to produce a fiber in which the form and stress birefringence is very low (5-8). However, even these fibers are subject to birefringence induced by external effects (5-9), the most important of which is bending. Bending introduces asymmetrical stress into the fiber that causes birefringence of magnitude

$$\Delta\beta_b = \frac{K_b}{\lambda} \frac{r^2}{R^2} \text{ rad/m} \qquad (5\text{-}8)$$

where K_b is a (slightly wavelength dependent) constant equal to about 0.85, λ is wavelength, r is the fiber radius, and R is the bend radius (Figure 5-7). The fast axis is in the plane of the bend. If the fiber is bent under tension, as for

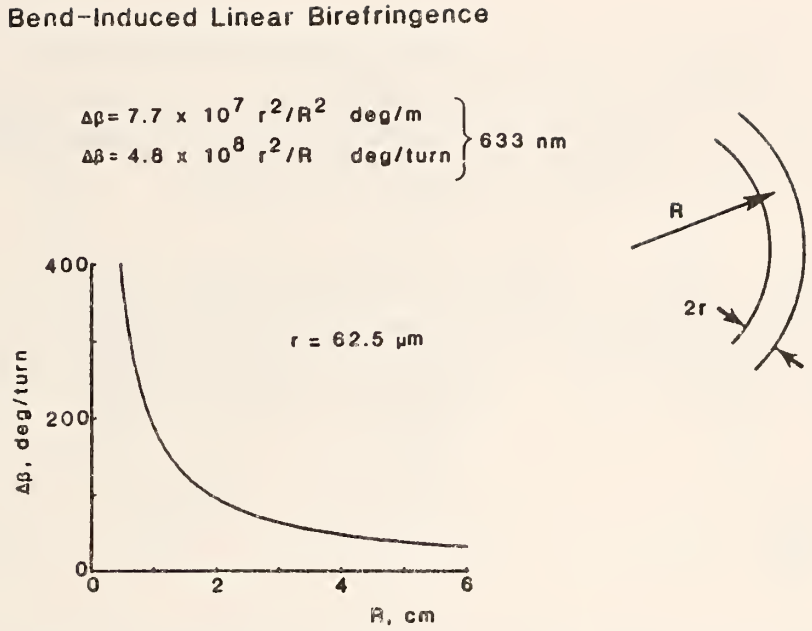

5-7 Geometry of bend-induced birefringence in single mode fiber and a numerical illustration for 125 μm diameter fiber at a wavelength of 633 nm.

example by winding it tightly around a coil former, there is an additional component to the bend birefringence, sometimes called "tension coiled birefringence" that takes the form

$$\Delta\beta_{tc} = \frac{K_{tc}}{\lambda}\frac{r}{R}\varepsilon_z \text{ rad/m}, \tag{5-9}$$

where K_{tc} is another (slightly wavelength dependent) constant equal to about 3.1 and ε_z is the longitudinal strain. As might be expected, transverse stress also induces linear birefringence in a fiber. The magnitude is given by

$$\Delta\beta_p = \frac{K_p}{\lambda}\frac{f}{r} \text{ rad/m} \tag{5-10}$$

where f is a line force (units of newtons/meter) and K_p is approximately 3×10^{11}.

Experience suggests that all of these effects are significant in determining the stability of a fiber current sensor. Tension coiled birefringence and transverse stress can be largely avoided through proper mechanical design. Bend

birefringence is more difficult to avoid. To determine the magnitude of the problem, one must compute the transfer function of a fiber sensor under various conditions.

The method of computation (5-10) is to use Jones calculus, a matrix technique of describing the changes in polarization state of light as it passes through anisotropic materials. The equation relating the polarization state at the output of a fiber current sensor to that at the input is as follows:

$$\begin{vmatrix} E_x(z) \\ E_y(z) \end{vmatrix} = \begin{vmatrix} \cos\frac{\phi z}{2} - j\frac{\Delta\beta}{\phi}\sin\frac{\phi z}{2} & -\frac{2F}{\phi}\sin\frac{\phi z}{2} \\ \frac{2F}{\phi}\sin\frac{\phi z}{2} & \cos\frac{\phi z}{2} + j\frac{\Delta\beta}{\phi}\sin\frac{\phi z}{2} \end{vmatrix} \begin{vmatrix} E(0) \\ E_y(0) \end{vmatrix} \qquad (5\text{-}11)$$

where

$$(\frac{\phi}{2})^2 = (\frac{\Delta\beta}{2})^2 + (F)^2,$$

E_x and E_y are the components of the optical electric field in and perpendicular to the coil, $\Delta\beta$ is the linear birefringence per unit length of fiber, and F is the induced Faraday rotation per unit length.

Utilizing Eqs. 3-3 and 5-10 it is then straightforward to compute the transfer function for various coil configurations and polarizer orientations. Figure 5-8 shows the result for two sensor designs, the coils having different diameters and number of turns and the polarizer configuration being that of Figure 3-7. In each case the transfer function is distorted for relatively low currents but approaches the ideal when the current becomes sufficiently large.

One technique for minimizing the effect of linear birefringence is to twist the fiber (5-11). Twisting introduces a torsional stress that, again through the stress-optic effect, causes a rotation of the plane of polarization in addition to the Faraday effect. In terms of the transfer function, it can be seen in Figure 5-9 that the effect is to shift the distorted portion of the transfer function away from the origin. For coils with diameters of about 10 cm or greater, it is usually possible to introduce enough twist to cause the slope at the origin to be effectively equal to that which would be measured without linear birefringence. The problem is that the twist-induced rotation is temperature dependent, which means that the origin (i.e., the parameter Φ in Eq. 2-2) shifts with temperature.

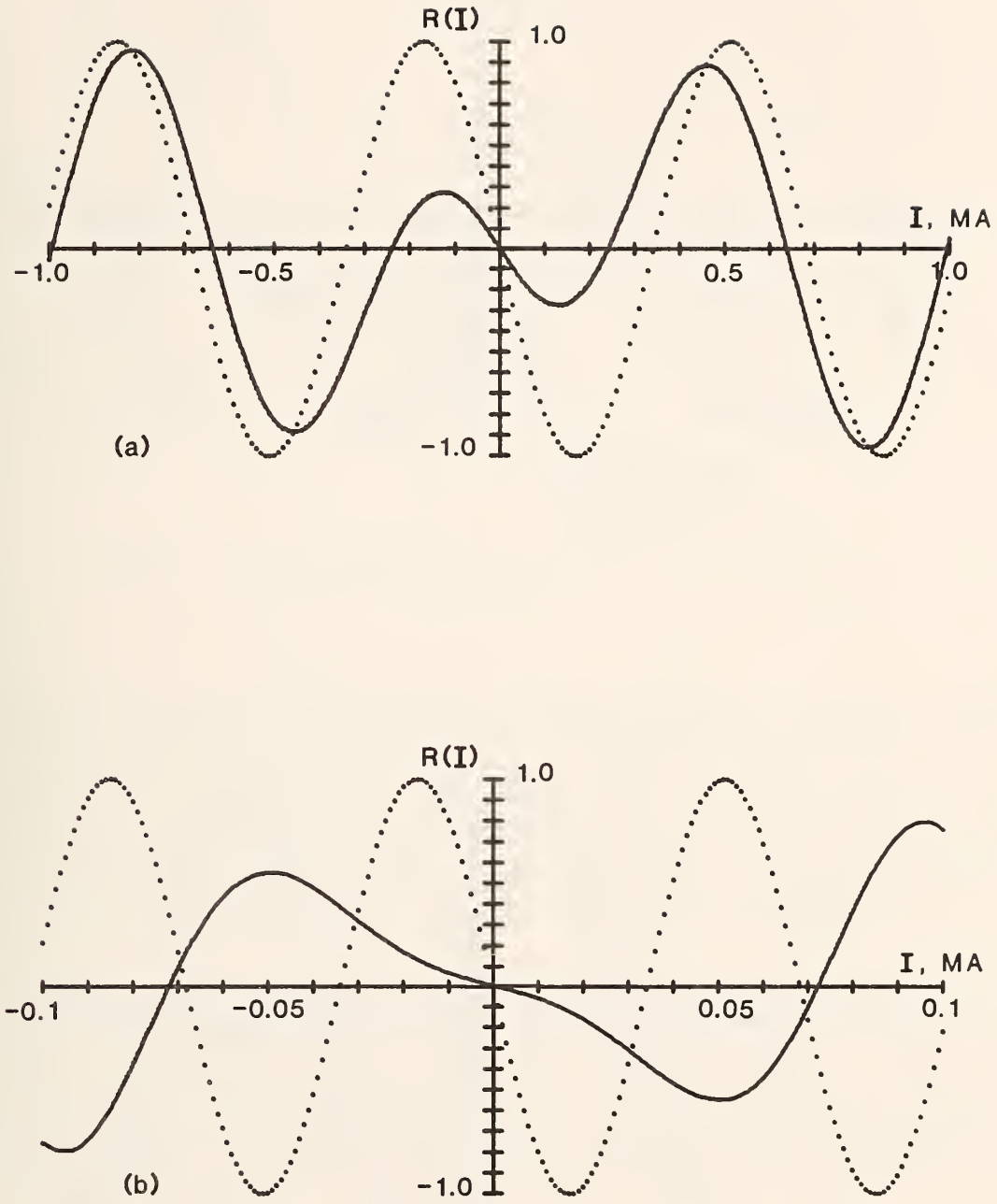

5-8 Transfer functions for two fiber current sensor configurations showing the effect of bend birefringence. Dotted curves assume no birefringence; solid include only bend birefringence. (a) 1 cm diameter coil, 1 turn; (b) 10 cm diameter coil, 10 turns. Both cases: 125 μm diameter fiber, wavelength 633 nm.

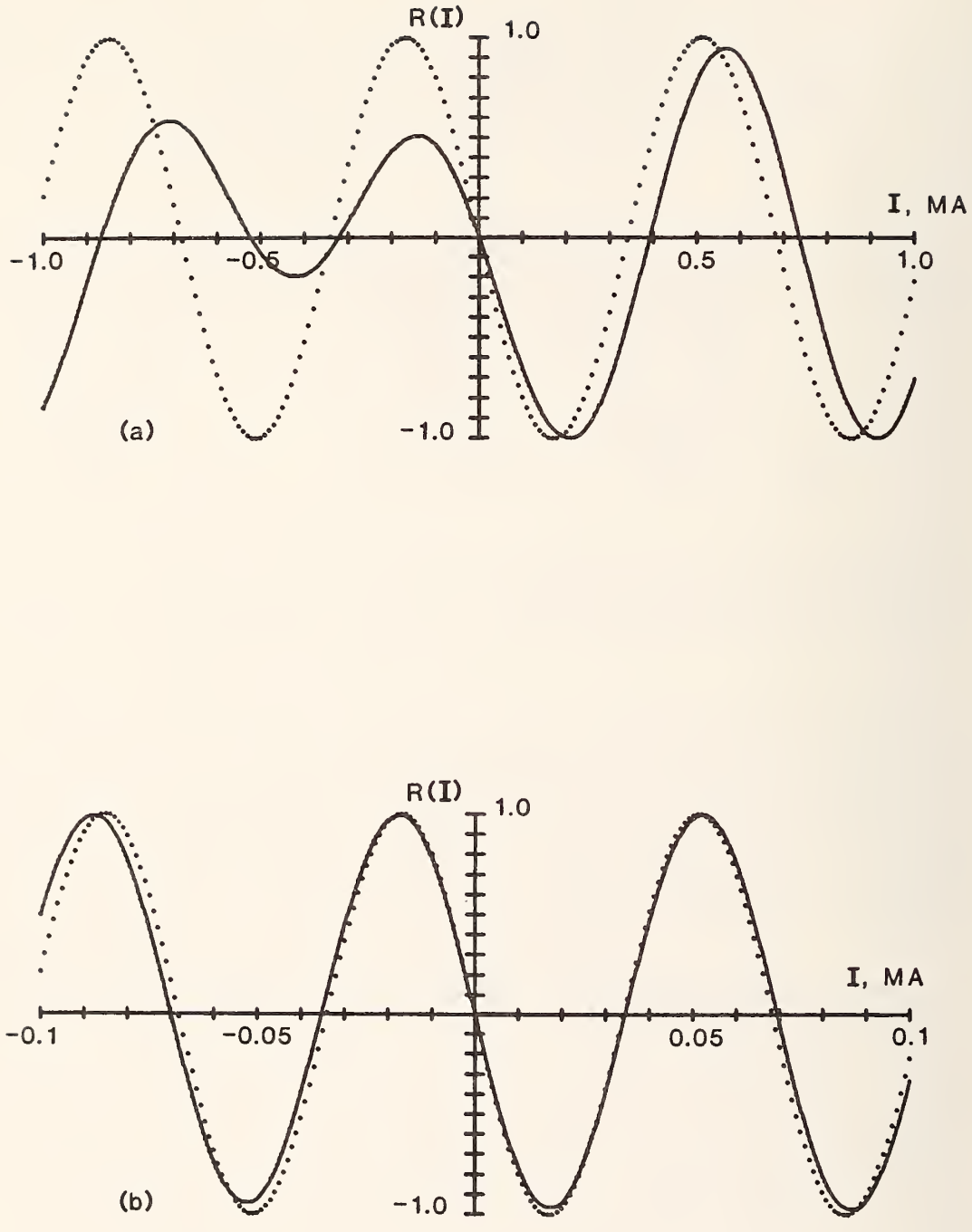

5-9 Transfer functions for the two coils of Figure 5-8, but with twisted fiber. (a) Twist rate 40 turns/meter; (b) twist rate 10 turns/meter. All other parameters same as Figure 5-8.

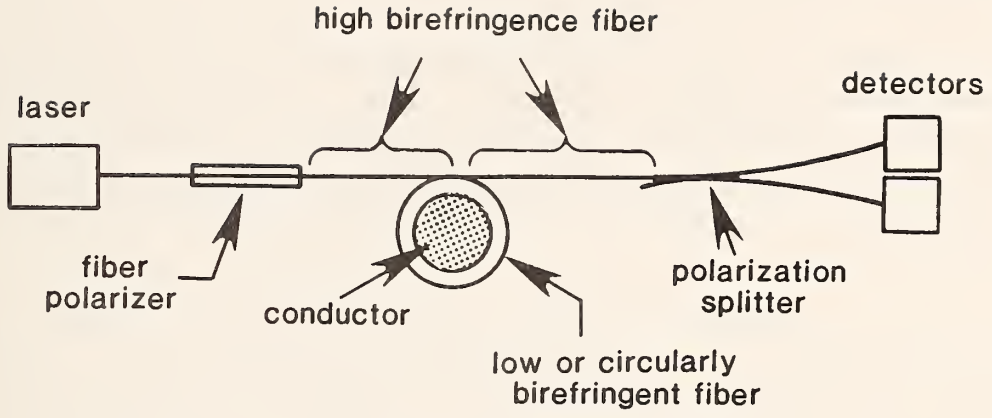

5-10 Possible configuration of an all-fiber current sensor.

An alternative technique is to relieve the bend induced birefringence by annealing (5-12). In this case the fiber is formed into the desired sensor configuration and then heated to temperatures of up to 800°C. After slow cooling, the birefringence of the coil is found to be greatly reduced. To date, coils as small as 3 cm diameter with as many as 20 turns have been annealed in our laboratory with reductions in birefringence by more than two orders of magnitude.

It is difficult to make general statements about the magnitude of linear birefringence that can be tolerated in a high precision current sensor. In relatively low precision sensors, a linear birefringence of roughly 50 deg, total, can generally be accepted without appreciable decrease in response. If the total birefringence is stable with temperature, it may be possible to accept nearly as much in high precision devices.

Another aspect of the problem with linear birefringence in fiber current sensors is that stress resulting from vibration or acoustic disturbances introduces noise into the sensor output. Mechanical design thus becomes critical in isolating the fiber from these perturbations.

Other Fiber Components

The optical fiber current sensor shown diagramatically in Figure 3-12 suggests that bulk polarization components might be used in conjunction with the fiber. In fact, one of the greatest long term attractions of a fiber current sensor is the possibility of producing an all-fiber system. Such a system is indicated in Figure 5-10. All of the components required have been demonstrated in research laboratories and most are available commercially.

Several types of fiber polarizers have been demonstrated experimentally (5-13). Of these, a design based on differential attenuation in a fiber with high linear birefringence is the only one available commercially. The requirements placed on the polarizer in this case are relatively mild and should be met acceptably by existing devices.

Polarization maintaining fiber (5-7) is used in the leads to the sensor coil. This is fiber designed to have a very high linear birefringence by deliberately avoiding cylindrical symmetry. If the birefringence is very large compared to any externally caused effects, linearly polarized light propagating along one of the axes of birefringence will remain linearly polarized. Polarization maintaining fiber is manufactured by several companies and is readily available.

Polarizing couplers are a more difficult problem. While demonstrations of principle have been achieved no practical devices are available (5-14). Two alternatives exist. One is to use a normal, nonpolarizing coupler and two fiber polarizers. This has the disadvantage of wasting half of the optical power and is subject to possible problems with changes in the coupling ratio with temperature. The other is to detect only one polarization, thereby obtaining a transfer function of the form shown in Figure 2-1. The disadvantages of this approach were discussed in Section 2.

Source and Detector Considerations

A semiconductor laser would likely be used in an all-fiber current sensor to take advantage of the improved coupling between source and fiber. The higher coherence is not expected to be a problem, with the exception that optical feedback from the system into the source must be avoided to minimize amplitude noise. Otherwise, the same source and detector requirements apply as in the case of the other configurations.

Temperature Compensation Techniques

In principle, a temperature compensated current sensor is more difficult to conceive that a temperature compensated field sensor because the current sensor is basically a distributed sensor, integrating the magnetic field around the conductor. Two possible approaches can be considered, however.

One possibility is to investigate new materials or material combinations in which dV/dT would be very small. Recent work in that direction [5-15] using mixtures of Yttrium Iron Garnet (YIG) and Terbium Iron Garnet (TbIG) which have temperature dependences of opposite signs. Preliminary data indicate that the Verdet constant of the resulting mixture, $(Y_{1-x}Tb_x)_3Fe_5O_{12}$, varies with temperature by much less than 1 percent over the temperature range from 300 to 415°C when x = 0.19. This material is ferromagnetic and exhibits saturation which makes it less than ideal for sensors, but it may be possible to extend the technique to other materials.

The second possibility is to define carefully and maintain the geometry of the sensor so that the sensing material need not be homogeneous. The optical path could then consist of several segments of two or more materials that have opposite signs of dV/dT. Such a device would not, in principle, be immune to stray fields from nearby conductors, but both that problem and the need to maintain the geometry can be addressed by increasing the number of segments. A greater question is whether diamagnetic materials can be found that have a negative dV/dT. If not it may be necessary to use paramagnetic materials which would limit the temperature range over which the balancing could be maintained.

Prognosis for High Precision Current Sensors

Eventually, most magneto-optic current sensors will be of the all-fiber type. The advantages include reduced size, greater flexibility, better sensitivity, avoidance of alignment problems, etc. and are significant. The technology is progressing steadily. It has already reached the stage where fiber current sensors are the preferred technology for certain types of applications, including pulsed current measurements and other situations where precision requirements are not severe. However, it is not yet possible to design, from readily available components, a sensor that will meet high precision requirements. With further, foreseeable progress in controlling the polarization properties of fiber it should be readily possible to achieve a sensor with a precision of around

2 percent over a temperature range of 100°C. This would be limited by the temperature coefficient of the Verdet constant in fused silica. Progress beyond that will require significant study of fiber materials.

For now and probably for the next few years high precision devices can be achieved more easily with bulk components than with fibers. Enough is now known about design principles to produce sensors that have a precision limited by the temperature dependence of the Verdet constant. A good choice of material for this purpose is the SF-57 glass, for reasons given previously. It is inexpensive and readily formed into desired component shapes. Based on measurements reported here, the calibration of such a device would remain constant to within about ±1 percent. Temperature compensation schemes must be employed to provide a sensor with a better precision. These are feasible, but more difficult than for electric field/voltage sensors.

References

5-1. M. J. Weber. Faraday Rotator Materials. Lawrence Livermore Laboratory, June 1982.

5-2. Optical Glass. Schott Optical Glass Inc., Duryea, PA 18642.

5-3. "Faraday effect in optical glasses, The wavelength dependence of the Verdet constant." Technical Information number 17, Schott Glaswerke, Mainz, F. R. Germany.

5-4. Herbert Piller. "Faraday Rotation," Ch. 3 in Semiconductors and Semimetals, Vol. 8, R. K. Willardson and A. C. Beer, Eds. Academic Press.

5-5. A. Sommerfeld. Optics. New York: Academic Press, 1964, Chapter III, Section 20.

5-6. G. W. Morey. Properties of Glass. Reinhold Co., 1938.

5-7. S. C. Rashleigh. "Origins and control of polarization effects in single-mode fibers." IEEE J. Lightwave Tech., 1983, vol. LT-1, p. 312-331.

5-8. D. N. Payne, A. J. Barlow, and J.-J. Ramskov Hansen. "Development of low- and high-birefringence optical fibres." IEEE J. Quantum Electron., 1982, vol. QE-18, p. 477-488.

5-9. G. W. Day. "Birefringence measurements in single mode optical fiber." Proc. SPIE 425, 1983.

5-10. G. W. Day, L. R. Veeser, G. I. Chandler, R. W. Cernosek. "Progress in the design of optical fiber sensors for the measurement of pulsed electric currents." Proc. Workshop on Meas. of Elect. Quant. in Pulse Power Systems, 1986, Gaithersburg, MD.

5-11. S. C. Rashleigh and R. Ulrich. "Magneto-optic current sensing with birefringent fibers." Appl. Phys. Lett., 1979, vol. 34, p. 768-770.

5-12. G. W. Day and S. M. Etzel. "Annealing of bend-induced birefringence in fiber current sensors." Technical Digest, 11th European Conference on Optical Communications/5th International Conference on Integrated Optical and Optical Communications, 1986, Venice.

5-13. See, for example: L. Li, et al. "Low cost metal/glass fibre polarisers produced in continuous lengths." Proceedings, 4th International Conference on Optical Fiber Sensors, 1986, Tokyo. K. Bohm, et al. "Simple metal-cladded fibre polarizer." Ibid. M. P. Varnham, et al. "Coiled birefringent-fibre polarisers." Electron Lett., 1984.

5-14. I. Yokohama, K. Okamoto, and J. Noda. "Fibre-optic polarizing beam splitter employing birefringent-fibre coupler." Electron. Lett., 1985, vol. 21, p. 415-416.

5-15. O. Kamada, Y. Tsujimoto, and Y. Hayashi. "Fiber-optical current sensors using mixed rare-earth iron garnet crystals." Proceedings, 3rd Sensor Symposium, (sponsored by IEE, Japan) Tsukuba, 1983.

Section 6

SUGGESTED APPROACHES TO THE DEVELOPMENT OF HIGH PRECISION OPTICAL CURRENT AND VOLTAGE SENSORS

During the course of this study it has become apparent that if high precision optical current and voltage sensors are to be developed and introduced into power systems, the process will be evolutionary. In this section we suggest and discuss three areas where increased emphasis would accelerate progress toward these goals.

1. The engineering and field testing of moderate precision current and voltage sensors specifically for power system configurations.

Based on our own work and on discussions with a number of manufacturers, we believe that it is possible to produce both current and voltage sensors that offer many of the advantages of optical sensors--high bandwidth (including dc), freedom from interference, small size, safe operation, modest cost, etc.--and moderate precision (roughly ±1 percent over a 100°C temperature range) using technology that has already been demonstrated in the laboratory or early prototypes. Such devices, fully suitable for use in the field, have not yet been produced but could be provided fairly quickly by several potential vendors, both domestic and foreign. Some technical issues remain to be resolved and would form the basis for final design and testing. These include

- Basic engineering design--configuration, placement, structure, insulation, etc.
- Transient temperature stability
- Vibration sensitivity
- Interface to existing instrumentation

2. The development of passive temperature compensation techniques for both voltage and current sensors.

If optical current and voltage sensors are to achieve a precision of the order of 0.1 percent over a temperature range of 100°C or greater, it is now clear that some form of temperature compensation must be used. Passive techniques--those in which the different properties of materials and components are exploited, rather

than measurement and adjustment or temperature control--are to be preferred for their simplicity and therefore cost. In this document we have proposed several such passive temperature compensation schemes. These need to be investigated further, including

- Accumulation of more data on the temperature coefficients of the linear electro-optic effect and the Faraday effect
- Laboratory demonstration of a temperature compensated electro-optic device
- Further analysis of schemes for temperature compensation in magneto-optic devices

3. Research and development on special fibers, fiber components, and planar waveguide electro-optic components.

We believe that, eventually, optical current sensors will be all-fiber devices and that the only non-fiber component in a voltage sensor will be an electro-optic crystal which will appear as a guided wave component. Such sensors will offer significant advantages in configuration, size, and cost. Optimism that they can be produced is based on recent rapid advances in the understanding and control of the polarization properties of fiber, the development of several new fiber types, and progress in planar waveguide technology. Three main areas of attack are suggested, as follows:

- Development and refinement of fiber components--circularly birefringent fibers, fiber polarizers, fiber couplers, and polarization splitters
- Investigation of the stability of such devices
- Fabrication and study of planar electro-optic modulators in 43 m crystals

Section 7

SUMMARY

We began this study and this report with the central question, "What precision can be achieved with an electro-optic voltage sensor or a magneto-optic current sensor?" We have pursued the answer in numerous ways--through an investigation of the basic properties of materials and components, both as reported in the literature and new data generated in our laboratory, through attempts to demonstrate the feasibility of overcoming certain limitations in the properties of components, through analysis of some fundamental limitations, through the proposal of new or refined designs, and through discussions with numerous other investigators.

We conclude that ease of obtaining high precision (in a power systems context) is not included among the many advantages of using optical sensors for measurement of electromagnetic quantities. The principal difficulty is with the necessity of designing sensors that will maintain their calibration over extremely broad temperature ranges (at least 100°C) without the possibility of temperature stabilization. We find, specifically, that using relatively standard approaches and an appropriate definition of precision, a precision not better than about ±1 percent can be expected. Achieving that level will require wise choices of materials, components, and design, but we have been able to offer numerous suggestions in this regard.

Judgments about the commercial viability of such devices should perhaps be left to those more expert in that subject than we. We should remember, however, that worst case situations are encountered infrequently, and therefore represent pessimistic assessments of performance in real applications. We also suspect that the other advantages of optical sensors may in some applications be dominant considerations. Safety is one example.

We are very optimistic about improving the precision of optical sensors by a desired order of magnitude or more, principally by investigating passive temperature compensation techniques. We have examined several of these analytically, and

suggest that they be further investigated. Other approaches, including temperature compensation by measurement and adjustment, could be considered, but were not discussed here. We are also optimistic about the development of all-fiber or nearly all-fiber sensors that could provide very simple, low cost measurements, even if the highest precision is not achieved, and have suggested further work in that area.

Appendix A

NOISE ANALYSIS FOR ELECTRO-OPTIC OR MAGNETO-OPTIC SENSORS

To examine the limitations imposed by noise on the precision of a sensor we assume that the sensor configuration is such that there are two detectors, one providing a transfer function of the form

$$R(x) = A \sin^2(x/x_0 + \pi/4)$$

and the other

$$R(x) = A \sin^2(x/x_0 - \pi/4)$$

yielding a difference

$$R(x) = A \sin(2x/x_0)$$

as indicated in Section 2.

We assume that each detector is followed by a transimpedance amplifier with a feedback resistor R_f. Such an amplifier is depicted in Figure 4-5. Assuming further that laser noise and amplifier noise are or can be made negligible, shot noise associated with the average detector current and Johnson noise associated with the feedback resistor remain as the fundamental noise sources.

The equivalent input noise current of each detector is given by

$$i_n^2 = [4kT/R_f + 2eI_{av}]$$

where k is Boltzmann's constant, T is absolute temperature, e is the electronic charge, and I_{av} is the average detector current (which produces an output from the detector of A/2). The change in detector current, per unit of the measurand, is $2I_{av}/x_0$. The noise equivalent measurand (NEM), that is the value of the measurand that produces a signal equal to the noise, is given for each detector by

$$NEM = [4kT/R_f + 2eI_{av}]^{1/2}/[2I_{av}/x_0].$$

Using two detectors as described increases the noise current by a factor of $2^{1/2}$ (assuming uncorrelated noise processes) and increases the signal by a factor of 2, thereby reducing the NEM by a factor of $2^{1/2}$ and yielding

$$NEM = [2kT/R_f + eI_{av}]^{1/2}/[2I_{av}/x_0].$$

Recalling that for a current sensor $1/x_0 = \mu_0 VN$ and for an electric field sensor $1/x_0 = C_{eo}/2$, we can now plot both the noise equivalent current (NEI) or the noise equivalent electric field (NEE) as a function of the value of the feedback resistor and the average detector current. Figure A-1 shows such a plot for a single turn current sensor using the Verdet constant of fused silica for an electric field sensor using the appropriate value of C_{eo} for a bismuth germanate crystal that is five times longer than its thickness, both assuming a wavelength of 633 nm.

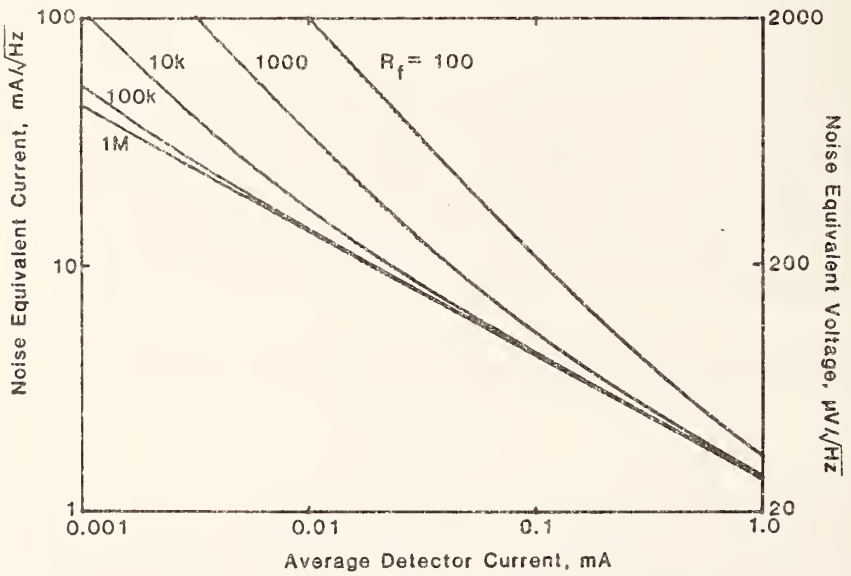

A-1. Noise equivalent current for a single turn current sensor of fused silica and noise equivalent voltage for a bismuth germanate voltage sensor with a length to thickness ratio of 5, both operated at a wavelength of 633 nm, as a function of amplifier feedback resistor size and average detector current.

Appendix B

OPTICAL DESIGN FOR BULK SENSORS

As shown in Appendix A, a major factor in determining the signal to noise performance of a sensor is the average detector current, which is assumed to be proportional to the average optical power incident on the detector. Particularly when bulk components are incorporated into a sensor, maximizing the power at the detector require several trade-offs in optical design. In this appendix we examine some of the choices that must be made.

The problem can be divided into two parts. One is maximizing the power launched from a source into the input fiber. The other is maximizing the transfer of power from one fiber, through a series of bulk components, and back into another fiber. Here we consider the case of a sensor using an LED source with multimode fiber.

MAXIMIZING LAUNCHED POWER

If maximizing the launched power were the only consideration, one would choose a large area (and therefore high power) LED, a fiber with an equally large core and as large a numerical aperture as possible. Assuming that there is no mismatch in area and that the LED is centered very near the end of the fiber, the coupling efficiency will depend on the radiation properties of the LED, the numerical aperature of the fiber and its refractive index profile.

The radiation pattern of an LED is normally symmetric about the axis of propagation, with an angular distribution given, to a useful approximation, by

$$I = I_0(\cos \alpha)^m \qquad \text{(B-1)}$$

where I and I_0 represent irradiance (units of power/area), α is angle with respect to the axis, and m ($m \geq 1$) is a parameter governing the angular width of the pattern. The case m = 1 corresponds to what is commonly known as a Lambertian source. The index profile of a multimode fiber is usefully approximated by the form

$$n(r) = \begin{cases} n_1[1 - 2\Delta(\frac{r}{a})^g]^{1/2} & r < a \\ n_1[1 - 2\Delta]^{1/2} & r > a \end{cases} \qquad \text{(B-2)}$$

and

$$\Delta = (n_1^2 - n_2^2)/2n_1^2$$

where $n(r)$ is the refractive index as a function of radius, n_1 is the refractive index at the center of the core, and n_2 is the refractive index of the cladding, and g is a parameter governing the shape of the profile. The case of $g = \infty$ corresponds to what is known as a step index fiber. Most fibers described as graded index fibers have $g \approx 2$.

Using Eqs. B-1 and B-2 one can compute the coupling efficiency, η, and find for $m = 1$

$$\eta = (\frac{g}{g+2})(NA)^2 \qquad \text{(B-3)}$$

where NA is the numerical aperture of the fiber [$NA = (n_1^2 - n_2^2)^{1/2}$]. In the case of a step index fiber the functional dependence on m is given by

$$\eta = (\frac{m+1}{2})(NA)^2. \qquad \text{(B-4)}$$

COUPLING BETWEEN FIBERS

The components of a bulk sensor usually represent an optical system that is relatively long compared to its transverse dimensions. One option is to place the end of the input fiber in the focal plane of a lens thereby collimating the light through the sensor components (Figure B-1). The beam passing through the sensor is smallest at the collimating lens and diverges with a half angle given by

$$\Omega = a/f \qquad \text{(B-5)}$$

where a is the radius of the fiber core and f is the focal length of the lens. This assumes that the refractive index of the sensor is 1, though it is of course

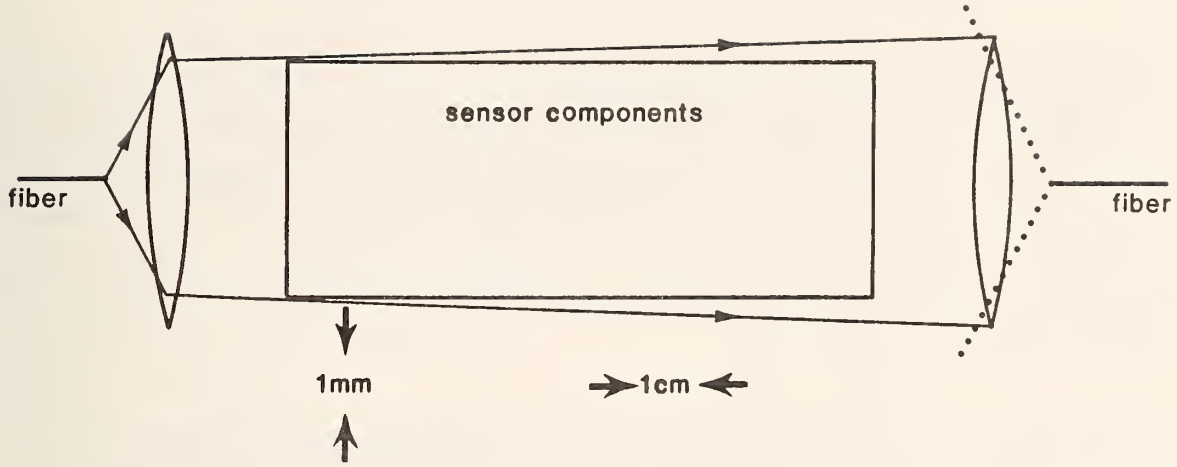

B-1 Illustration of optical coupling from one multimode fiber, through a series of sensor components, and back into an identical multimode fiber. In this case the light is collimated through the sensor. Dotted lines show acceptance cone of output fiber.

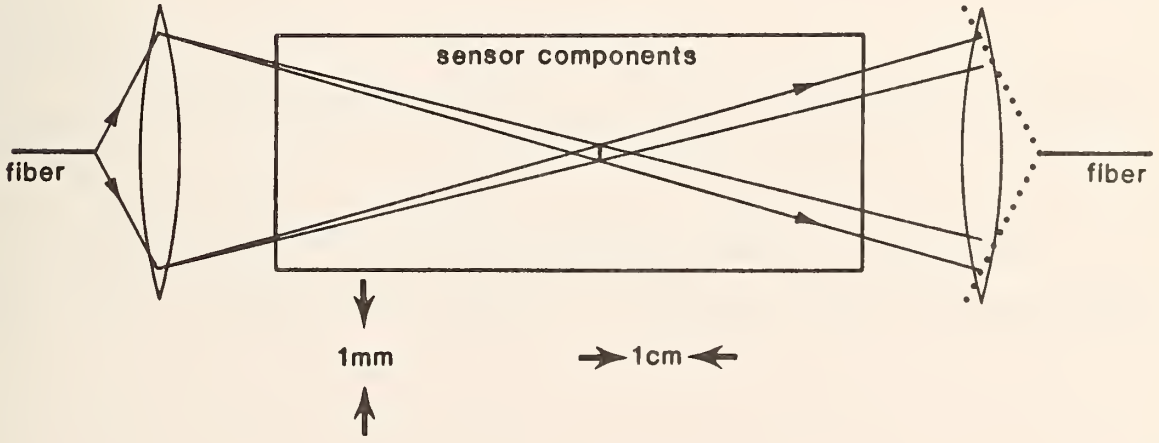

B-2 Same as B-1, except that the output end of the input fiber is imaged at a point somewhat greater than midway between the lenses. This results in a greater collection efficiency into the output fiber.

higher, and overstates the divergence accordingly. To avoid aperturing in the sensor or in the refocusing lens, it is therefore desirable to use an input fiber with as small a core as possible and a lens with as long a focal length as possible. The first of these considerations conflicts with the conditions for maximizing launched power. The second, coupled with the use of large numerical aperture fiber, may require a large diameter lens and result in a beam size that is unacceptably large, even where, at the lens, it is smallest.

An alternative and probably superior choice is to image the output of the input fiber somewhere in the middle of the sensor (Figure B-2). The image represents the minimum beam size, which can, in principle, be controlled through the choice of input lens and fiber location. The actual design may be fairly difficult when several components with different refractive indices are involved. In any case, this approach also works best when the input fiber has a small core and small numerical aperture.

The main point of this discussion therefore, is that optimizing the power delivered to the detector may not be best achieved by maximizing the light launched into the input fiber, but will in general involve an optimization of the input fiber type and a fairly detailed design of the optical system that transmits light from the input fiber, through the sensor, and back into the output fiber.

Reference

B-1 A. H. Cherin, An Introduction to Optical Fibers. McGraw Hill, 1983.

Appendix C

PROPERTIES OF SELECTED ELECTRO-OPTIC CRYSTALS OF POINT GROUP $\bar{4}3m$

In section 3 of this report, it was suggested that crystals of crystal class $\bar{4}3m$ were the most suitable for electro-optic voltage sensors. In this appendix the relevant properties of five materials having that crystal symmetry are tabulated. Numbers in parentheses are wavelengths in nanometers.

Material: Bismuth Germanate, $Bi_4Ge_3O_{12}$

Nominal transparent range (nm)	400 to 5000
Refractive index, n	2.0975 (633) [a]
Normalized temperature derivative of refractive index, (dn/dT)/n, (10^{-5}/K), at room temperature	2. (633) [b]
Thermal expansion coefficient, (dh/dT)/h, (10^{-6}/K), at room temperature	1. [b]
n^3r_{41} (pm/V)	8.8 (T) (631) [a]
Verdet constant, V (deg/cm-T)	16.5 (633) [c]
Relative dielectric constant, ε_r	NA

References:

[a]D. P. Bortfeld and H. Meier. "Refractive indices and electro-optic coefficients of the eulitities $Bi_4Ge_3O_{12}$ and $Bi_4Si_3O_{12}$." J. Appl. Phys., 1972, vol. 43, p. 5110-5111.

[b]G. W. Day, D. Conrad, K. S. Lee, and P. D. Hale. "Optical, electro-optical, and stress-optical properties of bismuth germanate, $Bi_4Ge_3O_{12}$," unpublished.

[c]M. J. Weber. "Faraday Rotator Materials." Lawrence Livermore Laboratory Report, 1982.

Material: Zinc Sulfide, ZnS

Nominal transparent range, nm	500 to 14000
Refractive index, n	2.3450 (650) [a] 2.3062 (850) [a] 2.2721 (1500) [a]
Normalized temperature derivative of refractive index, (dn/dT)/n, (10^{-5}/K), at room temperature	2.3 (650) [a] 2.1 (850) [a] 1.9 (1500) [a]
Thermal expansion coefficient, (dh/dT)/h, (10^{-6}/K), at room temperature	6.8 [b]
$n^3 r_{41}$ (pm/V)	28.1 (633) [c]
Verdet constant, V (deg/cm-T)	NA
Relative dielectric constant, ε_r	8.3 to 9.0 [a]

References:

[a]H. H. Li. "Refractive index of ZnS, ZnSe, and ZnTe and its wavelength and temperature derivatives." J. Phys. Chem Ref. Data, 1984, vol. 13, p. 103-150.

[b]Albert Feldman, Deane Horowitz, Roy M. Waxler, and Marilyn J. Dodge. "Optical materials characterization." Final technical report, Nat. Bur. Stand. (U.S). Tech. Note 993, 1979.

[c]"Landolt-Boernstein, Zahlenwerte und Funktionen aus Naturwissenschaften und Technik," Neue Serie, K.-H. Hellwege, Ed., Gruppe III:Band 11, Elastische, piezoelektrische, pyroelektrische, piezooptische, elektrooptische Konstanten und nichtlineare dielektrische Suszeptibilitaten von Kristallen. Springer-Verlag, 1979.

Material: Zinc Selenide, ZnSe

Nominal transparent range, nm	500 to 22000
Refractive index, n	2.5810 (650) [a] 2.5124 (850) [a] 2.4570 (1500) [a]
Normalized temperature derivative of refractive index, $(dn/dT)/n$ (10^{-5}/K), at room temperature	3.9 (650) [a] 3.1 (850) [a] 2.7 (1500) [a]
Thermal expansion coefficient, $(dh/dT)/h$, (10^{-6}/K), at room temperature	7.3 [b]
$n^3 r_{41}$ (pm/V)	34.3 (632) [c]
Verdet constant, V (deg/cm-T)	67.6 (633) [d]
Relative dielectric constant, ε_r	7.6 to 9.6 [a]

References:

[a]H. H. Li. "Refractive index of ZnS, ZnSe, and ZnTe and its wavelength and temperature derivatives." J. Phys. Chem. Ref. Data, 1984, vol. 13, p. 103-150.

[b]Albert Feldman, Deane Horowitz, Roy M. Waxler, and Marilyn J. Dodge. "Optical materials characterization." Final technical report, Nat. Bur. Stand. (U.S). Tech. Note 993, 1979.

[c]"Landolt-Boernstein, Zahlenwerte und Funktionen aus Naturwissenschaften und Technik." Neue Serie, K.-H. Hellwege, Ed., Gruppe III:Band 11, Elastische, piezoelektrische, pyroelektrische, piezooptische, elektrooptische Konstanten und nichtlineare dielektrische Suszeptibilitaten von Kristallen. Springer-Verlag, 1979.

[d]M. J. Weber. "Faraday Rotator Materials." Lawrence Livermore Laboratory Report, 1982.

Material: Gallium Arsenide, GaAs

Nominal transparent range, nm	1000 to 17000
Refractive index, n	3.50 (1020) [a] 3.347 (1900) [a] 3.313 (3000) [a]
Normalized temperature derivative of refractive index, $(dn/dT)/n$, $(10^{-5}/K)$, at room temperature	1.7 (>5000) [b]
Thermal expansion coefficient, $(dh/dT)/h$, $(10^{-6}/K)$, at room temperature	5.7 [c]
$n^3 r_{41}$ (pm/V)	61. (T) (1150) [a] 44. (T) (3390) [a]
Verdet constant, V (deg/cm-T)	NA
Relative dielectric constant, ε_r	12.3 to 13.2 [d]

References:

[a]"Landolt-Boernstein, Zahlenwerte und Funktionen aus Naturwissenschaften und Technik." Neue Serie, K.-H. Hellwege, Ed., Gruppe III:Band 11, Elastische, piezoelektrische, pyroelektrische, piezooptische, elektrooptische Konstanten und nichtlineare dielektrische Suszeptibilitaten von Kristallen. Springer-Verlag, 1979.

[b]Yet-ful Tsay, Bernard Bendow, and Shashanka S. Mitra. "Theory of the temperature derivative of the refractive index in transparent crystals." Phys. Rev. B, 1973, vol. 8, p. 2688-2696.

[c]William L. Wolfe. "Properties of Optical Materials." In Handbook of Optics, Optical Society of America/McGraw Hill, 1978.

[d]Amnon Yariv and Pochi Yeh. Optical Waves in Crystals. John Wiley, 1984.

Material: Gallium Phosphide GaP

Nominal transparent range, nm	500 to 13000
Refractive index, n	3.36 (640) [a] 3.24 (850) [a] 3.07 (1400) [a]
Normalized temperature derivative of refractive index, (dn/dT)/n, (10^{-5}/K), at room temperature	1.3 (????) [b]
Thermal expansion coefficient, (dh/dT)/h, (10^{-6}/K), at room temperature	5.3 [c]
$n^3 r_{41}$ (pm/V)	33. (T) (550...1300) [a]
Verdet constant, V (deg/cm-T)	NA
Relative dielectric constant, ε_r	10. [d]

References:

[a]"Landolt-Boernstein, Zahlenwerte und Funktionen aus Naturwissenschaften und Technik." Neue Serie, K.-H. Hellwege, Ed., Gruppe III:Band 11, Elastische, piezoelektrische, pyroelektrische, piezooptische, elektrooptische Konstanten und nichtlineare dielektrische Suszeptibilitaten von Kristallen. Springer-Verlag, 1979.

[b]Yet-ful Tsay, Bernard Bendow, and Shashanka S. Mitra. "Theory of the temperature derivative of the refractive index in transparent crystals." Phys. Rev. B, 1973, vol. 8, p. 2688-2696.

[c]William L. Wolfe. "Properties of Optical Materials." In Handbook of Optics, Optical Society of America/McGraw Hill, 1978.

[d]Amnon Yariv and Pochi Yeh. Optical Waves in Crystals. John Wiley, 1984.

Appendix D

PROPERTIES OF SELECTED DIAMAGNETIC GLASSES

In this section we summarize the properties of several glasses that have been used as the magneto-optic material in electric current sensors. Because it is difficult to specify glasses other than by commercial designation, those designations are provided in addition to the general glass type. This should not be construed as a recommendation or an implication that similar products from another supplier might not be equally or more suitable for the purpose. Numbers in parentheses are wavelengths in nanometers.

Material: Dense flint glass, Schott SF-57

Composition (compound/wt. %)	NA
Nominal transparent range (nm)	430 to 2400
Refractive index, n	1.81184 (633) [a] 1.82045 (852) [a] 1.83957 (1060) [a]
Stress-optic coefficient (pm/N)	0.03 (589) [a]
Verdet constant, V (deg/cm-T)	11.5 (633) [b] 3.8 (1060) [b]
Temperature coefficient of the Verdet constant, (dV/dT)/V	
Density (g/cm^3)	5.51 [a]
Thermal expansion coefficient, (dh/dT)/h, (10^{-6}/K), at room temperature	8.3 [a]

References:

[a]Optical Glass, Schott Optical Glass, Inc., York Avenue, Duryea, PA 18642.

[b]M. J. Weber. "Faraday Rotator Materials." Lawrence Livermore Laboratory Report, 1982.

[c]M. Deeter, T. Milner, G. W. Day. "The temperature dependence of the Verdet constant in diamagnetic glasses," unpublished.

Material: Flint glass, Schott SF-6

Composition (compound/wt. %)	SiO_2	27.35
	K_2O	1.50
	PbO	71.15
Nominal transparent range (nm)	400 to 2400	
Refractive index, n	1.77381 (633) [a] 1.78159 (852) [a] 1.65106 (1060) [a]	
Stress-optic coefficient (pm/N)	0.63 (589) [a]	
Verdet constant, V (deg/cm-T)	10.3 (633) [b] 3.5 (1060) [b]	
Temperature coefficient of the Verdet constant, (dV/dT)/V		
Density (g/cm^3)	5.18 [a]	
Thermal expansion coefficient, (dh/dT)/h, (10^{-6}/K), at room temperature	8.1 [a]	

References:

[a]Optical Glass, Schott Optical Glass, Inc., York Avenue, Duryea, PA 18642.

[b]M. J. Weber. "Faraday Rotator Materials." Lawrence Livermore Laboratory Report, 1982.

[c]M. Deeter, T. Milner, G. W. Day. "The temperature dependence of the Verdet constant in diamagnetic glasses," unpublished.

Material: Fused silica, SiO_2

Nominal transparent range (nm)	
Refractive index, n	1.4567 (644) [a] 1.4525 (852) [a] 1.4462 (1362) [a]
Stress-optic coefficient (pm/N)	3.36 (633) [a]
Verdet constant, V (deg/cm-T)	2.1 (633) [b] 1.2 (850) [b]
Temperature coefficient of the Verdet constant, (dV/dT)/V	[c]
Density (g/cm^3)	2.20 [d]
Thermal expansion coefficient, (dh/dT)/h, (10^{-6}/K), at room temperature	8.3 [d]

References:

[a] American Institute of Physics Handbook. McGraw Hill, 1972

[b] J. D. O. McFadden and G. W. Day, unpublished.

[c] M. Deeter, T. Milner, G. W. Day. "The temperature dependence of the Verdet constant in diamagnetic glasses," unpublished.

[d] Handbook of Optics. Optical Society of America/McGraw Hill, 1978.

Material: Borosilicate Crown glass, Schott BK-7

Composition, (compound/wt. %)	SiO_2	69.58
	B_2O_3	9.91
	Na_2O	8.44
	K_2O	8.37
	CaO	0.07
	BaO	2.54
	Al_2O_3	0.04
Nominal transparent range (nm)	330 to 2300	
Refractive index, n	1.51509 (633) [a]	
	1.50981 (852) [a]	
	1.50669 (1060) [a]	
Stress-optic coefficient (pm/N)	2.74 (589) [a]	
Verdet constant, V (deg/cm-T)	2.3 (633) [b]	
	1.0 (1060) [b]	
Temperature coefficient of the Verdet constant, (dV/dT)/V		
Density (g/cm^3)	2.51 [a]	
Thermal expansion coefficient, (dh/dT)/h, (10^{-6}/K), at room temperature	7.1 [a]	

References:

[a] Optical Glass. Schott Optical Glass, Inc., York Avenue, Duryea, PA 18642.

[b] M. J. Weber. "Faraday Rotator Materials." Lawrence Livermore Laboratory Report, 1982.

[c] M. Deeter, T. Milner, G. W. Day. "The temperature dependence of the Verdet constant in diamagnetic glasses," unpublished.

Appendix E

THE CHARACTERIZATION OF WAVEPLATES

In order to measure small changes in retardance of various types of waveplates, the measurement system shown in Figure E-1 was developed. It uses a quartz-halogen incandescent source with a temperature stabilized interference filter, usually placed near the detector, to define the wavelength of measurement. A prism polarizer at the input to the waveplate is adjusted to transmit light polarized at 45° to the axes of the waveplate. A prism polarizer at the output rotates about its axis at a rate of about 200 Hz yielding a signal at the detector of the form

$$I = I_0(1 + \cos\delta \sin\omega t) \qquad \text{(E-1)}$$

where δ is the retardance of the device.

Thus by measuring the ac and dc components of the detector output we can obtain cos δ.

The system is obviously most sensitive when $\delta \approx \pi/2$ so that it is ideal for the characterization of quarter-wave plates. The resolution in that case, depending on the wavelength of measurement, can be as good as 0.1 mrad. For the measurement of waveplates with retardances other than $\pi/2$ rad, it is possible to use a Babinet-Soleil compensator in series with the waveplate to achieve a net retardance of $\pi/2$.

For measuring the temperature dependence of various waveplates, the devices to be tested are placed on a small optical mirror mount inside a specially built oven. The oven has no windows, nor are there any other optical components between the two polarizers. The temperature inside the oven near the waveplate can be maintained to within about 0.1°C over a range from 15 to 100°C.

The system operates under the control of a desk-top computer which adjusts the oven heater, measures the temperature, the dc output of the detector, and the output of the lock-in amplifier, computes the birefringence, and plots the results.

Figure E-2 shows examples of the data obtained for a quartz waveplate and a polymer waveplate.

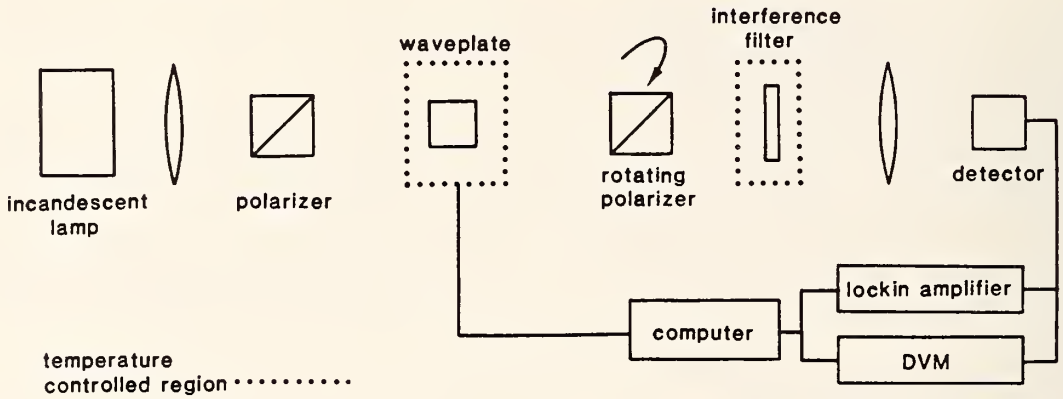

E-1 Measurement system for the determination of the temperature coefficient of the retardance of various waveplates.

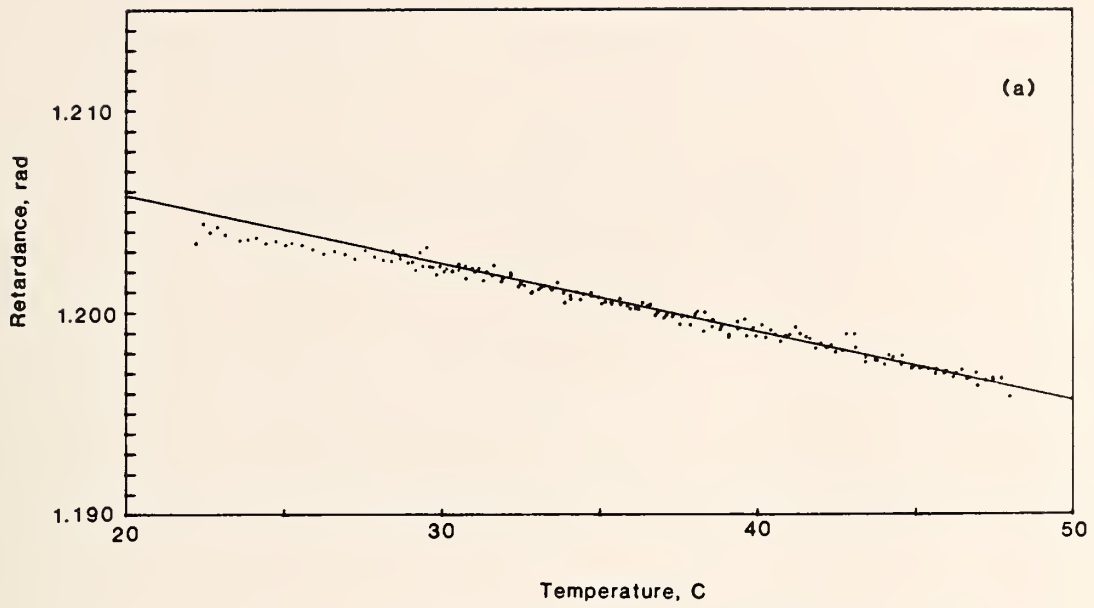

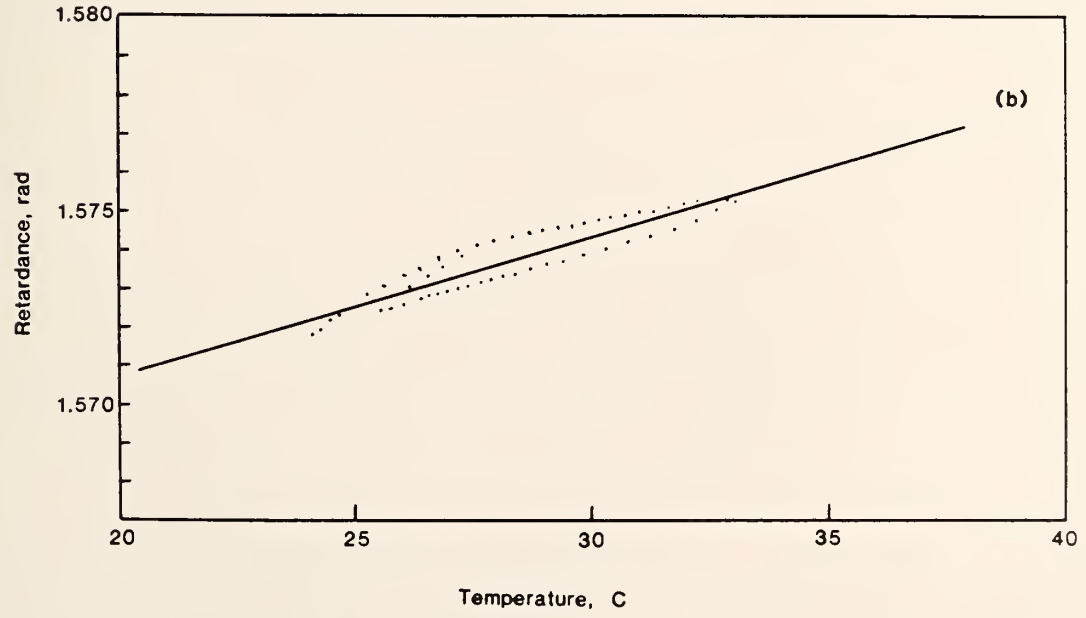

E-2 Retardance versus temperature for a mica quarter wave plate (a) and an acromatic polymer waveplate (b).

APPENDIX F

BIREFRINGENCE MEASUREMENTS IN SINGLE MODE OPTICAL FIBER

(Proc. SPIE, Vol. 425, 1983)

Birefringence measurements in single mode optical fiber

G. W. Day

Electromagnetic Technology Division, National Bureau of Standards
325 Broadway, Boulder, Colorado 80303

Abstract

Because their cores are not perfectly circular or because of stress, inherent to the structure or externally applied, practical single mode fibers are birefringent. These sources of birefringence are reviewed briefly. A simple model for the fiber consists of a combination of one linearly birefringent element and one circularly birefringent element. Depending on the magnitude of the birefringence, different techniques of evaluating the parameters of the model may be suitable. Several methods appropriate for low and high birefringence fiber are described and some of their advantages and disadvantages outlined.

In an idealized single mode optical fiber, in which none of the structural or optical parameters varies with the azimuthal coordinate, all polarization states within the fundamental mode are degenerate; that is, neither the phase nor group velocity depends on polarization. In practice, however, this degeneracy is usually lifted by non-circularity of the core, by inherent stress in the guiding structure, or by stress resulting from bending, pressure, or twisting. Light entering the fiber with an arbitrary polarization state will then be resolved into a pair of orthogonal polarization states that propagate with different velocities. As a phase shift develops between them, the state of polarization will vary periodically along the fiber. The orthogonal states may be linear, circular, or in general elliptical, depending on the specific mechanisms involved.

Birefringence is a measure of the difference in phase velocity between the two states and is precisely expressed as the difference between their effective refractive indices:

$$B = \delta n = \frac{\lambda}{2\pi}\Delta\beta$$

where $\Delta\beta$ is the difference between the two propagation constants. Alternatively, birefringence is sometimes taken to be synonymous with $\Delta\beta$ and is expressed in radians (or degrees)/unit length. Primarily for linear birefringence, a useful related quantity is the beat length (L_p) defined as the distance of propagation necessary for a phase shift of 2π radians to develop between the orthogonal states:

$$L_p = \frac{2\pi}{\Delta\beta} = \frac{\lambda}{B} .$$

For circular birefringence, it is more common to specify the rotation per unit length (Ω) of linearly polarized light that occurs in such a medium:

$$\Omega = \Delta\beta_{circular}/2 .$$

For some purposes, it will be necessary to use fiber with extremely low values of birefringence. In certain types of fiber sensor sytems, for example, magnetic field sensors based on the Faraday effect, the measured response to an external stimulus is a change in polarization. Birefringence in such devices may alter or even quench the desired effect; furthermore, it may render the device unstable as the birefringence changes with other external parameters. Also differences in phase velocity with polarization generally imply differences in group velocity that result in a form of signal distortion known as polarization mode distortion. Under certain circumstances, polarization mode distortion could represent a significant contribution to the total bandwidth limitation of a single mode fiber.

In other cases it will be helpful to use fiber designed to have extremely high values of inherent birefringence. Externally induced birefringence is then much less significant and light entering the fiber with a properly chosen input polarization will maintain that polarization over long propagation distances. Applications for high birefringence fiber include interferometric sensors and heterodyne communications systems. In each of these cases, random variations in polarization at the fiber output would represent a major source of noise. As a further enhancement of this type of fiber, it has recently been shown[1] that

the attenuation as well as the propagation constants of the two polarization states can be dramatically different, leading to a truly single polarization fiber.

Before examining methods for characterizing these fibers it will be useful to review the factors that contribute to fiber birefringence. Further detail can be found in a recent paper on the development of high and low birefringence fibers.[2]

If the cross section of the fiber is taken to be an ellipse, light linearly polarized with its electric field parallel to the minor axis has a higher phase velocity (smaller propagation constant) than the orthogonal linear polarization.[3] The magnitude of this linear birefringence increases with the ellipticity and with the refractive index difference (Δn) between the core and the cladding. This dependence on Δn means that fiber desinged to have a very low birefringence will typically have a low Δn and thus a relatively large core. Similarly, high birefringence elliptical fiber designs usually involve large values of Δn and very small core dimensions. The birefringence also depends on the normalized frequency (V) of the fiber, reaching a maximum at a V-value slightly less than the cut-off of the second mode.

Variations in the thermal expansion coefficient of fused silica with dopant and dopant concentration inevitably result in stress which alters the refractive index through the stress-optic (photoelastic) effect.[4] In a perfectly axially symmetric structure this stress would be radially directed and axially symmetric and would not therefore lead to birefringence. However, if the core is slightly elliptical the effect of stress will be anisotropic and will add algebraically to the linear birefringence resulting from ellipticity alone. To achieve low birefringence fiber one chooses dopants and structures that minimize differences in thermal expansion coefficients.[5] To achieve high birefringence fiber one may choose dopants that enhance these effects and may, as well, use other techniques to increase the azimuthal dependence of the stress.[6]

The direction of the axes of ellipticity or of the stress induced birefringence may well vary along the fiber, even in a straight, unperturbed fiber; this will modify the apparent macroscopic birefringence. It is, in fact, possible to eliminate effectively the intrinsic linear birefringence by fabricating the fiber in such a way that the axes of birefringence rotate with a pitch much greater than the intrinsic beat length (spun fiber).[7] In such a fiber the observed birefringence is almost entirely the result of externally applied stress.

Bending introduces linear birefringence with the fast axis in the plane of the bend, having a magnitude

$$B_b \approx 0.14 \frac{r^2}{R^2} \text{ or } \Delta\beta_b \approx \frac{0.85}{\lambda} \frac{r^2}{R^2} \text{ rad/m}$$

where r is the radius is the radius of the fiber, R is the radius of the bend, and λ is the wavelength in meters.[8] Furthermore, if the fiber is under longitudinal tension when bent, it incurs an additional ("tension-coiled") birefringence[9] having the same fast axis as bend birefringence and given by

$$B_{tc} \approx 0.49 \frac{r}{R} \text{ or } \Delta\beta_{tc} \approx \frac{3.1}{\lambda} \frac{r}{R} \epsilon_z \text{ rad/m}$$

where ϵ_z is the relative fiber elongation. A one-dimensional compressive force applied to a fiber normal to its axis produces a linear birefringence with the fast axis parallel to the applied force,[10] given by

$$B_p \approx 4.8 \times 10^{-12} \frac{f}{r} \text{ or } \Delta\beta_p \approx \frac{3.0 \times 10^{-11}}{\lambda} \frac{f}{r} \text{ rad/m}$$

where f is the applied force per unit length in newtons/m and r is in meters.

Twisting of a fiber causes a rotation of the axes of any linear birefringence that may be present; furthermore, it produces torsional stresses that give rise to circular birefringence. The net result of twisting depends on the rate of twist relative to the linear birefringence present.[11] If the linear birefringence is negligible the stress produces a rotation of

$$\Omega = g\xi$$

where g is a constant (≈ 0.073 for silica) and ξ is the twist rate. At the other extreme, if the linear birefringence is very large, the torsional stress is of little consequence, but rotation of the axes produces a rotation equal to the twist rate,

$$\Omega = \xi.$$

Intermediate cases require more complex descriptions.

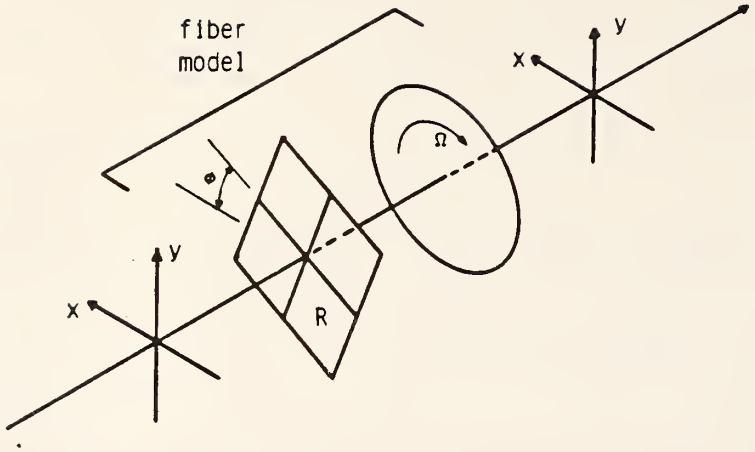

Figure 1. A simple model for the birefringence of an optical fiber consists of a linearly birefringent element of retardance R and orientation ϕ plus a circularly birefringent element (rotator) with rotation Ω.

An arbitrary fiber, exhibiting (potentially) all of the above effects at various points along its length could, in principle, be described by a model consisting of a series of differential optical retarders with varying retardation and orientation, interspersed with differential optical rotators (circular retarders) of varying strength. A prediction of the evolution of the polarization state along such a fiber would be very difficult. Fortunately, in many cases the microscopic characteristics of the fiber are much less important than its macroscopic or end-to-end characteristics. Furthermore, many of those cases where it is important to know the polarization state as a function of length involve high birefringence fibers where a single effect (or a small number of effects) predominates.

For end-to-end characterization it is possible to use a very simple model, for it can be shown in general that any system composed solely of linear retarders and rotators can be represented by a single retarder with an appropriate orientation and a single rotator.[12] The parameters of this model are the orientation of the retarder relative to an external coordinate system (ϕ), the value of the retardance (R), and the value of the rotation (Ω) (fig. 1). This simple characterization is most suitable for moderate to low birefringence fibers where specimens shorter than one beat length can be evaluated.

The model has at least one pair of orthogonal linear input polarization states for which the output state is also linear. These correspond to the axes of the retarder and are sometimes called principal axes. Less obviously, there is also a pair of generally elliptical input states that appear unaltered at the output and are generally called eigenstates. The existence of principal axes and eigenstates does not necessarily imply, however, that light launched into one of those states will not pass through other intermediate states during propagation.

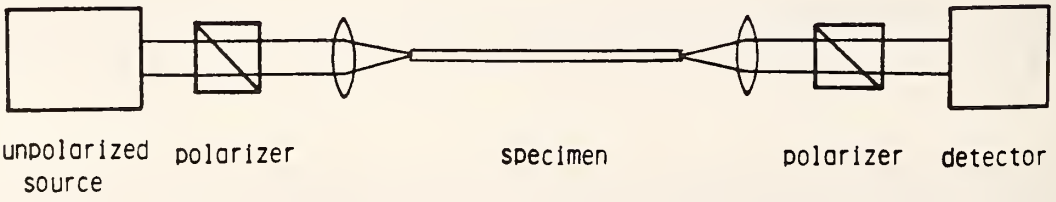

Figure 2. A basic system for birefringence measurements.

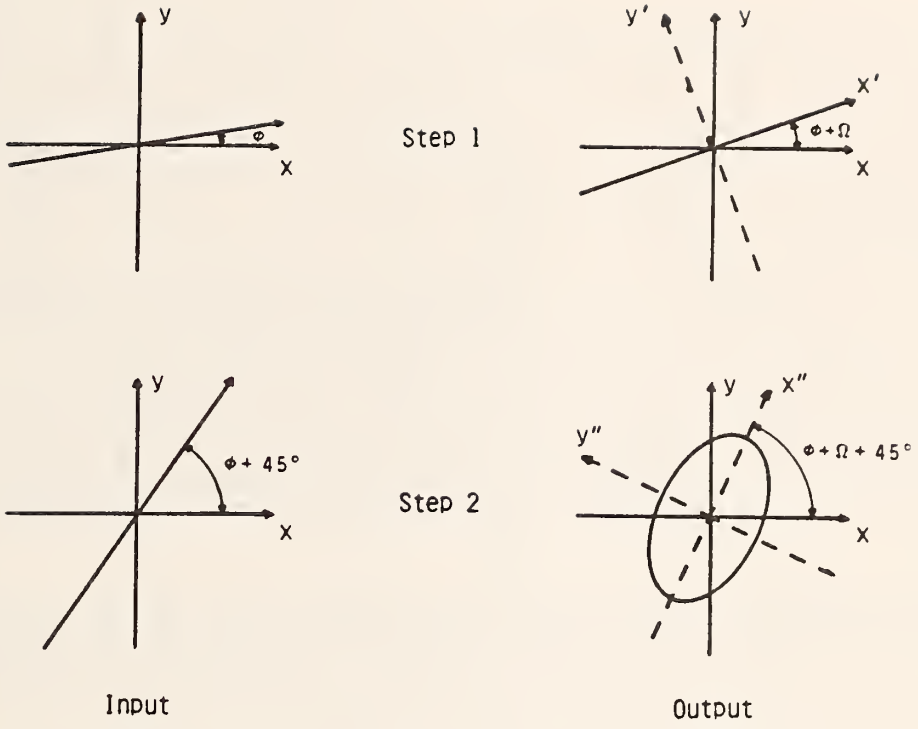

Figure 3. The first step in determining the parameters of the model is to rotate the input and output polarizers until a linear-input--linear-output condition is obtained. This gives ϕ and Ω. The second step is to launch linearly polarized light at 45° to the axes of the retarder element. This gives an elliptically polarized output from which R can be obtained.

The simplest apparatus for determining ϕ, R, and Ω is shown in figure 2. It consists of an unpolarized (or perhaps circularly polarized) light source, two low birefringence lenses (usually microscope objectives), two high quality polarizers, and a photodetector. With a specimen in place the polarizers are rotated iteratively until a null in the transmission occurs. In this linear-input-linear-output condition, the orientation of the input polarizer corresponds to one of the principal axes at orientation ϕ, and the output polarizer orientation corresponds to $\phi + \Omega + 90°$ (output polarizer parallel to y' in fig. 3).

Obtaining the retardance R is only slightly more difficult. The input polarizer is first rotated by exactly 45° so that the field components parallel to each of the principal axes are identical. Under these circumstances the output state will be an ellipse with its major or minor axis rotated by $\phi + \Omega + 45°$ from the positive x axis. The electric field components in the x' and y' direction are equal but differ in phase by R:

$$E_{x'} = Ee^{i\frac{R}{2}}; \quad E_{y'} = Ee^{-i\frac{R}{2}}.$$

A standard polarimetric method for determining R is to measure the power transmitted by a polarizer parallel to each axis of the ellipse ($I_{x"}$ and $I_{y"}$). With some simple mathematics one finds,

$$I_{x"} \equiv E^2_{x"} = \left(\frac{1}{\sqrt{2}} E_{x'} + \frac{1}{\sqrt{2}} E_{y'}\right)^2 = \frac{E^2}{2}\left(e^{i\frac{R}{2}} + e^{-i\frac{R}{2}}\right)^2 = 2E^2\cos^2\frac{R}{2}$$

$$I_{y"} \equiv E^2_{y"} = \left(-\frac{1}{\sqrt{2}} E_{x'} + \frac{1}{\sqrt{2}} E_{y'}\right)^2 = \frac{E^2}{2}\left(-e^{i\frac{R}{2}} + e^{-i\frac{R}{2}}\right)^2 = 2E^2\sin^2\frac{R}{2}$$

and

$$\frac{I_{x''} - I_{y''}}{I_{x''} + I_{y''}} = \cos R.$$

All three parameters in the model are thus determined, but subject to several ambiguities. Neither R nor Ω can be distinguished from values related by $\pm n2\pi$ radians. Furthermore, it was not determined whether the principal axis at the input angle ϕ was a fast or slow axis, which is equivalent to noting that the sign of R cannot be determined from the symmetric cosine function, or that values of Ω related by $\pm n\pi$ radians are indistinguishable. Finally, since the cosine function is dual valued within any one period, values of R are indistinguishable from those of $2\pi - R$ radians.

When these ambiguities cannot be resolved through a priori estimates of some of the values they may often by distinguished by multiple cutback methods. In this case the parameters ϕ, R, and Ω are determined for a successively shortened fiber and a uniform length dependence is assumed. This cut-back technique is widely applicable except that as a practical matter it becomes difficult when the birefringence is extremely high.

Alternatively, R may be determined from the output polarization ellipse (step 2, fig. 3) using a calibrated Babinet-Soleil compensator, a device that can be adjusted for any retardance. The compensator is placed between the fiber and the output polarizer and is oriented with its fast or slow axis parallel to x'. The output polarizer is oriented parallel to y". When the compensator is adjusted for a null in the detected signal the birefringence added to the system by the compensator is equal in magnitude and opposite in sign to R. (Equivalently, and sometimes more conveniently, the compensator may be placed at the input with its axes parallel to the principal axes.)

Compared to the first approach, the use of the compensator has several advantages. The measurement is generally simpler to perform. It yields much less ambiguous results; only the $\pm n2\pi$ ambiguities remain and the cut-back technique is therefore more easily employed. And finally, the compensator technique does not depend on source or coupling stability since only nulls and not relative power levels are required. A disadvantage is that the compensator used must be of high quality and carefully calibrated.

A third possibility for obtaining R from the output polarization ellipse is to place a quarter wave plate just before the output polarizer with its fast axis parallel to x". Under these circumstances, the elliptical state is converted to a linear state at an angle with respect to the positive x axis of $\phi + \Omega + 45° + \frac{R}{2}$. Ambiguities other than $\pm n2\pi$ do not appear.

It is easier to use the quarter-wave plate than a compensator, and this approach has been used to develop an automated measurement system.[14] However, a single Babinet-Soleil compensator can be calibrated and used at any wavelength of interest while separate quarter wave plates must be used for each wavelength.

Various types of polarization modulators have been used in systems similar to that outlined above to study crystals and other anistropic media. Generally the motivation for this approach is greater sensitivity, especially for low values of birefringence. One such technique that has been successfully applied to fiber characterization is the use of a photoelastic modulator.[15] A suitable device is a block of fused silica to which a piezoelectric transducer has been attached in such a way as to provide a uniaxial stress normal to the direction of propagation. The result is a linearly birefringence element, the retardance of which may be modulated at rates of several tens of kilohertz. A convenient method of using the modulator is to attach it directly to the output polarizer so that the two elements rotate together with a fixed relative orientation of 45°. The detected signal in general contains harmonics of the frequency at which the modulator is driven. It may be shown that

$$W_1 \propto \sin R \sin 2(\theta_1 - \phi)$$

and

$$W_2 \propto [\cos 2(\theta_1 - \phi) \sin (2\theta_2 - 2\Omega) + \cos R \sin 2(\theta_1 - \phi) \cos (2\theta_2 - 2\Omega)]$$

where W_1 is the magnitude of the modulation component at the drive frequency, W_2 is the corresponding value at twice the drive frequency, θ_1 is the angle of the input polarizer and θ_2 is the angle of the modulator axis, with respect to the x axis.

The procedure then simply consists of nulling the W_1 component by adjusting the input polarizer (W_1 does not depend on the orientation of the modulator-output polarizer combination) and then nulling the W_2 component to obtain Ω. To determine R one rotates the input

polarizer by 45° ($\theta_1 - \phi = +45°$). Then $W_1 \propto \sin R$ and $W_2 \propto \cos R$ from which R can be determined, again only with the $\pm n2\pi$ ambiguity.[1]

In certain cases, it may be desirable or necessary to evaluate unambiguously the evolution of polarization states along a fiber without changing its length. Examples include in situ measurements of low birefringence fiber where external stress may be significant and the characterization of very high birefringence fiber where cut-back techniques are impractical.

One approach in these cases is another class of modulation techniques in which the birefringence of the fiber itself is modulated at a point along its length and the corresponding change in polarization state at the output is determined. The essential basis for this approach is that in a system consisting of linearly and circularly birefringent elements the change in output state resulting from a local change in polarization state depends only on local parameters and not on the properties of the system preceding or following the point of modulation. Modulators inducing either linear birefringence or circular birefringence in the fiber have been used for this purpose.[15,16]

Circular birefringence may be introduced into a fiber by using a small electromagnet that provides a field parallel to the fiber axis.[16] The magnitude of the resulting change in polarization (Faraday effect) depends on the polarization state at the point of modulation. It is most effective when the polarization state is linear and is zero for a circular polarization. Therefore, by moving the magnet along the fiber one may, for example, directly determine the beat length as twice the distance separating points of maximum modulation. This technique is easy to employ and extremely useful for high birefringence fiber, though for extremely short beat lengths (L_p < 1 mm) it may be difficult to design a magnet to give sufficient spatial resolution.

A linear birefringence may be introduced into a fiber either by applying a large electric field normal to the axis (Kerr effect)[16] or by applying a tranverse stress[16] as described above. The beat length can be obtained, again by longitudinal translation of the modulation. Furthermore, since the azimuth of the induced birefringence can be varied it is possible to deduce the exact polarization state at the point of modulation.

Another technique that is widely used for nondestructive determiniations of the beat length is the observation of the length dependence of Rayleigh scattering normal to the axis.[18] If linearly polarized light is launched into the fiber at 45° to the principal axes and if the scattered light is viewed at the same azimuth, a series of bright and dark bands will appear along the length of the fiber. This results from the fact that the angular dependence of Rayleigh (dipole) scattering passes through a null along the dipole axis and a maximum normal to the dipole axis. Bright regions appear where the direction of observation is normal to the local plane of polarization, recurring with a periodicity equal to a beat length. This method is best suited to the evaluation of moderately high birefringence fibers (L_p ~ a few millimeters) in the visible region of the spectrum where the scattering is relatively large and the light and dark bands are easily seen.

Rayleigh scattering can also be used to determine the beat length using a modified form of optical time domain reflectometry (OTDR) known as polarization OTDR, or POTDR.[19] If a polarized probe pulse is used the backscattered light will show a time dependent polarization state that depends on the polarization state of the probe pulse at the point of scattering. The temporal periodicity observed in the backscattered light can therefore be directly related to the beat length.[20] A lack of sufficiently short pulses and pulse broadening within the fiber generally limit this technique to the measurement of fairly long beat lengths.

A final possiblity for studying the properties of high birefringence fibers nondestructively involves observing changes in the output state as the wavelength is scanned. For a length of fiber ℓ the total phase difference (retardance) between the orthogonal states is

$$R = \Delta\beta\ell \equiv kB\ell \equiv \frac{2\pi}{\lambda} B\ell.$$

For a frequency change Δk the corresponding change in retardance, ΔR, is

$$\Delta R = \ell\frac{d(\Delta\beta)}{dk} \Delta k - \ell[B + k \frac{dB}{dk}] \Delta k.$$

Assuming a fixed input state, the output state varies periodically with wavelength, the period corresponding to $\Delta R = 2\pi$.

If the dispersion of the birefringence (dB/dk) were negligibly small or known, it would be possible to measure unambiguously the fiber birefringence in this way. Unfortunately, dB/dk is generally not negligible.[21] Furthermore, it depends in a complicated way on the mechanisms producing the birefringence and so is not readily predictable. One may thus reliably determine only the the relative change in birefringence with wavelength in this way.[22]

Such a relative measurement does allow a prediction of the polarization mode distortion,[22] since the difference in group delays of the two states is given by

$$\Delta\tau_g = \frac{\ell}{c}\frac{d(\Delta\beta)}{dk}.$$

In high birefringence fibers this expression provides a good estimate of the pulse spreading that is measured on long fiber lengths. In low birefringence fiber the above expression usually overestimates substantially the observed pulse spreading. This is because in low birefringence fibers significant coupling between the orthogonal states serves to equalize the propagation times.

Acknowledgment

The author is greatly indebted to members of the Optical Communications Research Group at the University of Southampton, especially Dr. A. J. Barlow, for numerous fruitful discussions on this subject. Research at NBS on the polarization characteristics of optical fiber is supported in part by the Department of Defense, Calibration Coordination Group.

References

1. J. R. Simpson, F. M. Sears, J. B. MacChesney, R. H. Stolen, W. Pleibel, and R. E. Howard, "Single polarization fiber," Digest, OFC 83, New Orleans.
M. P. Varnham, D. N. Payne, R. D. Birch, and E. J. Tarbox, "Single polarization operation of highly birefringent optical fiber," Electron. Lett., Vol. 18, pp. 246-247. 1983.

2. D. N. Payne, A. J. Barlow, and J. J. Ramskov-Hansen, "Development of low and high birefringence optical fiber," IEEE J. Quantum Electron., Vol. QE-18, pp. 477-488. 1982.

3. R. B. Dyott, J. R. Cozens, and D. G. Morris, "Preservation of polarization in optical fiber waveguides with elliptical cores," Electron. Lett., Vol. 15, pp. 380-382. 1979.
J. D. Love, R. A. Sammut, and A. W. Snyder, "Birefringence in elliptically deformed optical fibers," Electron. Lett., Vol. 15, pp. 615-616. 1979.

4. A. J. Barlow and D. N. Payne, "The stress optical effect in optical fibers," IEEE J. Quantum Electron., Vol. QE-19, pp. 834-839. 1983.

5. S. R. Norman, D. N. Payne, M. J. Adams, and A. M. Smith, "Fabrication of single mode optical fibers with extremely low polarization birefringence," Electron. Lett., Vol. 15, pp. 309-311. 1979.

6. T. Okoshi and K. Oyamada, "Single polarization single mode optical fiber with refractive index pits on both sides of core," Electron. Lett., Vol. 16, pp. 712-713. 1980.
T. Hosaka, K. Okamoto, Y. Mika, Y. Sasaki, and T. Edahiro, "Low loss single polarization fibers with asymmetrical strain birefringence," Electron. Lett., Vol. 17, pp. 530-531. 1981.
R. D. Birch, D. N. Payne, and M. P. Varnham, "Fabrication of polarization maintaining fibers using gas-phase etching," Electron. Lett., Vol. 18, pp. 1036-1038. 1982.
T. Katsuyama, H. Matsumura, and T. Suganuma, "Los loss single polarization fibers," Electron. Lett., Vol. 17, pp. 473-474. 1981.

7. A. J. Barlow, D. N. Payne, M. R. Hadley, and R. J. Mansfield, "Production of single mode fibers with negligible intrinsic birefringence and polarization mode dispersion," Electron. Lett., Vol. 17, pp. 725-725. 1981.

8. R. Ulrich, S. C. Rashleigh, and W. Eickhoff, "Bending induced birefringence in single mode fibers," Opt. Lett., Vol. 5, pp. 273-275. 1980.

9. S. C. Rashleigh and R. Ulrich, "High birefringence in tension coiled single mode fibers," Opt. Lett., Vol. 5, pp. 354-356. 1980.

10. J. Sakai and T. Kimura, "Birefringence and polarization characteristics of single mode optical fibers under elastic deformations," IEEE J. Quantum Electron., Vol. QE-17, pp. 1041-1051. 1981.
A. M. Smith, "Single mode fiber pressure sensitivity," Electron. Lett., Vol. 16, pp. 773-774. 1980.

11. R. Ulrich and A. Simon, "Polarization optics of twisted single mode fibers," Appl. Opt., Vol. 18, pp. 2241-2251. 1979.

12. F. P. Kapron, N. F. Borrelli, and D. B. Keck, "Birefringence in dielectric optical waveguide," IEEE J. Quantum Electron., Vol. QE-8, pp. 222-225. 1972.

13. R. C. Jones, "A new calculus for the treatment of optical systems," J. Opt. Soc. Am., Vol. 31, pp. 388-493. 1941.

14. A. M. Smith, "Automated birefringence measurement system," J. Phys. E: Sci. Instrum., Vol. 21, pp. 927-930. 1979.
15. A. J. Barlow and D. N. Payne, "Measurement of fiber polarization properties using a photo-elastic modulator," Technical Digest, Symp. Opt. Fiber Meas. 82, Boulder, CO.
16. A. Simon and R. Ulrich, "Evolution of polarization along single mode fiber," Appl. Phys. Lett., Vol. 31, pp. 517-520. 1977.
17. N. Chinone and R. Ulrich, "Elasto-optic polarization measurements in optical fiber," Opt. Lett., Vol. 6, pp. 16-18. 1981.
18. A. Papp and H. Harms, "Polarization optics of index gradient optical waveguide fibers," Appl. Opt., Vol. 14, pp. 2406-2411. 1975.
I. P. Kaminow, "Polarization in optical fibers," IEEE J. Quantum Electron., Vol. QE-17, pp. 15-32. 1981.
19. A. J. Rogers, "Polarization optical time domain reflectometry," Electron. Lett., Vol. 16, pp. 489-490. 1980.
20. M. Nakazawa, T. Horiguchi, M. Tokuda, and N. Uchida, "Polarization beat length measurement in a single mode optical fiber by backward Rayleigh scattering," Electron. Lett., Vol. 17, pp. 513-515. 1981.
B. Y. Kim and S. S. Choi, "Backscattering measurement of bending induced birefringence in single mode fibers," Electron. Lett., Vol. 17, pp. 193-194. 1981.
21. S. C. Rashleigh, "Measurement of fiber birefringence by wavelength scanning: effect of dispersion," Opt. Lett., Vol. 8, pp. 336-338. 1983.
S. C. Rashleigh, "Wavelength dependence of birefringence in highly birefringent fibers," Opt. Lett., Vol. 7, pp. 294-296. 1982.
22. S. C. Rashleigh, "Polarization mode dispersion in single mode fibers," Opt. Lett., Vol. 3, pp. 60-62. 1978.

APPENDIX G

PROGRESS IN THE DESIGN OF OPTICAL FIBER SENSORS FOR THE MEASUREMENT OF PULSED ELECTRIC CURRENTS

(Proc. Workshop on Measurement of
Electrical Quantities in Pulse Power Systems,
March 1986, Gaithersburg, MD)

PROGRESS IN THE DESIGN OF OPTICAL FIBER SENSORS FOR THE MEASUREMENT OF PULSED ELECTRIC CURRENTS

G. W. Day
National Bureau of Standards
Boulder, CO 80303

L. R. Veeser and G. I. Chandler
Los Alamos National Laboratory
Los Alamos, NM 87545

R. W. Cernosek
Sandia National Laboratory
Albuquerque, NM 87185

ABSTRACT

The state of the art in the design of fiber sensors for pulsed electric currents is reviewed. Some of the more useful configurations are described and compared. Transfer functions are computed and used to illustrate the effect of linear birefringence and twisting on the characteristics of the sensors. The technique of annealing bend-induced birefringence is described and its present capabilities indicated. An analysis of the ultimate limits to noise equivalent current is given, suggesting that several orders of magnitude improvement should be obtainable.

INTRODUCTION

The measurement of pulsed electric currents must often be performed in the presence of substantial electromagnetic interference, making the use of conventional sensors difficult. Optical sensing techniques can effectively eliminate this interference.

In this paper we describe recent progress in the design of current sensors based on the Faraday effect in single-mode optical fiber. These sensors are being used successfully in several measurement systems at Los Alamos and Sandia National Laboratories where the pulse amplitudes range from about 100 A to 50 MA with durations as short as 1 μs. We anticipate that fiber current sensors can be used in a much broader range of applications, including those that require several orders of magnitude improvement in minimum detectable current.

BASIC SENSOR DESIGNS

The Faraday effect is a magnetically induced rotation of the plane of polarization of linearly polarized light (i.e., an induced circular birefringence), given by

$$\theta = V \int \vec{B} \cdot \vec{dz} \qquad (1)$$

where θ is the rotation, V is a material parameter known as the Verdet constant, $B = \mu H$ is the magnetic flux density, and z is the direction of propagation. In an optical fiber current sensor [1,2,3], one or more loops of single-mode optical fiber surround the electrical conductor. Then, since

$$\oint \vec{H} \cdot \vec{dz} = I \qquad (2)$$

about any closed path around a conductor carrying a current I, the plane of polarization of light propagating in the fiber is rotated by an amount

$$\theta = \mu VNI, \qquad (3)$$

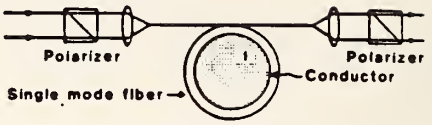

1. Schematic of an optical fiber current sensor. Linearly polarized light passing through one or more turns of fiber surrounding the conductor is rotated in proportion to the current. A polarizer at the output allows the rotation to be detected as a change in transmittance.

where N is the number of turns of fiber around the conductor. For a single turn of fused silica fiber ($\mu = \mu_0$) the ratio of rotation to current is approximately 265 deg/MA at a wavelength of 633 nm.

To measure this rotation the fiber is usually placed between polarizers and the transmitted light monitored with a high-speed photodiode (Fig. 1). The transmittance of the sensor as a function of current depends on the relative orientation of the polarizers. For two important cases, namely crossed polarizers and polarizers at 45 deg to each other, the transfer functions are given by (Fig. 2)

$$R(I) = \frac{1}{2}(1 - \cos 2\mu_0 VNI) \qquad (4)$$

and

$$R(I) = \frac{1}{2}(1 \pm \sin 2\mu_0 VNI), \qquad (5)$$

respectively.

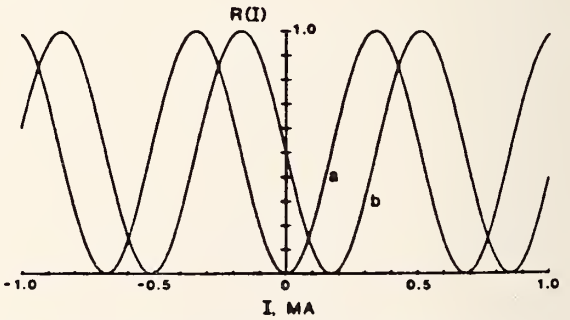

2. Computed transfer functions for the sensor shown in Fig. 1 for the case of polarizers aligned for minimum transmittance at zero current (a) and for polarizers oriented for a transmittance of 0.5 at zero current, i.e., the output polarizer at 45 deg to the minimum transmittance orientation (b).

When the currents to be measured are small, it is generally preferrable to use the latter case (Eq. (5)) to take advantage of the greater sensitivity. A further, two fold, increase in sensitivity can be obtained by using a polarizing beamsplitter at the output, detecting both the +45 and -45 deg components, and taking the difference electronically. From Eq. (5), the transfer function then becomes

$$R(I) = \sin 2\mu_0 VNI. \qquad (6)$$

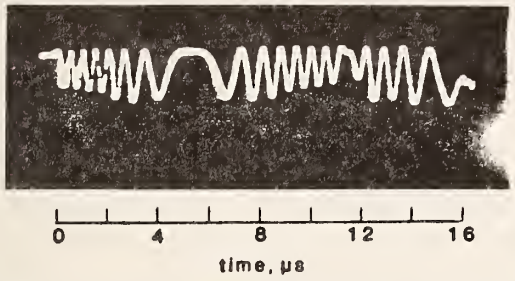

3. Raw data from a sensor similar to that shown in Fig. 1. The current was produced by a capacitor bank discharged into a low-impedance load and approximates a damped sinusoid with a peak amplitude of about 2.4 MA.

When the currents to be measured are large, the multivalued nature of this transfer function may be a problem. Often, however, the general shape of the waveform is known in advance so that ambiguities can be resolved by inspection. Examples of such cases are illustrated in Figs. 3 and 4. Figure 3 shows raw data from an experiment in which a capacitor bank was discharged into a very low impedance load. With the prior knowledge that the current waveform should approximate a damped sinusoid, it is easy to recognize the peak of the first half cycle at about 5.5 μs and the first zero-crossing at about 11.5 μs. Figure 4 shows some processed data from a two-stage, explosively driven flux compression generator. The current was initiated by capacitive discharge yielding a peak current of about 1 MA. After one stage of flux compression the peak current increased to about 10 MA (Fig. 4a) and after the second stage to more than 50 MA (Fig. 4b). Good agreement between the optical sensors and conventional sensors (Rogowski coils) also used in this experiment was observed except that the Rogowski coils in the second stage failed slightly earlier than the optical sensor.

When the general shape of the current waveform is not known in advance or when the data are processed automatically, a two polarization detection scheme can be used to resolve ambiguities [4]. Figure 5 shows such a system. The output of the fiber is split with a polarization-independent beamsplitter, allowing the detection of two separate polarization components. One polarizer/detector combination is oriented for minimum transmittance at zero current and therefore provides a cosinusoidal transfer function of the form of Eq. (4). The other polarizer/detector combination is oriented for a transmittance of 0.5 (i.e., at 45 deg to the first) and provides a sinusoidal transfer function of the form of Eq. (5). By examining the sign of the sine and cosine signals the rotation can be determined unambiguously within the range $-90 < \theta < +90$. Furthermore, if the signals are sampled at least once within each 90 deg of rotation, multiple rotations can be identified [4].

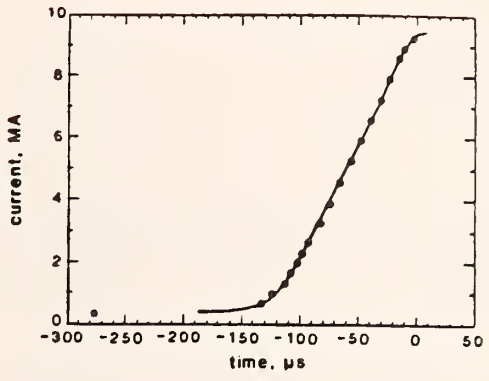

(a)

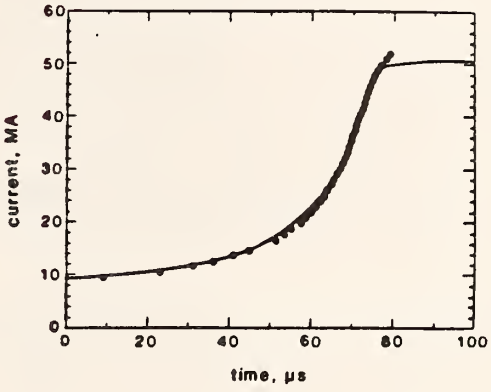

(b)

4. Processed data from a two stage high-explosive-driven flux compression generator. The upper curve is the current measured at the output of the first stage; the lower curve is the current at the output of the second stage. Time zero is the firing of the second stage. Points are from the optical sensor; solid lines are from a Rogowski coil. [After L. R. Veeser, et al. Proc. SPIE 506, San Diego, CA, 1984.]

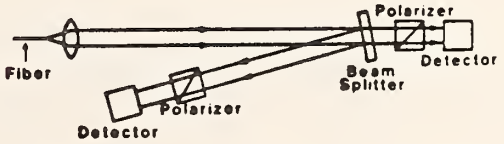

5. A two-polarization detection scheme that provides both sinusoidal and cosinusoidal transfer functions and therefore allows resolution of ambiguities resulting from the multivalued transfer function.

A sensor configuration that avoids the use of polarizers entirely is the Sagnac interferometer [5] shown in Fig. 6. As in an optical fiber gyroscope, a coupler divides the input light into equal amplitude, counter-propagating waves in a fiber coil. The coupler, like a beamsplitter in an interferometer, introduces a 90 deg phase shift between its two output beams. Therefore, if the field acts on the counter-propagating waves reciprocally, the two components combining at the output port cancel and all the power is returned to the input port. Any nonreciprocal effects in the coil, specifically those produced by rotation

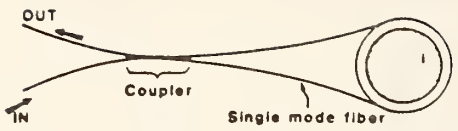

6. Schematic of a Sagnac interferometer used as a current sensor. No polarizers are required. The transfer function, which is identical to that shown in Fig. 2a, is independent of the input polarization state.

about the coil axis, a magnetic field, or time dependent effects, cause power to appear at the output port. For the case of Faraday rotation, the transfer function can be obtained either by considering the change in polarization state of the counter-propagating beams or by resolving the input state into orthogonal circular states and considering the induced phase shifts. The result, somewhat surprisingly, is independent of input polarization state, and is identical to that found for a coil placed between crossed polarizers (Eq. (4)).

In all of the configurations described above, the induced rotation or circular birefringence is converted to a change in transmittance. In some cases it may be desirable to observe the induced birefringence directly. This can be done using a rotating linear input polarization state [6,7,8].

A rotating linear polarization state is equivalent to orthogonal circular polarization states shifted in (optical) frequency by the rotation rate. The induced circular birefringence produced by the magnetic field can therefore be observed as a change in phase of the rotating linear polarization.

High rotation rates are most easily produced by starting with frequency shifted, orthogonally linearly polarized beams which can be produced by Zeeman splitting of a gas laser [7] or acousto-optic modulation [8]. When passed through a quarter wave plate the desired rotating linear polarization is produced (Fig. 7). Changes in the phase of the rotation can be observed by detecting the input and output signals through linear polarizers and using standard phase measurement electronics.

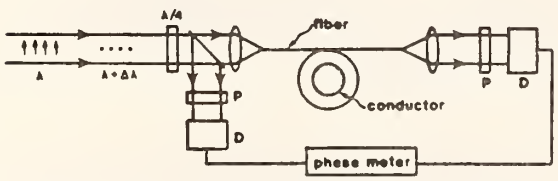

7. Schematic of a sensor using a rotating input polarization. Two input signals, differing in optical frequency by $\Delta\lambda$ and having orthogonal linear polarizations, are passed through a quarter wave plate to yield the required input state.

A particular advantage of this technique is that it can be used to raise the detection frequency above the range where laser noise dominates. Also, since most phase meters provide both sine and cosine outputs, ambiguities arising from the multivalued transfer function are more easily resolved than with the two-detector method described above.

EFFECT OF LINEAR BIREFRINGENCE IN THE FIBER

The sensor characteristics described in the preceeding section can be achieved only when, in the absence of applied fields, the propagation characteristics of the fiber are independent of polarization state. This is not, in general, a good assumption. Indeed, the primary difficulty with fiber current sensors is that linear birefringence in the fiber, resulting from inherent geometrical imperfections and stress or induced by applied stress, can seriously distort the transfer function.

Inherent linear birefringence can be effectively eliminated using certain manufacturing techniques. Birefringence resulting from applied stress, particularly from bending, remains a problem. Bend-induced linear birefringence can be predicted analytically [9] and is highly reproducable [10]. It is given by

$$\Delta\beta = K_\lambda \, r^2/R^2, \tag{7}$$

where r is the fiber radius, R is the bend radius, and K_λ is a parameter equal to about 7.7×10^7 deg/m for silica fibers at a wavelength of 633 nm.

Faraday rotation in a linearly birefringent medium such as a fiber coil can be modeled using Jones calculus. The relationship between the input and output polarization states is given by [11]

$$\begin{vmatrix} E_x(z) \\ E_y(z) \end{vmatrix} = \begin{vmatrix} \cos\frac{\phi z}{2} - j\frac{\Delta\beta}{\phi}\sin\frac{\phi z}{2} & -\frac{2F}{\phi}\sin\frac{\phi z}{2} \\ \frac{2F}{\phi}\sin\frac{\phi z}{2} & \cos\frac{\phi z}{2} + j\frac{\Delta\beta}{\phi}\sin\frac{\phi z}{2} \end{vmatrix} \begin{vmatrix} E_x(0) \\ E_y(0) \end{vmatrix} \tag{8}$$

where E_x and E_y are complex electric-field amplitudes, $\Delta\beta$ is the birefringence per unit length, F is the Faraday rotation per unit length, and

$$(\tfrac{\phi}{2})^2 = (\tfrac{\Delta\beta}{2})^2 + (F)^2. \tag{9}$$

Inspection of Eqs. (8) and (9) indicates that when $F \ll \Delta\beta$ the matrix in Eq. (8) approaches that of a pure linear retarder, indicating that the rotation is effectively quenched. When $F \ll \Delta\beta$ the matrix approaches that of a pure rotation (circularly birefringent) element.

This behavior can be observed in the computed transfer functions shown in Fig. 8. Figure 8a shows the transfer function of a sensor consisting of a single 3 cm diameter turn of 125 μm diameter fiber between crossed polarizers and operated at 633 nm. The bend-induced birefringence is approximately 127 deg, leading to significant distortion in the amplitude of the transfer function for rotations less than about 180 deg (about 0.7 MA). Figure 8b shows the transfer function for a 10 turn, 10 cm coil of the same fiber, in which the total birefringence is about 382 deg. In this case, both the amplitude and the periodicity of the transfer function show significant distortion.

TWISTED FIBERS

One technique for overcoming induced linear birefringence is to twist the fiber. Twisting, like the Faraday effect, induces a rotation or circular birefringence in the fiber. The magnitude of the rotation is given by

$$\Omega = g'\xi, \tag{10}$$

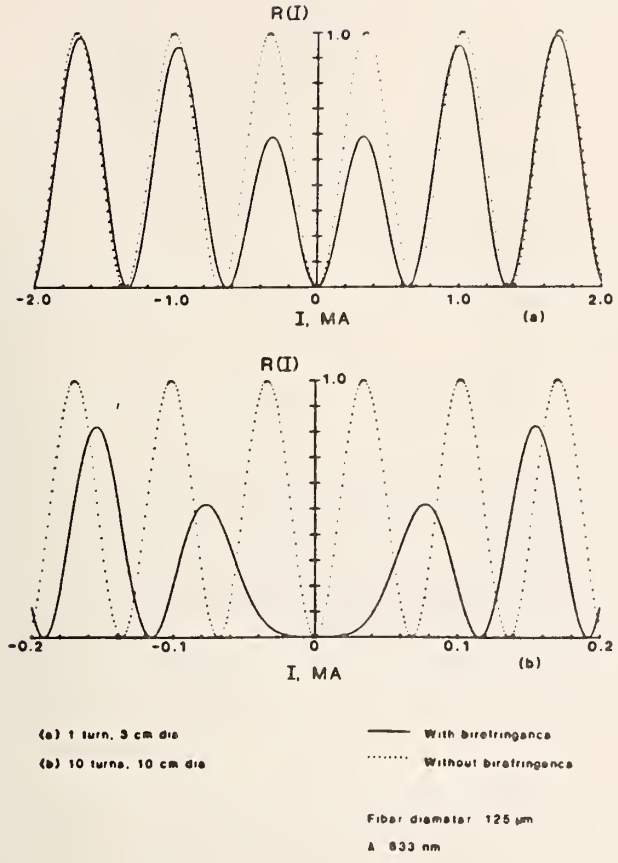

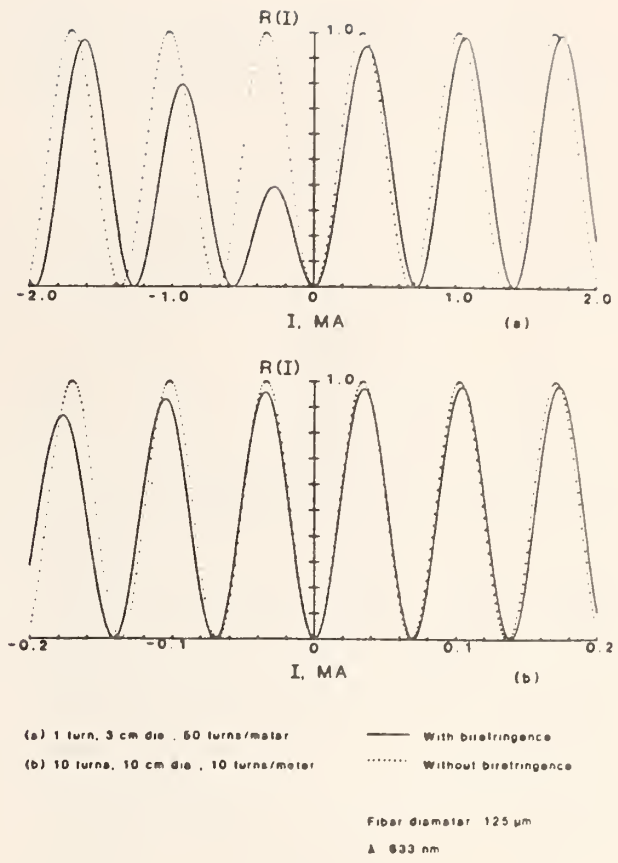

8. Computed transfer functions of fiber current sensors showing the effect of bend-induced linear birefringence in the fiber. (a) One turn, 3 cm coil diameter, 125 μm fiber diameter, 633 nm operating wavelength. (b) 10 turns, 10 cm coil diameter, 125 μm fiber diameter, 633 nm operating wavelength. The linear input polarization is aligned with one of the axes of birefringence. Dotted curves show the transfer functions that would be observed if linear birefringence were not present.

9. Computed transfer functions of the same sensors illustrated in Fig. 7 showing the effect of twisting the fiber. (a) The 3 cm diameter coil using a twist rate of 50 turns per meter. (b) The 10 cm diameter coil using a twist rate of 10 turns per meter. Dotted curves assume no linear birefringence.

where Ω is the rotation per unit length, ξ is the twist per unit length, and g' is a material parameter which at a wavelength of 633 nm is equal to about 0.08. The twist-induced rotation may be added algebraically to the magnetically-induced rotation in Eq. (8). This is illustrated in Fig. 9 which shows that the effect of twisting is, in essence, to bias the sensor away from the distorted part of the transfer function. The extent to which the transfer function can be shifted depends on the relative magnitude of the linear birefringence and twist-induced rotation per turn. Since for a rotation p given twist per unit length the twist per turn increases (linearly) with coil diameter and bend-induced birefringence per turn decreases (inversely) with the coil diameter, twisting becomes much more effective with larger coil diameters (Fig. 9b versus Fig. 9a).

Many 125 μm silica fibers will withstand twists of between 40 and 50 turns/m; with care, some will reach 80 or 90 turns/m. For small coils this may not bias the transfer function sufficiently to measure dual polarity waveforms, though for single-polarity waveforms less bias is required (Fig. 9a).

Another difficulty with twisting is that the parameter g defined in Eq. (10) is slightly temperature dependent so that when large amounts of twist are used the bias in the transfer function may drift. One technique for eliminating this problem is to twist the fiber in opposite directions about its center [2]; any drift in the twist-induced rotation in one half tends to be compensated by an equal drift in the other half. The effect of alternate twisting on the transfer function is to shift the distortion in both directions from the origin. Thus it is most useful in sensors designed to measure small currents and which therefore use polarizers oriented at 45 deg. The transfer function of a 10 turn, 10 cm diameter coil in that configuration, without twisting and with alternate twisting is shown in Fig. 10.

The effect of twisting on a Sagnac current sensor is qualitatively similar to the effect of alternate twisting in a polarimetric sensor. Specifically, the transfer function remains symmetric about zero current and the distortion caused by linear birefringence shifts away from the origin (Fig. 11). One of the most important properties of the Sagnac, its independence on input polarization state, is retained, at least for the symmetric geometry considered here.

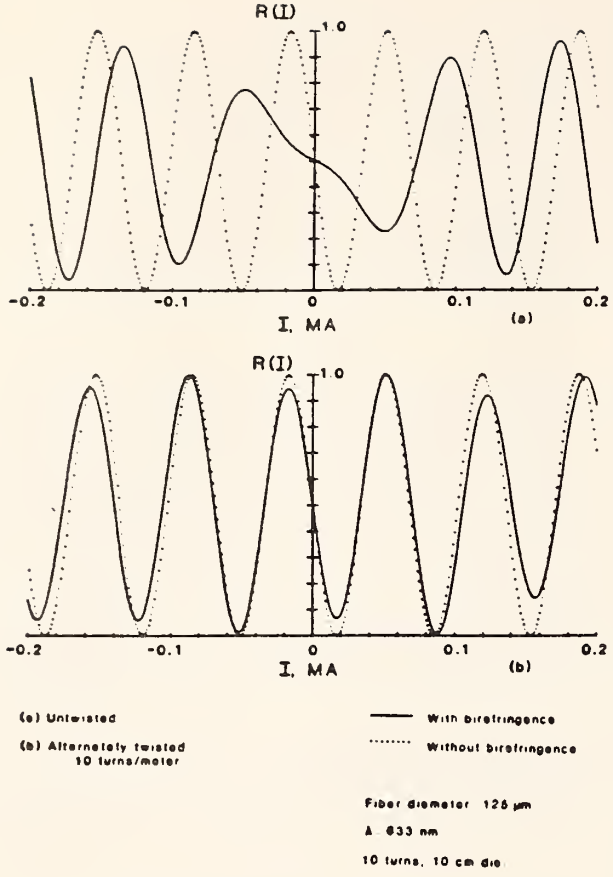

10. Computed transfer function showing the effect of alternate twisting. Coil is the same as in Figs. 8b and 9b except that the polarizers are oriented for a transmittance of 0.5 at zero current. (a) The fiber is not twisted. (b) The fiber is twisted at a rate of 10 turns per meter about its center. Dotted curves assume no linear birefringence.

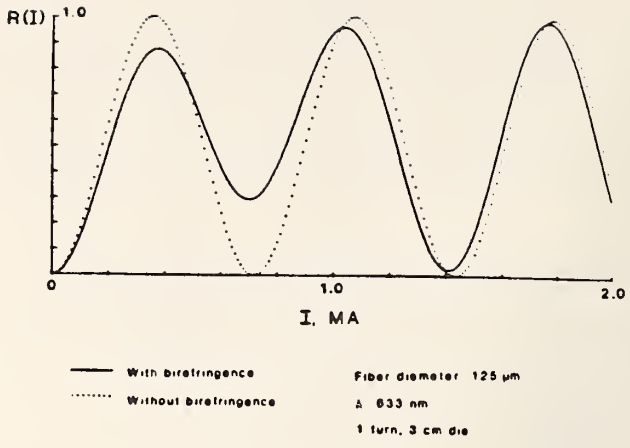

11. Computed transfer function for a Sagnac interferometer configuration showing the effect of twisting. Coil is the same as in figures 8a and 9a. Twist rate is 50 turns per meter. Dotted curve assumes no linear birefringence.

ANNEALING OF BEND-INDUCED BIREFRINGENCE

To produce multiple turn coils much smaller than 10 cm diameter, one must consider other techniques for minimizing the bend-induced birefringence. One technique that has been successful in reducing the birefringence of coils as small as 3 cm diameter is annealing at high temperatures [13].

With all coatings removed, fibers are placed into a ceramic fixture (Fig. 12) that determines their ultimate configuration. By heating the coil to temperatures in the vicinity of 700°C, maintaining those temperatures for periods of several days, and cooling slowly, the birefringence can be reduced by an order of magnitude or more. When cool, the fibers retain their coiled form without confinement and can, if desired, be removed from the annealing fixture. They are strong enough to be handled but could be encapsulated for further protection.

Most of the testing to date has been performed on coils with five and a half turns of fiber. These coils show the sensitivity that would be expected for coils without linear birefringence.

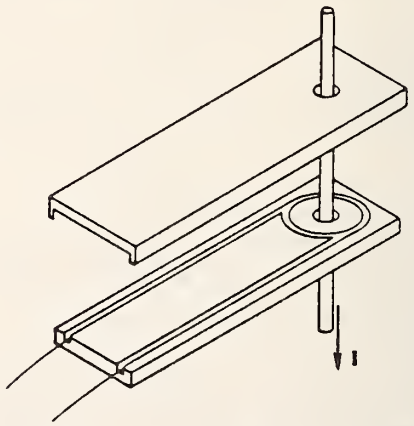

12. Fixture used for annealing bend birefringence. The material is machinable ceramic. The fiber lies in a 3 mm wide channel and makes several 3 cm diameter turns around a hole through which a conductor can be placed.

SIGNAL/NOISE ANALYSIS

It is widely believed that the relatively small Verdet constant of fiber limits the application of fiber current sensors to applications involving very large currents. Actually, if other noise sources can be reduced to the point that shot noise in the detector is the limiting factor, quite small currents can be measured.

Numerous parameters must be considered in determining the noise equivalent current of a fiber current sensor. The signal level is determined by the Verdet constant, the number of turns of fiber, the optical power propagating in the fiber, the responsivity of the detector and its load resistance. The noise level is normally set by fluctuations in the optical power (laser noise) in combination with the Johnson noise of the detector load resistance and/or the shot noise associated with the average detector current.

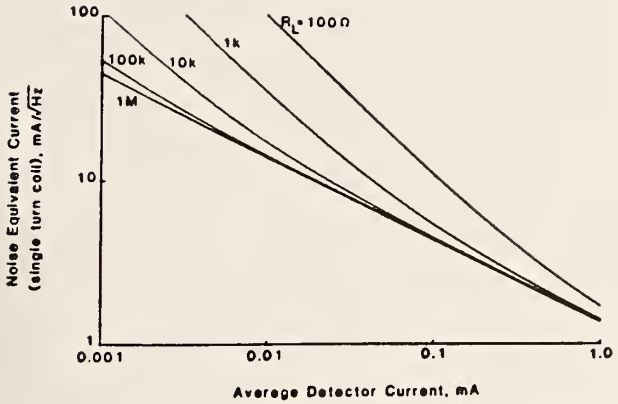

13. Computed noise equivalent current for a single-turn sensor as a function of detector load resistance and average detector current. Laser noise is assumed to be insignificant.

For a sensor based on a single turn of fiber, with a beamsplitting polarizer and two detectors at the output as described above, the noise equivalent current (NEI) can be computed as a function of average detector current and detector load resistance. The transfer function is assumed to be as given by Eq. (6). Laser noise and acoustic noise are assumed to be negligible. The result is shown in Fig. 13.

For small load resistances and small average detector currents, the slope of the curves is unity, indicating a Johnson noise limitation. For larger load resistances and/or larger average currents, the slope of the curves shifts to one half, indicating a shot noise limitation. At an average detector current of 1 mA the noise equivalent current ranges from 1 to 2 $mA/Hz^{1/2}$ for a broad range of load resistances.

An average detector current of 1 mA is probably a practical upper limit for such a sensor system. Other options for decreasing the NEI of a sensor based on this configuration are using more turns and using a fiber with a higher Verdet constant.

Increasing the number of turns of fiber to improve the sensitivity is limited by the extent to which linear birefringence can be controlled and to which a reduction in the response time of the sensor can be tolerated. Calculations similar to those presented above suggest that, using relatively large (e.g., 10 cm diam.) coils of twisted fiber, it may be practical to use more than 100 turns. Such a device should provide a NEI of the order of 10 $\mu A/Hz^{1/2}$. The transit time of a 100 turn, 10 cm diameter coil is about 160 ns.

Several research groups are now exploring the possibility of producing fibers with a higher Verdet constant [14,15,16,17]. Among the possibilities are fibers containing lead and various rare earth elements. An examination of data for various commercial bulk glasses suggests an increase in the Verdet constant of a factor of 10 to 20 might be achieved in this way. If so, it is reasonable to anticipate fiber current sensors with a NEI of the order of 1 $\mu A/Hz^{1/2}$.

ACKNOWLEDGMENTS

Research on optical fiber current sensors at the National Bureau of Standards has been supported in part by the U. S. Department of Energy through Los Alamos and Sandia National Laboratories and the Bonneville Power Administration, and also by the Empire State Electric Energy Research Corporation and the Electric Power Research Institute through the Bonneville Power Administration. This paper represents U.S. Government work and is therefore not subject to copyright.

REFERENCES

1. A. M. Smith, Polarization and magnetooptic properties of single-mode optical fiber, 17, 52-56 (1978).
2. S. C. Rashleigh and R. Ulrich, Magneto-optic current sensing with birefringent fibers, 34, 768-770 (1979).
3. A. Papp and H. Harms, Magnetooptical current transformer. 1: Principles. Appl. Opt. 19 3729-3734 (1980).
4. W. F. Hemsing, VISAR: $2^{1/2}$ minutes for data reduction, Proc. SPIE 427, San Diego, 1983.
5. H. J. Arditty, Y. Bourbin, M. Mapuchon, and C. Puech, Current sensor using state-of-the-art fiber-optic interferometric techniques, Technical Digest, Third International Conference on Integrated Optics and Optical Fiber Communications, San Francisco, 1981.
6. D. L. Mitchell and R. F. Wallis, Interband Farday Rotation in Germanium, Phys. Rev. 131, 1965-1971 (1963); E. D. Palik, The use of polarized infrared radiation in magneto-optical studies of semiconductors, Appl. Opt. 2, 527-539 (1963).
7. T. Yoshino and M. Nara, Some fiber-optic sensors using differential heterodyne method, Proc. 4th Sensor Symposium, 1984, Institute of Electrical Engineers of Japan.
8. G. I. Chandler, P. R. Forman, and F. C. Jahoda, Measurement of Faraday rotation in twisted optical fiber using rotating polarization and analog phase detection, Proc. SPIE, 566, San Diego, 1985.
9. R. Ulrich, S. C. Rashleigh, and W. Eickhoff, Bending-induced birefringence in single-mode fibers, Optics Lett., 5, 273-275 (1980).
10. G. W. Day, D. N. Payne, A. J. Barlow, and J. J. Ramskov Hansen, Design and performance of tuned fiber coil isolators, IEEE J. Lightwave Tech., LT-2, 56-60 (1984).
11. W. J. Tabor, A. W. Anderson, and L. G. VanUitert, Visible and infrared Faraday rotation and birefringence of single-crystal rare-earth orthoferrites, J. Appl. Phys., 41, 3018-3021 (1970).
12. R. Ulrich and A. Simon, Polarization optics of twisted single-mode fibers, Appl. Opt., 18, 2241-2251 (1979).
13. G. W. Day and S. M. Etzel, Annealing of bend-induced birefringence in fiber current sensors, Technical Digest, ECOC/IOOC 1985, Venice.
14. P. Sanders, D. Krohn, and M. Maklad, Faraday rotator single-mode fiber, SPIE 566, 1985, August 1985, San Diego.
15. K. Shiraishi, K. Nishino, and S. Kawakami, Temperature-insensitive fiber Faraday rotator, Appl. Opt. 24, 1896-1897 (1985).
16. K. Shiraishi, S. Sugaya, and S. Kawakami, Fiber Faraday rotator, Appl. Opt. 23, 1103-1106 (1984.
17. S. Poole and D. N. Payne, Fabrication of optical fibers containing low levels of rare earth ions, Technical Digest, ECOC/IOOC 1985, Venice.

☆ U.S. GOVERNMENT PRINTING OFFICE: 1987—775-316/65135

NBS-114A (REV. 2-8C)

U.S. DEPT. OF COMM. BIBLIOGRAPHIC DATA SHEET (See instructions)	1. PUBLICATION OR REPORT NO. NBS/TN-1307	2. Performing Organ. Report No.	3. Publication Date March 1987

4. TITLE AND SUBTITLE

Limits to the Precision of Electro-Optic and Magneto-Optic Sensors

5. AUTHOR(S)

G.W. Day, P.D. Hale, M. Deeter, T.E. Milner, D. Conrad, S.M. Etzel

6. PERFORMING ORGANIZATION (If joint or other than NBS, see instructions)

NATIONAL BUREAU OF STANDARDS
DEPARTMENT OF COMMERCE
WASHINGTON, D.C. 20234

7. Contract/Grant No.

8. Type of Report & Period Covered

9. SPONSORING ORGANIZATION NAME AND COMPLETE ADDRESS (Street, City, State, ZIP)

Bonneville Power Administration (BPA), Empire State Electric Energy Research Corp. (ESEERCO), and the Electric Power Research Institute (EPRI)

10. SUPPLEMENTARY NOTES

☐ Document describes a computer program; SF-185, FIPS Software Summary, is attached.

11. ABSTRACT (A 200-word or less factual summary of most significant information. If document includes a significant bibliography or literature survey, mention it here)

The principles of electro-optic and magneto-optic sensors suitable for use in power system applications are reviewed with particular attention to the properties of materials and components that limit the precision of such sensors. Data on a number of materials are collected and presented. For high-precision electro-optic sensors, it is recommended that crystals of point symmetry $\bar{4}3m$ be used. For high-precision magneto-optic sensors, a lead glass with a low stress-optic coefficient is recommended. Choices for other components are also suggested. For both types of sensors, a precision of roughly ± 1 percent over a 100 °C temperature range should be attainable. To achieve a precision better than that, it will be necessary to use temperature compensation techniques, several of which are proposed and discussed.

12. KEY WORDS (Six to twelve entries; alphabetical order; capitalize only proper names; and separate key words by semicolons)

current; electric power; electro-optic; fiber optic sensors; magneto-optic; measurements; power systems

13. AVAILABILITY

☒ Unlimited

☐ For Official Distribution. Do Not Release to NTIS

☒ Order From Superintendent of Documents, U.S. Government Printing Office, Washington, D.C. 20402.

☐ Order From National Technical Information Service (NTIS), Springfield, VA. 22161

14. NO. OF PRINTED PAGES 128

15. Price

NBS Technical Publications

Periodical

Journal of Research—The Journal of Research of the National Bureau of Standards reports NBS research and development in those disciplines of the physical and engineering sciences in which the Bureau is active. These include physics, chemistry, engineering, mathematics, and computer sciences. Papers cover a broad range of subjects, with major emphasis on measurement methodology and the basic technology underlying standardization. Also included from time to time are survey articles on topics closely related to the Bureau's technical and scientific programs. Issued six times a year.

Nonperiodicals

Monographs—Major contributions to the technical literature on various subjects related to the Bureau's scientific and technical activities.

Handbooks—Recommended codes of engineering and industrial practice (including safety codes) developed in cooperation with interested industries, professional organizations, and regulatory bodies.

Special Publications—Include proceedings of conferences sponsored by NBS, NBS annual reports, and other special publications appropriate to this grouping such as wall charts, pocket cards, and bibliographies.

Applied Mathematics Series—Mathematical tables, manuals, and studies of special interest to physicists, engineers, chemists, biologists, mathematicians, computer programmers, and others engaged in scientific and technical work.

National Standard Reference Data Series—Provides quantitative data on the physical and chemical properties of materials, compiled from the world's literature and critically evaluated. Developed under a worldwide program coordinated by NBS under the authority of the National Standard Data Act (Public Law 90-396). NOTE: The Journal of Physical and Chemical Reference Data (JPCRD) is published quarterly for NBS by the American Chemical Society (ACS) and the American Institute of Physics (AIP). Subscriptions, reprints, and supplements are available from ACS, 1155 Sixteenth St., NW, Washington, DC 20056.

Building Science Series—Disseminates technical information developed at the Bureau on building materials, components, systems, and whole structures. The series presents research results, test methods, and performance criteria related to the structural and environmental functions and the durability and safety characteristics of building elements and systems.

Technical Notes—Studies or reports which are complete in themselves but restrictive in their treatment of a subject. Analogous to monographs but not so comprehensive in scope or definitive in treatment of the subject area. Often serve as a vehicle for final reports of work performed at NBS under the sponsorship of other government agencies.

Voluntary Product Standards—Developed under procedures published by the Department of Commerce in Part 10, Title 15, of the Code of Federal Regulations. The standards establish nationally recognized requirements for products, and provide all concerned interests with a basis for common understanding of the characteristics of the products. NBS administers this program as a supplement to the activities of the private sector standardizing organizations.

Consumer Information Series—Practical information, based on NBS research and experience, covering areas of interest to the consumer. Easily understandable language and illustrations provide useful background knowledge for shopping in today's technological marketplace.

Order the **above** *NBS publications from: Superintendent of Documents, Government Printing Office, Washington, DC 20402.*

Order the **following** *NBS publications—FIPS and NBSIR's—from the National Technical Information Service, Springfield, VA 22161.*

Federal Information Processing Standards Publications (FIPS PUB)—Publications in this series collectively constitute the Federal Information Processing Standards Register. The Register serves as the official source of information in the Federal Government regarding standards issued by NBS pursuant to the Federal Property and Administrative Services Act of 1949 as amended, Public Law 89-306 (79 Stat. 1127), and as implemented by Executive Order 11717 (38 FR 12315, dated May 11, 1973) and Part 6 of Title 15 CFR (Code of Federal Regulations).

NBS Interagency Reports (NBSIR)—A special series of interim or final reports on work performed by NBS for outside sponsors (both government and non-government). In general, initial distribution is handled by the sponsor; public distribution is by the National Technical Information Service, Springfield, VA 22161, in paper copy or microfiche form.

U.S. Department of Commerce
National Bureau of Standards
Gaithersburg, MD 20899